

THE ROLE OF HEAT SHOCK PROTEIN 90 IN MITIGATING FACIAL ALLODYNIA AND
IMPROVING BLOOD BRAIN BARRIER INTEGRITY IN A MIGRAINE MODEL
UTILIZING CORTICAL SPREADING DEPRESSION

by

Seph Michael Palomino

Copyright © Seph Michael Palomino 2022

A Dissertation Submitted to the Faculty of the

DEPARTMENT OF MEDICAL PHARMACOLOGY

In Partial Fulfillment of the Requirements

For the Degree of

DOCTOR OF PHILOSOPHY

In the Graduate College

THE UNIVERSITY OF ARIZONA

2022

THE UNIVERSITY OF ARIZONA
GRADUATE COLLEGE

As members of the Dissertation Committee, we certify that we have read the dissertation prepared by: Seph Palomino, titled: The Role of Heat Shock Protein 90 in Mitigating Facial Allodynia and Improving Blood Brain Barrier Integrity in a Migraine Model Utilizing Cortical Spreading Depression, and recommend that it be accepted as fulfilling the dissertation requirement for the Degree of Doctor of Philosophy.




Dr. John Streicher

Date: 4/14/22




Dr. Tally Largent-Milnes

Date: 4/14/2022



Dr. Todd Vanderah

Date: 4/14/2022

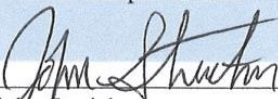


Dr. Nam Lee

Date: 4/14/2022

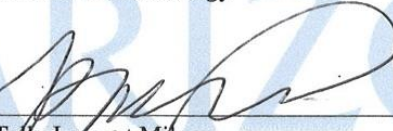
Final approval and acceptance of this dissertation is contingent upon the candidate's submission of the final copies of the dissertation to the Graduate College.

We hereby certify that we have read this dissertation prepared under our direction and recommend that it be accepted as fulfilling the dissertation requirement.



John Streicher
Dissertation Committee Co-Chair
Medical Pharmacology

Date: 4/14/22



Tally Largent Milnes
Dissertation Committee Co-Chair
Medical Pharmacology

Date: 4/10/22

ACKNOWLEDGEMENTS

First and foremost, I would like to acknowledge my dad, Richard Palomino, for making sure I was provided and cared for throughout my life and given the means to succeed. I would not have been able to accomplish this achievement without you. I would like to thank my other immediate family members for their care and support. My siblings Jason Alshouse and Kaitlyn Fournier as well as my mother Stacey Fournier and Stepfather Andre Fournier. I would also like to thank my cousin and mentor Dr. Christopher Campos for helping me understand what type of scientist I wanted to become. My close friends have also helped me in keeping on track and focused. Anyang I appreciate you and your families support over the last 13 years. My friends and lab mates Katherin Gabriel, Aidan Levine, Jared Wahl, David Duron, Justin Lavigne, Erica Williams, Robert Betterton, Jessy Bowden, and Christopher Campbell for their intellectual advice and fun times while in graduate school.

I would like to thank my advisors Dr. John Streicher and Dr. Tally Largent-Milnes. Thank you Dr. Streicher for believing in me and accepting me into your lab and giving me the opportunity to work under you. From you I have learned many molecular pharmacology techniques that will be helpful in my future career. Dr. Largent-Milnes I am thankful for you allowing me the opportunity to work in your lab and I have appreciated your kindness and especially your patience when teaching me animal surgeries and behaviors which I will be able to take with me in my career. I want to thank my other committee members Dr. Todd Vanderah and Dr. Nam Lee. Dr. Vanderah I appreciate your help in teaching me the importance of communication improving my presentation abilities. Dr. Lee I appreciate your support and help regarding my project and thought you had a fun attitude about science which was very helpful in keeping me optimistic.

Table of Contents

LIST OF FIGURES	8
LIST OF ABBREVIATIONS	10
ABSTRACT.....	12
CHAPTER 1: INTRODUCTION TO HEADACHE PAIN AND TREATMENT.....	18
1.1 Primary and Secondary Headache Disorders	19
1.2 Migraine Overview	20
1.2.1 Migraine with Aura	23
1.3 Cortical Spreading Depression	25
1.4 Trigeminal Nociceptive System in Migraine	28
1.4.1 Transmission and Modulation of Head and Facial Pain from the Trigeminal Pathways.....	29
1.5 Prominent Molecular Systems Implicated in Migraine Pain.....	31
1.5.1 Endocannabinoid System and its Role in Headache.....	34
1.6 The Blood Brain Barrier (BBB).....	36
1.6.1 Impact of Migraine with Aura on the Blood Brain Barrier.....	37
1.7 Heat Shock Protein 90 and its Role in Pain.....	40
1.8 Hypothesis.....	41
CHAPTER 2: CSD EVENTS INDUCED BY CORTICAL INJECTION ALTERS TRANSPORTER FUNCTION IN THE BBB ALLOWING FOR INCREASED SUMATRIPTAN TRANSPORT AND INCREASED EFFICACY IN TREATING PAIN ASSOCIATED WITH AURA.....	43
2.1 NHE1 Expression is Critical for Sumatriptan Blood to Brain Uptake Increasing Sumatriptan Efficacy in Rats Subjected to Cortical Spreading Depression	44
2.1.1 Introduction:	44
2.1.2 Methods and Materials.....	45
2.1.3 Results	52
2.1.3.1 Loss of functional NHE1 activity facilitates sumatriptan uptake in vitro.....	52
2.1.3.2 NHE1 inhibition with zonisamide causes periorbital allodynia but enhances sumatriptan efficacy after cortical injection of KCl in vivo	54
2.1.3.3 Total expression of NHE1 was decreased in cortex and PAG samples at 90 min after dural manipulation.	57
2.1.4 Conclusion	59
2.2 Sumatriptan Blood to Brain Uptake post KCl Insult is Mediated by OATP In Vitro, but not In Vivo	60
2.2.1 Introduction.....	60
2.2.2 Methods and Materials.....	62

2.2.3 Results	68
2.2.3.1 Oatp1a4 in bEnd.3 endothelial cells dynamically facilitate sumatriptan uptake during CSD progression in vitro	68
2.2.3.2 Oatp1a4 transport of sumatriptan during CSD in vivo	73
2.2.3.3 CSD induction regulates Oatp1a4 in vivo in a regionally and time-dependent manner	75
2.2.4 Conclusions.....	77
CHAPTER 3: INHIBITION OF HSP90 PRESERVES BLOOD-BRAIN BARRIER INTEGRITY AFTER KCl INDUCED CORTICAL SPREADING DEPRESSION VIA CLAUDIN-5 UPREGULATION.....	78
3.1 Introduction.....	79
3.2 Methods and Materials.....	80
3.3 Results	84
3.3.1 CSD-like Environments Increase HSP90a Expression in Brain Endothelial Cells In Vitro.....	84
3.3.2 Inhibition of HSP90 Prevents Paracellular Breaches of the BEB/BBB	84
3.3.3 17-AAG Prevents Paracellular Leak Induced by KCl In Vitro	87
3.3.4 17-AAG Increases Functional Expression of Claudin 5 Which May Prevent Paracellular Leak of the BBB In Vivo.	90
CHAPTER 4: HSP90 INHIBITION MITIGATES FACIAL ALLODYNIA IN A CSD MODEL THROUGH MODULATION OF ENDOCANNABINOID SYSTEM IN THE PAG.....	95
4.1 Introduction.....	96
4.2 Methods and Materials.....	97
4.3 Results	104
4.3.1 Cortical Spreading Depression Increases Expression of HSP90 in the PAG of Rats 90 Minutes Post KCl Injection	104
4.3.2 Periorbital Allodynia Associated with Cortical Spreading Depression is Mitigated by 24-hour Pretreatment with HSP90 Inhibitor 17-AAG.....	106
4.3.3 Effects of HSP90 Inhibitor 17-AAG on Periorbital Allodynia is Reversed by the Presence of CB1R Antagonist Rimonabant.....	110
4.3.4 Expression Levels of CB1R and AHA1 Were Not Increased in the PAG of Rats 90 Minutes Post KCl or aCSF Injection in Either Vehicle or 17-AAG Pretreated Groups.....	113
4.3.5 GTP γ S Binding in 24-hour Pretreated 17-AAG or Vehicle Rat PAG Tissue 90 Minutes Post KCl or aCSF Injection Using Specific CB1R Agonist PrNMI Reveal Right-ward Shift in Potency.....	116
4.3.6 CSD Affects Endocannabinoid Lipid Levels in a Region-specific Manner 90 Minutes Post KCl, and 24-hour Pretreatment with 17-AAG Increases AEA Lipid Levels in PAG 90 Minutes Post KCl Injection	119
4.3.7 FAAH but not HSP70 Expression in Rat PAG 90 Minutes Post KCl Induction is Affected by 17-AAG Pretreatment.....	122

4.3.8 CSD Induction Promotes Neuroinflammation in the PAG in a Time Dependent Manner.....	124
4.4 Conclusion	128
CHAPTER 5: ENDOGENOUS 2-AG LEVELS IN THE BRAIN INFLUENCE FACIAL ALLODYNIA AND BLOOD-BRAIN BARRIER INTEGRITY	130
5.1 2-AG Levels in the Brain Influence Facial Allodynia and Blood-brain Barrier Integrity	131
5.1.1 Introduction.....	131
5.1.2 Methods and Materials.....	132
5.1.3 Results	138
5.1.3.1 Inhibition of 2-AG degradation by ABHD6 prevents and reverses CSD induced periorbital allodynia in CBR -independent and -dependent manners, respectively ..	138
5.1.3 Conclusion	144
5.2 Assessing Blood-brain Barrier Integrity in a Chronic Morphine Medication Over-use Headache Model.....	145
5.2.1 Introduction.....	145
5.2.2 Methods and Materials.....	146
5.2.3 Results	149
5.2.3.1 Assessment of brain endothelial barrier exposed to acute and chronic morphine in vitro using trans-endothelial electrical resistance measurements and ¹⁴ C-sucrose	149
5.2.3.2 Sustained infusion of morphine in rats induced significant periorbital allodynia	153
5.2.3.3 Assessment of blood-brain barrier integrity of morphine induced MOH in rats	155
5.2.4 Conclusion	157
CHAPTER 6 DISCUSSION AND CLOSING STATEMENT	158
6.1 Spreading Depression Can Alter ASIC Transporter Function in the Cerebral Vasculature Improving Efficacy of Anti-migraine Therapeutics.....	160
6.2 HSP90 Inhibition Improves BBB Integrity Showing Claudin 5 to be Integral as a Neuroprotective Tight Junction Protein During and After CSD Events	166
6.3 HSP90 Inhibition Modulates Endocannabinoid System in the PAG Causing Antinociceptive Effects in a CSD Model of Migraine.....	169
6.4 2-AG is Essential in Modulating Pain and Maintaining BBB Integrity Post CSD Events.....	173
6.5 Morphine Induced MOH Compromises BBB Integrity In Vivo	175
6.7 Concluding Remarks and Significance	176
Appendix:.....	178

References 179

LIST OF FIGURES

Chapter 1

- Figure 1. The multiple phases of migraine22
- Figure 2. Reaction diffusion chart outlining SD propagation.....26
- Figure 3. Anatomy of the trigeminovascular system ascending projections.....30
- Figure 4. Propagation of SD across the dense cerebral vascular network and the neurovascular unit39

Chapter 2

- Figure 5. NHE1 inhibition enhanced KCl induced transport of sumatriptan *in vitro*.....53
- Figure 6. Systemic inhibition of NHE1 by zonisamide induced periorbital allodynia alone.....55
- Figure 7. Systemic inhibition of NHE1 by zonisamide influenced the overall efficacy of sumatriptan.....56
- Figure 8. Total expression of NHE1 was decreased in cortex and PAG samples at 90 min after dural manipulation.....58
- Figure 9. Localization and Expression of Oatp1a4 in mouse brain endothelial cells under physiological KCl and CSD KCl concentration.....69
- Figure 10. Suma succinate crossing from luminal to abluminal compartments of *in vitro* endothelial barrier.....71
- Figure 11. Suma succinate crossing from luminal to abluminal compartments of *in vitro* endothelial barrier.....72
- Figure 12. ³H-sumatriptan uptake in cortex and brainstem of rats post cortical injection of KCl with or without Oatp1a4 inhibitor74
- Figure 13 Expression of Oatp1a4 in cortex and brainstem at timepoints post cortical injection of KCl or aCSF76

Chapter 3

- Figure 14. KCl stimulation increases HSP90a and the co-chaperone endoplasmic in murine brain endothelial cells.....85
- Figure 15. Selective inhibition of HSP90 with 17-AAG reduced 60mM KCl insult associated with CSD to blood-brain barrier leak *in vitro*.....86
- Figure 16. Selective inhibition of HSP90 with 17-AAG reduced 60mM KCl insult associated with CSD induced blood-brain barrier paracellular leak *in vitro*.....88
- Figure 17. 17-AAG reduced cortical spreading depression associated blood-brain barrier leak *in vivo*.....91
- Figure 18. 17-AAG reduced cortical spreading depression associated blood-brain barrier leak *in vivo*.....92
- Figure 19. Summary of findings.....94

Chapter 4

- Figure 20. Total expression of HSP90 in key brain regions associated with CSD post cortical injection of aCSF or KCl.....105
- Figure 21. HSP90 inhibition with 17-AAG applied over dura mater alleviates frequency of periorbital allodynia.....108
- Figure 22. I.P. Injection of CB1R antagonist/ inverse agonist rimonabant blocks antinociceptive effects of 24-hour pretreatment with 17-AAG.....111

- Figure 23. CNR1 mRNA transcript and CB1R along with AHA1 protein levels assessed in 17-AAG pretreated PAG tissue.....114
- Figure 24. ³⁵S-GTPγS coupling assay using PrNMI for CB1R functionality and CB1R competitive antagonist rimonabant with agonist PrNMI to validate CB1R specificity in PAG tissue 90 min post acsf/KCl injection and with vehicle or 17-AAG pretreatment.....117
- Figure 25. Reduction in 90-minute PAG tissue of eCB levels after CSD in female rats, 17-AAG pre-treatment increases eCB levels in CSD induced rats.....120
- Figure 26. FAAH and HSP70 protein levels assessed in PAG of 17-AAG pretreated female rats followed by KCl induced CSD.....123
- Figure 27. Elisa for prostaglandin E2 in PAG tissue collected post CSD induction.....125
- Figure 28. Neuroinflammatory associated markers increased post CSD.....126
- Figure 29. Summary of HSP90 regulation of AEA levels.....129

Chapter 5

- Figure 30. Pharmacological inhibition of ABHD6 during CSD prevention paradigm...139
- Figure 31. Pharmacological inhibition of ABHD6 during CSD reversal paradigm.....140
- Figure 32. Inhibition of DAGLα with LEI106 compromises blood brain barrier integrity142
- Figure 33. TEER measurement of acute and chronic morphine exposure on BEB in vitro.....150
- Figure 34. Chronic morphine exposure to blood endothelial barrier prevents paracellular leak caused by high extracellular KCl.....152
- Figure 35. Assessment of periorbital allodynia after continuous infusion of morphine for seven days.....154
- Figure 36. Assessment of blood-brain barrier integrity in morphine induced MOH model.....156

LIST OF ABBREVIATIONS

2-AG- 2-arachidonoyl glycerol
AA- arachidonic acid
ABHD6- α/β -hydrolase domain-containing 6
aCSF- artificial cerebrospinal fluid
AD- Alzheimer's Disease
ADP- adenosine diphosphate
AEA- N-arachidonoyl ethanolamine
ALS- amyotrophic lateral sclerosis
ANOVA - Analysis of variance
ASIC- acid-sensing channel
ATP- adenosine triphosphate
BBB - blood brain barrier
BEB- blood endothelial barrier
BL - baseline
BSA - bovine serum albumin
Ca⁺- calcium ions
CB1R- cannabinoid receptor type 1
CB2R- cannabinoid receptor type 2
CED- Clinical Endocannabinoid Deficiency
CGRP - calcitonin gene related peptide
CH- Cluster headache
CNS - central nervous system
CSD- cortical spreading depression
CTCF- corrected total cell fluorescence
DAGL- Diacylglycerol lipase
DMEM - Dulbecco's modified Eagle's medium
DMSO- dimethyl sulfoxide
DPM- disintegrations per minute
DRG - dorsal root ganglion
EDTA- Ethylenediaminetetraacetic acid
eNOS- Endothelial nitric oxide synthase
ERK- extracellular signal regulated kinases
ERK- extracellular signal regulated kinases
ES- endocannabinoid system
FAAH- Fatty acid amide hydrolase
FHM- Familial hemiplegic migraine
GPCRs- G-protein coupled receptors
HPLC- high performance liquid chromatography
HSP70- Heat shock protein 70
HSP90- Heat shock protein 90
i.p.- Intraperitoneal
IACUC- Institutional Animal Care and Use Committee
KCl- potassium chloride
MAGL- monoacylglycerol lipase

MAO- monoamine oxidase
MAPK- mitogen-activated protein kinase
MCAO- middle cerebral artery occlusion
MMP-9- matrix metalloproteinases
MOH- medication overuse headache
Na+- sodium ions
NHE1- sodium-hydrogen exchanger type 1
NVU- Neurovascular unit
OATPs/Oatps- organic anion transporters polypeptides
P-gp- p-glycoprotein
PAG- periaqueductal gray
PBS - phosphate buffered solution
PBS - phosphate buffered solution
PET- positron emission tomography
PFA- Paraformaldehyde
PGE2- Prostaglandin E2
PH- paroxysmal hemicrania
RVM- rostral ventromedial medulla
SD- standard deviation
SEM- standard error of the mean
SERT- serotonin reuptake transporters
SUNCT- short lasting unilateral neuralgiform headaches with conjunctival injection and tearing
TACs- Trigeminal Autonomic Cephalgias
TBI- traumatic brain injury
TBST- tris-buffered saline with Tween 20
TEER- Transepithelial/transendothelial electrical resistance
TG- trigeminal ganglion
TJ- tight junction
TLR4- Toll-Like Receptor 4
TNC- trigeminal nucleus caudalis
TRPV1- transient receptor potential cation channel subfamily V member 1
TTH- Tension Type Headaches
WB- Western blot

ABSTRACT

The Blood-brain barrier and related pharmacokinetics are subjects of intense research in neurological pathologies such as traumatic brain injury, ischemic stroke, epilepsy, and encephalopathies. Aside from direct physical damage, the barrier also undergoes stress from the surrounding microenvironment. There is evidence which suggests chronic pain can also compromise blood-brain barrier integrity through various mechanisms, including inflammation. In recent years migraine with aura, a neurological disease afflicting billion world-wide, has been a subject of debate as to whether the disease affects blood-brain barrier integrity. Preclinical research has shown that cortical spreading depression (CSD), the underlying mechanism of an aura, can at least cause transient paracellular leaks. Clinical studies utilizing imaging technology to observe the vasculature of the brain suggests that if these changes are occurring, they are not significant. However, clinical reports have shown that migraine with aura is strongly correlated with increased likelihood of stroke. Additionally, studying the effects of CSD on the microenvironment of the neurovascular unit is crucial in relation to pharmacokinetics and drug delivery.

There is evidence which suggest dysregulation of pH in the brain during and after a CSD event. In this study we observed the effects of inhibiting an acid-sensing channel (ASIC) sodium-hydrogen exchanger 1 (NHE1) during CSD conditions on blood brain barrier modulation, periorbital allodynia, and drug delivery. We first explored how NHE1 inhibition, with specific NHE1 inhibitor zoniporide, would affect the drug delivery across a blood-endothelial barrier in vitro. Results showed increased sumatriptan transport across the BEB in the presence of zoniporide and high extracellular KCl. We observed that NHE1 inhibition with zoniporide alone caused periorbital allodynia and did not ameliorate the effects of KCl induced CSD in female rats. However, increased the efficacy of sumatriptan in CSD induced female rats.

Tissue western blot results revealed a decrease in NHE1 expression during post CSD event correlating with pH dysregulation. This suggests pH changes may affect transporters of the BBB and modulate drug delivery to the brain.

To better understand the increased efficacy of sumatriptan in rats and seek a mechanism for increased sumatriptan transport in vitro we studied Oatp1a4 in the context of CSD. Oatp1a4 had previously been suggested to have a role in sumatriptan transport. Our studies revealed no change in expression or localization of Oatp1a4 in high extracellular KCl in vitro in bEnd.3 mouse cells. Secondly, in an in vitro evaluation of sumatriptan transport E3S, an Oatp inhibitor, was used to treat the BEB monolayer decreasing the amount of sumatriptan transport in the presence of high extracellular KCl. In vivo in situ brain perfusions with ³H-sumatriptan were performed utilizing E3S pretreatment before CSD induction we observed no significant difference in sumatriptan transport post CSD but we did observe a time dependent effect on transport of sumatriptan across ass groups. This study indicates Oatp1a4 is not a major transporter of sumatriptan and depending on the timing from CSD induction there is less sumatriptan uptake in the brain.

Molecular mechanisms for BBB dysregulation and pain behavior and modulation are poorly understood in migraine with aura. In this study we researched the effect of HSP90 inhibition in our models of CSD in relation to migraine with aura. HSP90 inhibition has previously been shown to be neuroprotective of the BBB in a ischemic stroke model. In this study we explored how it would affect the BBB in conditions related to spreading depression. In vitro HSP90 inhibition reduced the drop in TEER of a BEB monolayer of bEnd.3 mouse cells caused by the presence of high extracellular KCl. Also in vitro pretreated BEB monolayers were shown to have reduced paracellular leak in the presence of high extracellular KCl. In vivo insitu

brain using ^{14}C -sucrose assessed BBB integrity in female rats, 17-AAG pretreated animals showed a significant reduction in sucrose uptake in the cortex of the brain suggesting reduced paracellular leak. Tissue western blots revealed animals pretreated with 17-AAG had increased protein detection levels of tight junction protein claudin 5 in the cortex and PAG regions of the brain showing HSP90 inhibition and upregulation of claudin 5 to be neuroprotective of the BBB in CSD conditions.

Regarding pain associated with migraine with aura we utilized our in vivo CSD model in female rats and assessed periorbital allodynia with pretreatment of 17-AAG. We observed HSP90 inhibition showed ameliorating effects on CSD induced periorbital allodynia with an intermediate dose of 0.5 nmol over the dura mater. The theory of clinical endocannabinoid deficiency in patients with headache has shown to correlate with data collected in our lab, HSP90 has co-chaperones which affect the endocannabinoid system. In this study we tested the relationship of HSP90 inhibition and the CB1R system in vivo. We repeated behavioral experiments with 17-AAG pretreatment of female rats, 30 minutes before CSD induction in 17-AAG pretreated rats we gave CB1R antagonist/invers agonist rimonabant. We observed the ameliorative effects of 17-AAG pretreatment to be ablated suggesting CB1R involvement in pain modulation associated with HSP90 inhibition during CSD. For molecular experiments ex vivo we focused on the PAG of the brain as we previously observed significant effects from CSD on HSP90 protein expression as well as previous research suggest endocannabinoid dysregulation in this region. We found that 17-AAG pretreatment significantly increased anandamide (AEA) in the PAG 90 minutes post CSD induction using LC/MS. We also report that 17-AAG pretreatment caused a significant decrease in expression of AEA hydrolysis enzyme FAAH 90 minutes post CSD induction. We also observed no change in expression of the CB1R using

western blots and a right ward shift in CB1R activity using ^{35}S -GTP γ functional binding in PAG tissue pretreated with 17-AAG and harvested 90 minutes post CSD induction in female rats. These results suggest HSP90 inhibition positively modulates the endocannabinoid system to cause pain relieving effects through descending pain modulation post CSD to prevent headache associated periorbital allodynia in female rats.

To further explore possible therapeutics for migraine with aura we assessed the efficacy of ABHD6 inhibition to increase 2-AG levels in our in vivo model of CSD in female rats. Previous work has shown decreased 2-AG levels in the brain could lead to headache pain. In this study we observed ABHD6 inhibition to be effective in both the prevention and reversal of periorbital allodynia post CSD induction. Also, we utilized both CB1 and CB2 receptor inhibitors in the prevention and reversal paradigm to understand which receptor may play a role in headache pain modulation. We report the CB1R to have a major role in ABHD6 inhibition in the reversal of headache pain but not prevention leaving further studies to be warranted. We also investigated the role of 2-AG in BBB maintenance in vitro and in vivo. We report in this study that with use of LEI106, a DAGL α inhibitor, as 2-AG depletion mechanism there was a decrease in TEER using a bEnd3 BEB monolayer. Using in situ brain perfusions with ^{14}C -sucrose we assessed BBB integrity 120m minutes post LEI106 I.P. injections into female rats. We observed a significant increase of sucrose in the PAG region of the brain and a near significant increase in the cortex suggesting 2-AG is important for BBB maintenance in key regions of the brain associated with headache and migraine pathology.

Finally, in this study we assessed BBB integrity after acute and chronic morphine treatment like what is observed in medication induced headache. Previous results showed a decrease in 2-AG in the PAG of female rats with morphine induced medication over-use

headache (MOH). As 2-AG depletion has shown to be important for BBB maintenance in the PAG specifically we investigated how morphine induced MOH affected the BEB in vitro using bEnd3 mouse cells. We report no significant change in TEER between acute and chronic morphine. To further investigate the effects of chronic morphine on paracellular leak we used ¹⁴C-sucrose to assess the integrity of the BEB in vitro, morphine alone had no effect on paracellular leak however morphine in the presence of high extracellular KCl seemed to reduce the transient leak caused by KCl. In vivo assessment of female rats continuously administered morphine for seven days with MOH induced periorbital behavior were assessed using in situ brain perfusions of ¹⁴C-sucrose for 15 minutes to determine BBB integrity. We show significant uptake of sucrose in the PAG region of the brain, however at this time more control animals are necessary for confirmation.

The results presented in this dissertation demonstrate that CSD affects ASIC channels which can alter the microenvironment of the BBB which can affect drug delivery. These changes can be led to new strategies for treatment of migraine pain. Also, HSP90 inhibition with 17-AAG has proven to be useful in ameliorating BBB leak and headache pain associated with migraine with aura. 17-AAG has also provided insight into molecular mechanisms associated with the positive effect of HSP90 inhibition and provided new avenues for research topics in the field of headache and migraine. Topics related to claudin 5 regarding its neuroprotective effects of the BBB and further knowledge into how clinical endocannabinoid deficiency can be regulated to provide pain relief for headache pain. Evidence is provided for ABHD6 inhibition as a therapeutic target for headache. Its mechanism of action is reliant on CB1R activity. Investigation into the PAG region for confirmation that the therapy is due to action in descending modulation is further needed. Low 2-AG levels also affect BBB integrity further evidenced by

the effect of morphine induced MOH on the BBB in the PAG. Based on previous results with HSP90 inhibition, future studies involving HSP90 in morphine induced MOH models may be of interest.

**CHAPTER 1: INTRODUCTION TO HEADACHE
PAIN AND TREATMENT**

1.1 Primary and Secondary Headache Disorders

Primary headache disorders are characterized by their lack of underlying causative disease pathology such as infection or trauma [1]. Primary headaches account for most cases of reported headache pain and include Migraine, Tension Type Headaches (TTH), and Trigeminal Autonomic Cephalgia's (TACs) [2]. Of the primary headache disorders, tension type and migraine affected about 3 billion people worldwide in 2016 [1]. TTH is poorly understood but commonly diagnosed affecting 60-80% of the population [1]. It is described as a pressure like pain and is often episodic, the chronic variant being rare [3]. TTH rarely impacts activities associated with daily living in comparison to migraine. Migraine is the second most prevalent disorder affecting at least 30% of the adult population [4]. There is difference in prevalence amongst females versus males for migraine, 18% of females compared to 6% of males experience migraine [4]. TACs are characterized by unilateral trigeminal distribution of pain with ipsilateral cranial autonomic symptoms [2]. TACs include cluster headache (CH), paroxysmal hemicrania (PH), and short lasting unilateral neuralgiform headaches with conjunctival injection and tearing (SUNCT) [2, 3]. Like migraine headaches, TACs are quite disabling with a high frequency of attacks considered incredibly painful. TACs are distinct, allowing for clinicians to properly diagnose and treat these disorders. Other notable forms of primary headache include Thunderclap, cough, exertional, and sexual headache [5].

Secondary Headache disorders differ from primary headache as they are the result of exogenous etiologies such as stroke or an insult. Primary headaches, although painful and disabling, are not life threatening. Secondary headaches may be due to dangerous underlying pathologies such as head trauma, cerebral vascular disorders, or meningeal infection [6]. It is important to differentiate between primary and secondary headache as this will determine treatment in the clinic. To discern Primary from Secondary headache, it is important to know the

patient's history as well as observe for signs/symptoms which can suggest underlying conditions causing the headache. Signs and symptoms to watch for could be related to disease such as: Fever, rash, infections, high blood pressure [6]. There could be neurological signs/symptoms such as change in level of consciousness, pulsatile tinnitus, weakness, ataxia, seizure [6]. The onset of the headache is also telling, sudden onset where pain reaches maximum level instantly versus older onset where the pain is gradual throughout the day [6]. Understanding and proper diagnosis of headache will ensure proper treatment which will lead to relief for the patient. The work done in this thesis focuses on Migraine, a common but highly disabling primary headache disorder.

1.2 Migraine Overview

There are 2 common types of episodic migraine headache, migraine with and without aura [2]. Migraine attacks occur in 3-4 documented phases depending on the subtype [2, 4]. Both can cause a combination of intense pain, debilitating neurological symptoms, as well as high chance of triggering a second attack during the postdrome phase, the sensitivity during the postdrome phase has a substantial impact on quality of life. There are several reported triggers for migraine attacks which are experienced by 90% of people with the disease including excessive levels of stress and anxiety [2]. In women, fluctuating hormone levels when going through the menstrual cycle can also lead to a migraine attack [7, 8]. The most common triggers aside from those associated with menstruation are related to diet/metabolism and disturbance in sleep cycles [3, 9]. Aside from these commonly reported triggers, there are also genetic causes linked to migraine [2, 10, 11]. Familial hemiplegic migraine (FHM) are hereditary mutations linked to migraine with aura [2]. They identified these mutations in three genes (CACNA1A, ATP1A2, and SCN1A) [11-14]. Identifying these genetic mutations have allowed for greater

molecular research into the pathology allowing greater expansion on etiology and treatment of the disease.

The more common type of migraine is migraine without aura, with only 15 – 30% of sufferers experiencing migraine with aura [4, 15, 16]. Both forms of migraine have at least 3 phases (**figure 1**): prodrome, headache, and postdrome [3]. The prodrome or premonitory phase, presents signs and symptoms such as fatigue, stiff neck, nausea, and photophobia, days to hours before some or all headaches [2]. People who experience migraine with aura will normally have the aura phase as part of the prodromal period of migraine, all of the neural symptoms experienced during the aura are temporary as well [2]. Migraine with aura includes neurological signs and symptoms such as visual disturbances (flashing lights, dark spots), phosmia (olfactory hallucinations), and motor disturbances (speech and movement difficulties) [2, 3, 17, 18]. The aura phase develops in 5 to 30 minutes and lasts up to 60 minutes [2, 19]. The headache phase begins 30 minutes to 24 hours after the prodromal or aura phase. The headache phase in both forms of migraine can last up to 72 hours [2]. A summary of features during the headache phase are detailed as: Typically unilateral with no side preference, in the ocular, temporal, or frontal regions of the head along with throbbing or pulsating pain with sharp periorbital “ice-pick” pains of moderate to severe intensity [2]. People can experience photophobia or phonophobia as well as nausea, and about half of people vomit during the headache phase [3, 20, 21]. The post-dromal phase of migraine presents symptoms like the prodromal phase of migraine: fatigue, photophobia, muscle stiffness, depression, and allodynia [3, 20, 21].

Figure 1

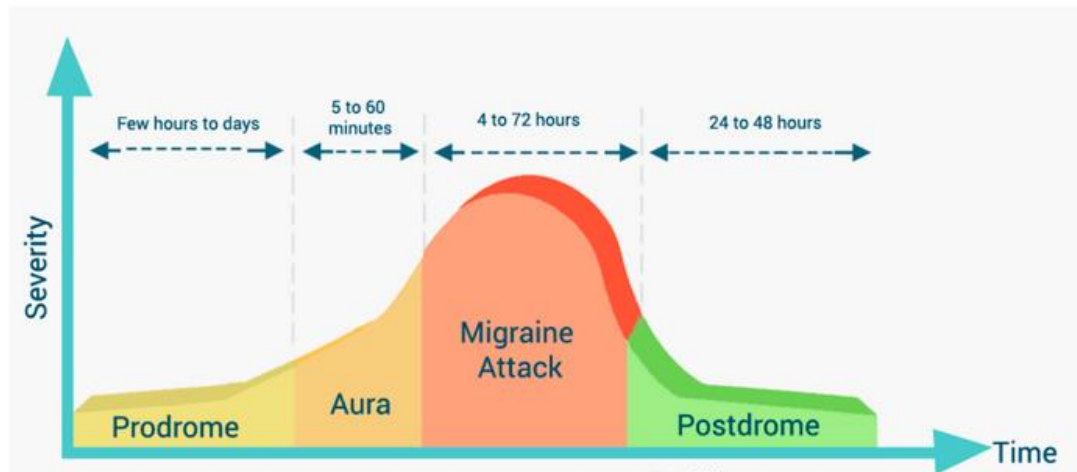


Figure 1. The multiple phases of migraine. Migraine has multiple phases: premonitory, aura, headache, post-drome and interictal (in between headaches). The premonitory phase can occur 3 days before the headache phase, and it involves complex interactions between various parts of the brain. The headache phase involves activation of the pain system.

Migraines occur over many years or over the course of the individual's lifetime. The frequency of attacks these individuals experience varies and are diagnosed as either episodic or chronic migraine and treated accordingly [2]. Episodic migraine is defined as headaches which occur 15 times or fewer in a month [2, 22]. Chronic migraines are defined as headaches which occur at least 15 days per month for at least 3 months with features of migraine on at least 8 days per month [23]. Differential diagnosis between episodic and chronic migraine is important clinically as patient treatment can be dictated by this distinction [22]. It is possible for episodic migraine to progress to chronic migraine in patients depending on factors related to their genetics and lifestyle [22]. A major confounding factor in the diagnosis of episodic and chronic migraine would be the presentation of medication overuse headache (MOH) in migraine patients [22].

MOH is defined as a headache occurring on 15 or more days per month in a patient with pre-existing primary headache and developing as consequence to overuse of acute or symptomatic headache medication on 10 to 15 or more day per month [23]. MOH is classified as a secondary headache disorder and can be difficult to diagnose and manage in chronic migraine patients [23].

1.2.1 Migraine with Aura

About a third of migraineurs experience an aura phase [1, 18], mostly comprised by patients who experience sporadic migraine; however, those who suffer from FMH predominantly experience migraine with aura [23]. The aura phenomenon is a reversible neurological event involving visual, olfactory, speech and/or motor symptoms which precedes the headache phase in migraine[18, 23, 24]. The aura phase does not typically last longer than 60 minutes, and all symptoms associated with the phase clear up [23]. The role of cortical spreading depression (CSD) as a mechanism associated with aura has been widely accepted by researchers, as it is supported by a large body of studies [18, 23]. Diagnosis of migraine with aura is described in the International Headache Classification Disorders III edition.

At least two attacks with one or more of the following reversible neurological symptoms: visual, sensory, motor, brainstem, retinal and at least three of the following six characteristics; one aura symptom which spreads gradually greater than 5 minutes, two or more aura symptoms occurring in succession, each individual aura symptom lasting between 5-60 minutes, at least one aura symptom is unilateral, at least one aura symptom is positive, and/or the aura is accompanied or followed by a headache within 60 minutes. People with FMH typically experience brainstem related symptoms; patients are recommended to time and record these symptoms for accurate diagnosis [23].

There are three types of FHM which cause migraine with aura [11, 25]. With FHM, migraine attacks occur due to genetic mutations causing defects in ion channel function [25]. As previously mentioned, there are three mutations which lead to ion channel dysfunction. The most common heritable form is FHM type 1 caused by a mutation in the CACNA1A gene[12-14]. This is an autosomal dominant gene mutation which affects the structure of the pore forming unit of the P/Q type calcium channel CaV2.1[11-13]. There have been 17 mutations on this channel identified, all of which result in varying degrees of pathology, but overall linked to increased potential of suffering from cerebral edema, stroke, epilepsy, and migraine [11, 25]. These mutations in the calcium channel allow for a lower membrane threshold for CSD initiation, becoming more sensitive to slight changes in the osmotic environment. The other two forms of FHM are less common but also contribute to the initiation of CSD by lowering cellular membrane potential allowing for increased likelihood of cellular depolarization or interfering with repolarization of cells. FHM type 2 is a mutation in the ATP1A2 gene encoding the Na⁺/K⁺-ATPase [26, 27]. This ATPase is heavily expressed on astrocytes which help maintain cellular membrane potential. This mutation leads to higher resting membrane potential in astrocytes, which makes it more difficult for repolarization to occur contributing to systemic hyperpolarization of surrounding cells. FHM type 3 mutation is located on the SCN1A gene encoding a sodium channel, Nav 1.1, alpha subunit [11, 28]. People with FHM suffer additional symptoms such as motor weakness and difficulty waking up [23]. Either before or in conjunction with aura symptoms, regional cerebral blood flow has been observed to be decrease in the cortex [23]. The reduction is above ischemic levels and spreads from the occipital lobe to the frontal lobe over the course of several hours followed by increase in cerebral blood flow in the same regions [23]. This physiological change has been linked to the CSD phenomenon.

1.3 Cortical Spreading Depression

Migraine was originally considered to be a vascular disease as vasodilation was observed during migraine attacks [9]. Today it is widely accepted as a neurovascular coupled disease; CSD has led to changes in vascular activity which have been linked to headache pain [9]. Cortical Spreading Depression as stated above, is an electrical phenomenon brought about by hyperexcitable neurons in the occipital or parietal lobes. The neurons depolarize systemically, leading to a fluctuation in osmotic pressure, and release of excitatory neurotransmitters, which causes long term hyperpolarization of both the neurons and surrounding astrocytes [9, 23]. The critical driver for this event would most arguably be high extracellular potassium $[K^+]$ ions, because of depolarized cells inability to bring K^+ back into the cells [9, 29-31]. Thresholds involving extracellular $[K^+]$ vary depending on species, age, and brain region [32, 33]. This massive $[K^+]$ efflux into the extracellular space can raise the resting normal levels from about 3 mM to 30-80 mM in most species and tissue [9, 34-36]. In response to the increased extracellular $[K^+]$ there is a change in intracellular $[Na^+]$, $[Cl^-]$, and $[Ca^{2+}]$, making the cells take in more of these ions and causing a shift in the ion gradient. The cells swell in response and conversely shrink the surrounding extracellular space [29, 37, 38]. The influx of sodium and calcium triggers the releases of many neurotransmitters and neuromodulators from the neurons such as glutamate, GABA, catecholamines, prostaglandins, adenosines, aspartate, and glycine [9, 39-41]. **Figure 2** shows a simple reaction diffusion chart outlining SD propagation [9].

Figure 2

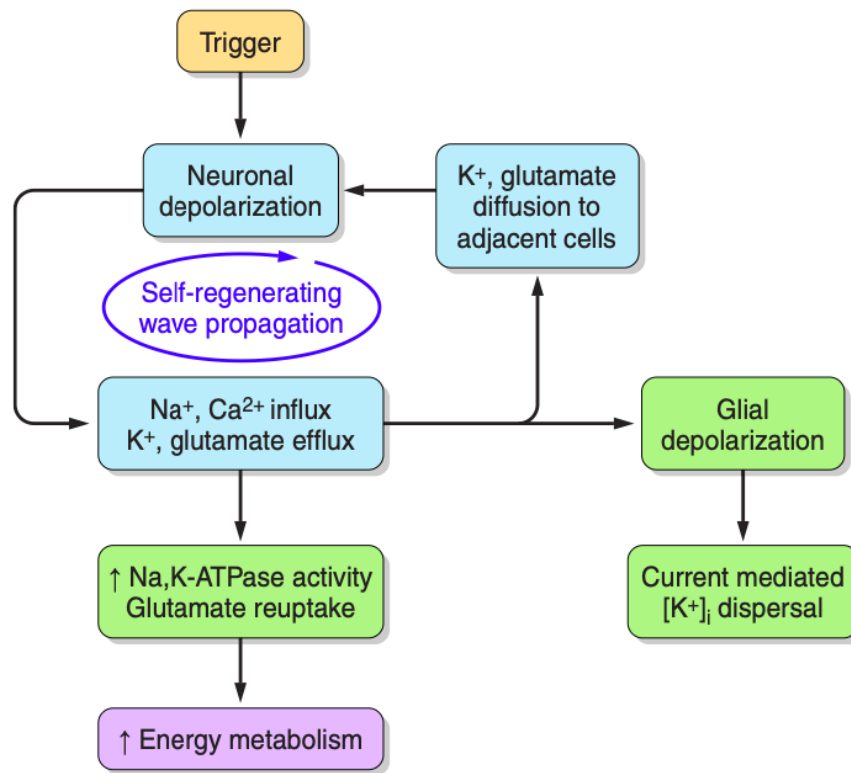


Figure 2. Reaction diffusion chart outlining SD propagation. Reaction-diffusion model of SD propagation and regenerative processes. Basic mechanisms believed to be responsible for the self-regenerating propagation of SD within contiguous grey matter and the mechanisms of recovery. [17]

This large scale hyperexcited event causes an outward circular self-propagating spread of depolarization in neurons and astrocytes moving across the cortex at a rate of 1.5-9.5 mm/min[9, 42, 43]. Complete membrane depolarization in neurons sequesters action potentials and suppresses both spontaneous and evoked electrical activity, rendering the region incapable of performing synaptic transmissions [9]. CSD seems to only be limited by the presence or absence of gray matter in its path, as studies have shown that lesions in the cortex interfere its spread [9,

44]. Interestingly, SD cannot penetrate white matter and thus white matter acts as a barrier to interrupt SD as well [9, 44]. The CSD event has shown to also initiate a spreading wave of hyperemia followed by prolonged vasoconstriction in the cerebral vasculature[45]. CSD is believed to be the underlying mechanism for aura in migraine with aura, however CSD is also involved in other pathologies such as epilepsy, traumatic brain injury, and ischemic stroke. In terms of reference to brain injuries and stroke, it would be more accurate to refer to it as spreading depolarization rather than depression [9]. The vascular effects of CSD are not as constant, as the electrophysiology across species and tissue, and certain factors such as experimental conditions, brain region, and vascular bed may vary [9].

Understanding the metabolic impact of CSD in the brain allows for greater understanding behind the hemodynamic response. It has been noted that ATP consumption in brain cells is high in the first few minutes of a CSD event [9, 46, 47]. There have been studies which show increased levels of ADP and AMP during SD as well, which support high expenditure of ATP [48]. This is most likely due to active transport mechanisms in neuronal and glial cells being overworked in an attempt to maintain homeostasis during the change in osmotic pressure, and the need to replenish and recycle neurotransmitters post depolarization [49]. The challenge on tissues during CSD is high and requires a lot of energy leading to a high demand of glucose and oxygen [9, 39, 48]. Increased glucose metabolism during a CSD causes up to a 60 percent decrease in tissue glucose within a minute of peak depolarization, and this effect varies by brain region [9, 47, 50, 51]. Along with a decrease in tissue glucose, there is also at least a 0.5 unit decrease in pH depending on the tissue and species (pH 6.80-6.90), close to observed pH levels during ischemia (pH of 6.75) [52-55]. Interestingly there have been studies which have shown a decrease of intracellular pH in neurons, and an increase of intracellular pH in astrocytes[9, 56].

Changes in pH can affect neuronal signaling which can lead to sensitization of circuits related to pain. Changes in pH can also affect the blood brain barrier and drug kinetics which may interfere or enhance treatment of disease states such as migraine. These intracellular pH changes do not last long however, usually lasting for only a few minutes, with the change in extracellular pH lasting roughly about 10 minutes, and full pH recovery can take up to 30 minutes [46, 53, 57]. This rapid change in pH and demand of glucose in reaction to widespread depolarization is a major trigger for release for vasoactive molecules such as CGRP and nitric oxide, which also contribute to hemodynamic changes during CSD [9, 58, 59]. Aside from changes in the microenvironment of the brain and cerebral vasculature, CSD has been implicated in trigeminal nerve activation and sensitization of meningeal nociceptors which can be associated with migraine pain [60, 61].

1.4 Trigeminal Nociceptive System in Migraine

Activation of the trigeminovascular system is the primary theory behind how CSD can lead to migraine headache pain [21, 62, 63]. The trigeminal nerve, commonly known as the fifth cranial nerve, operates as the major primary afferent for the relay of facial and scalp sensory information to the brain [64, 65]. The trigeminal ganglion innervates almost all cranial tissue as well as a few cervical afferents from the upper cervical DRG, which innervate the occipital region. The trigeminal nerve is divided into 3 main branches: the ophthalmic nerve, maxillary nerve, and mandibular nerve [64, 65]. The ophthalmic division has been considered the most relevant in migraine pain since the distribution of head pain is in proximity to the periorbital region. The trigeminal afferents consist mainly of myelinated A δ - and unmyelinated C- fibers which synapse centrally on the second-order relay neuron, located in the dorsal horn of the trigeminal nucleus caudalis [21, 66-68]. There are also indirect projections from the

trigemino-cervical complex into the parabrachial nucleus [21, 69, 70]. Recently, there has been evidence of direct projections from the trigeminal ganglion synapsing in the ipsilateral parabrachial nucleus in mice [71, 72]. This could explain some autonomic features of headache pain, as well as increased perception of painful stimuli in the head and face. Since there is an association with the limbic system, it is speculative that the trigeminal synapse to parabrachial nucleus could influence the affective motivational aspect of pain.

1.4.1 Transmission and Modulation of Head and Facial Pain from the Trigemino-cervical Pathways

As in the primary afferents located throughout the body, headache pain transmission begins with noxious stimuli introduced into the sensory nerve endings of the head and scalp. The stimuli can range from mechanical, thermal, or chemical signals. The initiation of these stimuli leads to the opening of voltage gated sodium channels (NaVCH), which propagate the noxious signal along the nerve fiber to a bundle of cell bodies located in the periphery. In the trunk of the body, these cell bodies are referred to as dorsal root ganglion (DRG). The equivalent in the head and scalp would be the trigeminal ganglion (TG), located in the lateral region of the brainstem. Trigeminal nociceptive fibers located in the dura project to the caudal medulla and the upper spinal cord referred to as the trigemino-cervical complex [9, 21, 73, 74]. Trigemino-vascular sensory information is relayed to the rostral ventromedial medulla, nucleus raphe magnus, and parabrachial medulla. The TG also synapses with the periaqueductal gray and locus coeruleus as well as the hypothalamic nuclei. **Figure 3** [21] is a simplistic representation of the ascending pathway associated with TG activation. These projections also largely target ventroposteromedial thalamic nuclei [21, 67, 75].

Figure 3

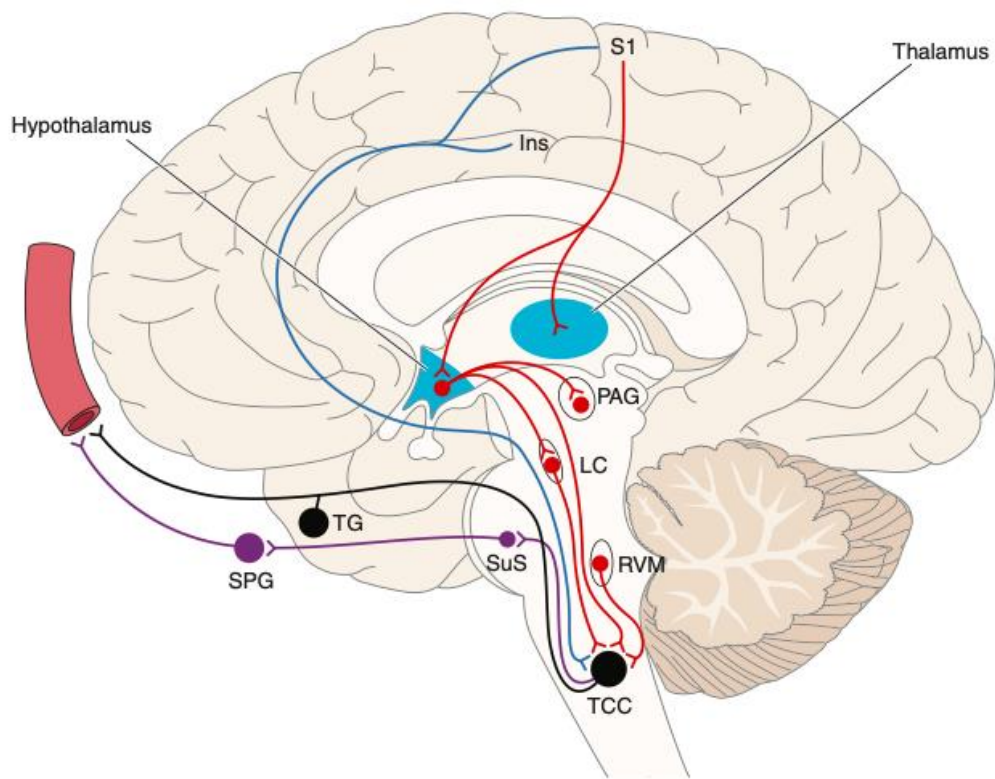


Figure 3. Anatomy of the trigeminovascular system ascending projections. The trigeminal ganglion (TG) gives rise to pseudounipolar trigeminal primary afferents which synapse on intra- and extra-cranial structures (blood vessels) as well as the spinal cord trigeminothalamic complex (TCC). Second-order neurons from the TCC ascend in the quintothalamic (trigeminothalamic) tract synapsing on third order thalamocortical neurons. Direct and indirect ascending projections also exist to the locus coeruleus (LC), periaqueductal grey (PAG), and hypothalamus.

Recently, the brainstem has garnered increased attention due to its potential involvement during migraine pain. More specifically the periaqueductal gray (PAG), as there is evidence of activation during spontaneous migraine attacks, and studies have shown lasting activation post triptan treatment which mitigates the pain state in most migraineurs [72, 76]. The PAG may have a role in the switch from episodic to chronic migraine [72, 77] since patients with increased number of migraine attacks have shown central sensitization leading to stronger synaptic response in higher order cortical structures associated with pain [72, 78]. The PAG shows distinct activation post dural vascular nociception, signifying its importance in migraine and headache pain processing [79-81]. Patients who have reported allodynia during migraine attacks have reduced mass volume in the midbrain region, which includes the PAG, in comparison to people who do not suffer from migraine [72, 82]. Currently the exact mechanism of the PAG's involvement pertaining to antinociception in migraine is unknown, aside from studies in which direct injections of either CGRP antagonists or 5-HT_{1B/1D} agonists into the PAG have ablated pain induced by CGRP injections [72, 83, 84]. Besides the experiments with treatments directly injected into the PAG, its role in antinociception in descending modulation is not well understood. The PAG is part of descending modulation as well there are projections from the PAG into the rostral ventral medulla (RVM). The RVM has ON and OFF neurons which modulate descending pain to the spinal dorsal horn. The ON cells receive nociceptive input which is modulated by endogenous opioids. OFF cells are tonically active, and they interfere with the activation of ON cells[21].

1.5 Prominent Molecular Systems Implicated in Migraine Pain

Although the role of aura in migraine pain has been debated in the field of headache pain, there has been evidence that CSD can stimulate trigeminovascular nociception [72, 85]. As

previously stated, CSD causes a release of several chemical signaling molecules which can lead to both transduction of pain signals and processing by second order neurons, leading to sensitization of the central nervous system. In preclinical models of CSD in rats, the event can lead to acute prolonged activity of the trigeminovascular system [72, 86]. Currently, the most effective treatment for migraine has been pharmacological and biological agents which inhibit the activity of the CGRP molecule [62].

The CGRP system was implicated in migraine when it was noticed to be elevated in the sera of patients experiencing a migraine attack [62]. The CGRP biologics have shown to be effective in both migraine and migraine with aura. The CGRP neuropeptide is a common signaling molecule in the peripheral nervous system including the TG and meningeal vasculature. Release of CGRP from peripheral nerve terminals not only signals to secondary neurons in the trigeminal nucleus caudalis (TNC), but also into other tissues. This causes sensitization of CNS to noxious stimuli and the production of nitric oxide, which can lead to vasodilation in the vasculature. It is notable that immunohistochemistry in both rat and human tissues show unmyelinated C-fibers innervating cerebral and meningeal arteries expressing CGRP [62, 87]. A δ fibers in the region were also shown to express RAMP1, the CGRP receptor, which could mean signaling from C-fibers can sensitize local A δ fibers [62, 87]. To further support this theory the humanized monoclonal CGRP antibody prevents A δ fibers from firing but not C-fibers [62, 87]. Interestingly, CGRP did not evoke a response from dural mast cells in human tissues [88]. Other studies have shown that CGRP can activate satellite cells, indicating glial activity's involvement in CGRP signaling in migraine pathology [62]. Preclinical and clinical research have shown CGRP signaling to be involved in both neuronal signaling and vasculature function, playing a key role in migraine pathophysiology.

Before the advancement in the field regarding the role of CGRP in migraine, the most prominently studied molecular pathway was the serotonergic system. There have been documented changes of serotonergic metabolism and processing of central serotonin mediated responses between and during migraine attacks in the past 20 years. Initially, it was believed that migraine patients suffered from a neurochemical imbalance of low serotonin in the brain, in which increased amounts of the neurotransmitter could lead to a migraine attack [89]. Many serotonergic neurons are in the raphe nucleus of the brainstem, and these neurons project throughout the rest of the brain [89]. Neurons projecting from the raphe nucleus are responsible for regulation of many physiological functions such as pain, stress, mood, and sleep [90, 91]. Peripheral 5-HT receptors which may contribute to migraine, are involved with platelet function and regulation of smooth muscle tone in the vasculature [89]. Serotonin is either degraded by monoamine oxidase (MAO), metabolized into 5-HIAA, or is recycled into the presynaptic neuron via serotonin reuptake transporters (SERT).

There are seven families of 5-HT receptors composed of six G-protein coupled receptors and the 5-HT₃ receptor which is a ligand gated ion channel. At least two of these receptor types have been targeted for pharmacological treatment of migraine, the 5-HT_{1B/1D} and the 5-HT_{1F} receptors, which are inhibitory auto-receptors located on the presynaptic neuron [92]. The triptan class of drugs are abortive, which target the 5-HT_{1B/1D} receptor and are effective in treating pain in at least 40% of people suffering migraine attacks [93]. Ditans, which act on the 5-HT_{1F} receptor, are similar to triptans except they are more specific and do not affect blood vessels as much thereby lowering their side effects [94]. A neuroimaging study performed in migraine patients using a selective 5-HTT ligand and photon emission computed tomography reported increased availability of 5-HTT in the brainstem [89, 95]. This implicates dysregulation of the

serotonergic system in the brainstem, further establishing the important role the brainstem plays in migraine pathophysiology. As mentioned before, there have been PET imaging studies in which increased blood flow to the brainstem occurs during a migraine, near the raphe nucleus region, however, this increase persisted after sumatriptan treatment, headache pain, and migraine symptoms were alleviated [76, 89]. The triptan class of drugs are effective to a point, but there have been studies which concluded that it is best to take triptans during the headache phase rather than aura phase for them to be more effective[96]. Additionally, based on epidemiological data taken from patients, it has been noted that sumatriptan is less effective as acute therapy for migraine with aura versus migraine without aura, however, there have also been studies which suggest increased efficacy of triptans when given during the aura phase [97, 98].

1.5.1 Endocannabinoid System and its Role in Headache

The endocannabinoid system (ES) has garnered attention in the field of migraine as there have been several studies demonstrating its dysregulation can lead to migraine headache phenotypes both preclinically and clinically [99]. The best characterized receptors are the cannabinoid 1 and 2 receptors (CB1R and CB2R), both inhibitory ($G_{i/o}$) GPCRs utilizing pathways associated with such receptor types. The ES is also unique in the fact that it is a system which utilizes retrograde signaling. CB1R are expressed throughout the body but have particularly dense population in the central nervous system [100-102]. CB1R is found in GABAergic interneurons, astrocytes, and glutamatergic, serotonergic, cholinergic, and glycinergic neurons in the brain [101-103]. There have been studies which suggest CB1R located on astrocytes are $G_{q/11}$ coupled receptors [103-105]. CB1Rs are abundant in synaptic terminals, indicative of their importance in regulating synaptic transmission [106]. CB2Rs are primarily expressed in immune cells such as microglia, and generally their activation leads to anti-

inflammatory effects [102]. The two major endogenous endocannabinoid neuromodulators associated with the ES are 2-arachidonoyl glycerol (2-AG) and N-arachidonoyl ethanolamine (anandamide or AEA), both of which have a high affinity for the CB1R but can also activate the CB2R [102]. These two lipid signaling molecules also have the potential to activate other GPCRs, nuclear receptors, and ion channels [107, 108]. Aside from that 2-AG being important in lipid metabolism, it is also the precursor for arachidonic acid (AA) which is important in the synthesis of prostaglandins [109].

There has been evidence which suggests the ES involvement in migraine pain in the last decade. CB1R agonists had been shown to reduce CSD amplitude, duration, and propagation in a rat model in a dose dependent fashion [110, 111]. Studies have shown treatment with mixed CB1/CB2 receptor agonist WIN55,212-2, as inhibiting trigeminocervical complex A and C-fiber activity linked to migraine pain [110, 112]. Secondly, the ES is involved with several molecular systems associated in migraine pain and treatment, such as, glutamate, GABA, serotonin, and arachidonic acid/prostaglandins. [99, 110]. The ES is also involved in regulating CGRP release which is tied to both vasodilation and central sensitization [110, 112]. There is also a high density of CB1 receptors located in the PAG, shown to play a part in modulation of 5-HT_{1B/1D} receptors, which may modulate ascending nociceptive signals from the trigeminovascular system [110, 113]. There may also be a role for the ES in descending modulation from the PAG and RVM as there are CB1 and TRPV₁ receptors present in these regions. AEA may signal through these receptors as studies which utilize an FAAH inhibitor, a hydrolyzing enzyme for AEA, showed enhanced analgesia in models of neuropathic pain when injected into the PAG [114, 115].

Further studies involving sex differences in the expression of endocannabinoids in the cortex and PAG in rats, showed basal differences in endocannabinoid levels in females versus males [116]. Tissue harvested from naïve males and estrous cycled females were processed and analyzed via liquid chromatography mass spectrometry, unlabeled proteomics, and immunohistochemistry. The study showed significantly decreased 2-AG levels in the PAG of females compared to males with no difference between estrous cycle [116]. These differences may contribute to the development of chronic pain states as well as the mechanism as to why females are more likely to have migraines than males. A follow up study showed that 2-AG depletion using the specific DAGL alpha inhibitor, LEI106, in rats caused facial allodynia and photophobia without extracephalic allodynia [116]. These studies, as well as the regulatory role of the ES reported to be involved in migraine pain, suggests further research and understanding of the ES in headache pain would be a beneficial contribution to the field preclinically and clinically.

1.6 The Blood Brain Barrier (BBB)

The blood brain barrier is the tightly regulated interface between the peripheral circulatory system and the CNS. It is a multicellular structure composed of microvascular endothelium, pericytes, astrocytes, and neurons which comprise the neurovascular unit (NVU) [117]. Homeostasis of the BBB is crucial to CNS health, as it maintains the microenvironment of the brain and spinal cord, and regulates substances crossing into the CNS [117]. In addition to these cells, the extracellular matrix and microglia have a role in maintenance and homeostasis of the BBB. Transmembrane proteins known as tight junctions (TJ) located between the endothelial cells prevent paracellular diffusion of water-soluble substances in the blood from entering the brain [117]. Aside from TJ proteins there are active influx and efflux transporters located in the

BBB which further regulate substances from entering the CNS from peripheral blood vessels [64, 118]. Constant or prolonged dysregulation of the BBB can have negative consequences for the CNS. Disease states involving chronic inflammation or pathogenic mechanisms which interfere with the function or structure of cells, or their components involved in BBB integrity, can have dire effects. Other than maintaining a healthy CNS, the BBB has been an important structure for pharmacologists to study, as it can assist or interfere with drug delivery and therefore treatment. Given this knowledge, it is important to study the BBB under pathologic conditions such as headache to better understand how the disease can affect both CNS health and the efficacy of drug treatment.

1.6.1 Impact of Migraine with Aura on the Blood Brain Barrier

The CNS is both the most critical and sensitive system in the body; for proper neuronal function the extracellular environment needs to be highly regulated. This system becomes threaten when a CSD event occurs due to the large change to the microenvironment of the brain, **figure 4** portrays how a CSD may affect the NVU [9]. The BBB although tightly regulated and maintained can also become sensitive to changes during a CSD. As mentioned earlier, a CSD can bring about ionic, metabolic, and structural changes that can disrupt the BBB and lead to damaging consequences for the CNS. A clinical study observed that patients with both migraine with and without aura had elevated matrix metalloprotease-9 (MMP-9) levels during days 1-6 of their migraine attack regardless of pain [60]. Elevated MMP-9 levels have been correlated with increased BBB permeability [119, 120]. This suggested there could be long term changes to the BBB for patients who experience regular recurring migraine attacks. Preclinical research has shown CSD caused by 0.5 μ injections of 1 M KCl injections into the V1M region of the cortex can lead to increased BBB permeability specifically in the cortex using ¹⁴C-sucrose [7]. This

Study suggests there could be a disruption of TJ proteins since sucrose does not have a transporter in the brain. This same study demonstrates increased sumatriptan transport into the brainstem but not the cortex [7]. This could indicate a change in transporter tone which would increase facilitation of the drug into the CNS post CSD, but further investigation is required at this time. Overall, further research of the BBB during and after a CSD event would be beneficial for treatment of the disease. Understanding the acute and long-term changes on the BBB due to migraine could also help us better understand the progression from episodic to chronic migraine.

Figure 4

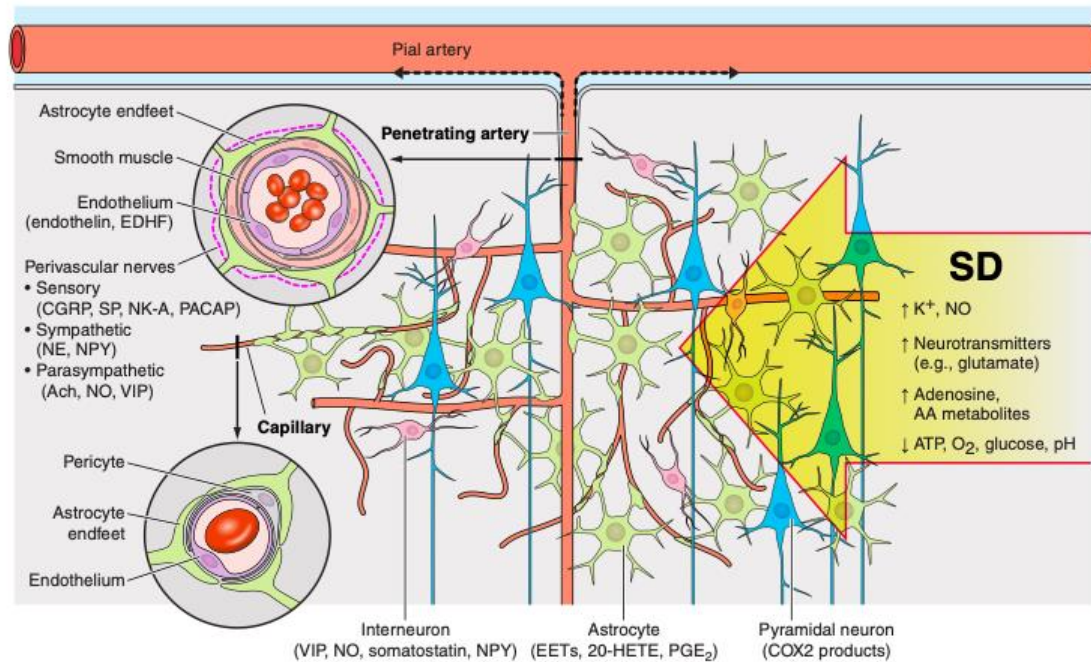


Figure 4. Propagation of SD across the dense cerebral vascular network and the neurovascular unit. SD invading the tissue profoundly impacts all cells and constituents of the cerebrovascular unit. The intense depolarization causes massive extracellular ionic, neurotransmitter, and metabolic changes. The cerebrovascular response is the result of numerous complex processes and interactions within the unit, mediated by key cell types and molecular signals, some of which are listed.

1.7 Heat Shock Protein 90 and its Role in Pain

Heat shock protein 90 (HSP90) is a central regulator of protein homeostasis under physiological and pathogenic conditions. This molecular chaperone facilitates maturation of its substrates, and plays a part in proper protein folding and trafficking [121]. Its substrates or client proteins include kinases, transcription factors, steroid hormone receptors, and E3 ubiquitin ligases [121]. HSP90 is ubiquitously expressed throughout the body comprising 2-3% of the total protein content of the cell under physiological conditions [122]. There are also four isoforms present in different compartments of the cell [122]. The chaperone is a homodimer which will bind with substrates based on a conformational change which is dependent upon ATP hydrolysis [121]. Recently HSP90 has been studied in the context of pain, specifically with opioid signaling [122, 123]. It has also been studied in the context of different disease states such as Alzheimer's, cancer, and rheumatoid arthritis. To date, there has been extensive research into HSP90 in the field of cancer since it is upregulated and can lead to increased cancer cell proliferation leading to higher chance of metastasis [122]. Currently there are several generations of HSP90 inhibitors which have undergone clinical trials, and these compounds can be repurposed for use in other clinical uses [122]. This protein is of particular interest because it can regulate hundreds of receptor systems as well as downstream signaling effectors. This could be critical in disease states which have activity across multiple physiological systems such as migraine, stroke, and traumatic brain injury.

Research has shown that HSP90 could be manipulated pharmacologically to possibly yield a therapeutic outcome in the context of pain. HSP90 inhibitors have shown to reduce Toll-Like Receptor 4 (TLR4) activity, mitigating hyperalgesia and allodynia associated with TLR4 pro-inflammatory signaling [122]. Inhibition of HSP90 in animal models of arthritis have shown to be effective at reducing inflammation and allodynia [124]. Groups using KU-32, a C-terminal

HSP90 inhibitor, noted similar amelioration of allodynia and hyperalgesia in neuropathic models of pain, but not through anti-inflammatory mechanisms [122]. KU-32 showed to be broadly neuroprotective, improving mitochondrial energetics, blocking apoptosis, and preserving neurons in neuropathic pain models [123]. Moreover, a study showed HSP90 inhibition in the spinal cord enhanced opioid antinociception in paw incision, chemotherapy therapy induced neuropathic pain, and tail flick response [123]. The group found that HSP90 inhibition in the spinal cord enhanced ERK MAPK signaling, which was believed to be responsible for the enhanced antinociception, since utilizing ERK inhibitors reversed the observed enhancement [123]. As previously mentioned, HSP90 is a protein with many functions and its manipulation in a disease state could reveal new therapeutic targets within its signaling network.

1.8 Hypothesis

In these studies, we had 4 major investigative aims. the first being to investigate how blockade of sodium-hydrogen exchanger 1 (NHE1) can affect pain and drug delivery during cortical spreading depression events. In this investigation, we hypothesized that inhibition of NHE1 would improve transport of sumatriptan across the blood-brain barrier. Additionally, we hypothesized that NHE1 inhibition would improve the efficacy of anti-migraine medication sumatriptan in relieving periorbital allodynia in our model of CSD induction with cortical KCl injection.

Our second aim was to determine the role of Oatp1a4 transporter in increasing sumatriptan levels in the brain of female rats post CSD induction. These studies were based on previous research in our group as well as follow up investigation from the first aim as pH can affect Oat1a4p transporter function. For this study, we hypothesized that Oat1a4 was responsible

for increased transport of sumatriptan into the brain in our in vivo model of CSD with cortical KCl injection.

Our third aim was to determine how HSP90 inhibition with 17-AAG would affect both blood-brain barrier integrity and periorbital allodynia in our in vitro and in vivo models of cortical spreading depression. There has been beneficial effect of HSP90 inhibition in neuroinflammatory pathologies and we wanted to investigate how it would affect CSD related pathologies. For this aim, we hypothesized HSP90 inhibition with 17-AAG would improve blood-brain barrier integrity in our models of cortical spreading depression. Additionally, we hypothesized that HSP90 inhibition would ameliorate periorbital allodynia in our in vivo model of CSD induction with cortical KCl injection.

Our fourth aim was to determine the therapeutic efficacy of increasing 2-AG levels to prevent or reverse periorbital allodynia associated with CSD induction in our animal model. We also wanted to determine how 2-AG would affect BBB integrity as previous data has shown deficiency in the brain can cause headache pain associated with CSD. We hypothesized that inhibition of ABHD6 to increase endogenous 2-AG levels would prevent and reverse periorbital allodynia post CSD induction. In addition, we hypothesize that reduced 2-AG levels would compromise blood-brain barrier integrity.

**CHAPTER 2: CSD EVENTS INDUCED BY
CORTICAL INJECTION ALTERS TRANSPORTER
FUNCTION IN THE BBB ALLOWING FOR
INCREASED SUMATRIPTAN TRANSPORT AND
INCREASED EFFICACY IN TREATING PAIN
ASSOCIATED WITH AURA**

2.1 NHE1 Expression is Critical for Sumatriptan Blood to Brain Uptake Increasing Sumatriptan Efficacy in Rats Subjected to Cortical Spreading Depression

2.1.1 Introduction:

Fluctuations in pH are linked to paracellular leaks and changes in transporter expression of the BEB in vitro, this could translate to influence of pharmacokinetics of drugs in the body. A primary gene family maintaining intracellular pH (pHi) is SLC9, the sodium-hydrogen exchange (NHE) antiporters. Three members of SLC9/NHE family, specifically the NHE1, NHE3, and NHE5, encoded by SLC9A1, SLC9A3, and SLC9A5 genes, mediate electroneutral exchange of one Na⁺ for one H⁺ across plasma membranes to regulate internal cellular pH (pHi)[125]. NHE1 plays a crucial role in the regulation of intracellular pH in neurons and endothelial cells in the brain [126-128]. Previous research has shown that pharmacological inhibition of NHE1 protein with its inhibitors has neuroprotective effects in experimental stroke models and prevents BBB damage [129-132]. Changes in NHE1 expression and function after CSD induction had not yet been studied. It is known that the pH is a regulator of BBB integrity [133-136] and transport of xenobiotics across the BBB[137, 138]. There is evidence which suggests CSD induces regional changes in pH [35]. The direct connection between pH change induced by a CSD event affects drug uptake and efficacy has not been observed. The goals of the studies herein focus on NHE1 as one of the main regulators of pH and how it is implicated in cortical KCl-induced changes which could alter drug efficacy resulting from pH dysfunction and regulation of sumatriptan blood to brain uptake. Results indicate sumatriptan uptake in vitro and analgesic effects in vivo were enhanced when NHE1 function was impaired. This data indicates a vital role that NHE1 expression and function plays at the BBB and highlights that comprise of NHE1 may affect pharmacokinetics of therapeutics for treatment of migraine with aura.

Disruption of blood-brain barrier integrity and dramatic failure of brain ion homeostasis including fluctuations of pH occurs during cortical spreading depression (CSD) events associated with several neurological disorders, including migraine with aura, traumatic brain injury and stroke. NHE1 is the primary regulator of pH in the central nervous system. The goal of this study was to investigate the role of sodium-hydrogen exchanger type 1 (NHE1) in blood brain barrier (BBB) and how it affects transport of sumatriptan during CSD events. Using immortalized cell lines and pharmacologic inhibition, we showed loss of functional NHE1 in endothelial cells facilitated uptake of the anti-migraine therapeutic, sumatriptan. In female rats, cortical KCl but not aCSF selectively reduced total expression of NHE1 in cortex and PAG but increased expression in trigeminal ganglia; no changes were seen in trigeminal nucleus caudalis. In vitro and ex vivo observations suggest there may be significance in vivo to increase brain sumatriptan levels and drug efficacy against headache associated allodynia. Pharmacological inhibition of NHE1 prior to cortical injections of KCl enhanced the efficacy of sumatriptan at early time-points but induced facial sensitivity alone. The results suggest that dysregulation of NHE1 contributes to drug penetrance, and the behavioral sensitivity to the antimigraine agent, sumatriptan.

2.1.2 Methods and Materials

Drugs and reagents

Ketamine/xylazine was purchased from Sigma-Aldrich (St. Louis, MO) and isoflurane from VetOne (IL, USA). Zoniporide (SML0076) was purchased from Sigma-Aldrich (St. Louis, MO), dissolved in water at 1 mM concentration for *in vitro* experiments, which was further diluted in the appropriate media. The final concentration of zoniporide was 10 nM. Sumatriptan succinate (S1198) was purchased from Sigma-Aldrich (St. Louis, MO). For *in vivo* experiments,

saline was used as a diluent for zonisamide and sumatriptan with an injection volume of 1 mL/kg. All other chemicals, unless noted were purchased from Sigma-Aldrich (St. Louis, MO).

Animals

Female Sprague Dawley rats (200–250 g), purchased from Envigo (Indianapolis, IN), were housed in a climate-controlled room on a regular 12 h light/dark cycle with lights on at 7:00 am with food and water available *ad libitum*. Animals were initially housed 3 per cage but were individually housed after dural cannulation. All procedures were performed during the 12-hour light cycle according to the policies/recommendations of the International Association for the Study of Pain and the NIH guidelines for laboratory animals, and with IACUC approval from the University of Arizona.

Dural cannulation

Dural cannulation was performed as previously described [7, 139]. Briefly, anesthesia was induced with intraperitoneal 80:10 mg/kg ketamine:xylazine or 45:5:2 mg/kg cocktail of ketamine:xylazine:acepromazine. Rats were placed in a stereotaxic frame (Stoelting Co.), and a 1.5- to 2-cm incision was made to expose the skull. A 0.66- to 1-mm hole (Pinprick/KCl: -6.5 mm A/P, -3 mm M/L from bregma) was made with a hand drill (DH-0 Pin Vise; Plastics One) to carefully expose, but not damage, the dura. A guide cannula (D/V: -0.5 mm from top of skull, 22 GA; Plastics One, C313G) was inserted into the hole and sealed into place with glue. Two additional 1 mm holes were made rostral to the cannula to receive stainless-steel screws (Small Parts, MPX-080-3F-1M), and dental acrylic was used to fix the cannula to the screws. A dummy cannula (Plastics One, C313DC) was inserted to ensure patency of the guide cannula. Rats were housed individually and allowed 6–8 d to recover. Cannula placement and dural integrity at screw placement was confirmed postmortem.

Cortical injections, treatment with zoniporide and sumatriptan

Cortical injections were performed using a Hamilton injector (30 GA, #80308 701 SN, Hamilton Company) customized to project 1.0 mm into and beyond the dura into the occipital cortex. The injector was inserted through the guide cannula to deliver a focal injection of 0.5 μ l of 1 M KCl (~60mM final concentration at site) or artificial CSF (aCSF: 145 mM NaCl, 2.7 mM KCl, 1 mM MgCl₂, 1.2 mM CaCl₂, and 2 mM Na₂HPO₄, pH 7.4), and the solution was passed through a 0.2- μ m syringe filter before injection. A second set of animals received dural application of aCSF or KCL (5 μ L) rather than a cortical injection. Zoniporide was dissolved in saline (1 mL/kg) and injected intraperitoneally at 1 mg/kg or 5mg/kg doses, 10 min before cortical KCl injection. Sumatriptan succinate (0.6 mg/kg, dissolved in saline) was dosed subcutaneously 30 min post-cortical KCl administration. Dural injections of saline or lidocaine (2%) were performed using a customized injector which was flush with the end of the dural guide cannula at a volume of 5 μ L.

Periorbital mechanical allodynia

Periorbital allodynia was evaluated before and at 30, 60, 90, 120, and 180 minutes after cortical injection of KCl or aCSF by an observer blinded to drug and cortical conditions. Rats were grouped based on their postsurgical baseline to ensure equivalent pre-injection thresholds (6-8g). Any rats exhibiting excessive postsurgical, but pre-pharmacological manipulation allodynia, (threshold <6 g) were removed from the study. Rats were acclimated to testing box 1 hour prior to evaluation of periorbital mechanical allodynia with von Frey filaments as previously described [140, 141]. Behavioral responses were determined by applying calibrated von Frey filaments perpendicularly to the midline of the forehead at the level of the eyes with enough force to cause the filament to slightly bend while held for 5 seconds. A response was

indicated by a sharp withdrawal of the head, vocalization, or severe batting at the filament with attempts to eat it.

Tissue collection for Western immunoblotting

Rats were anesthetized with ketamine/xylazine mix as above, then transcardially perfused with ice cold 0.1 M phosphate buffer at rates to not burst microvasculature (i.e., 3.1 mL/min). After decapitation, tissue samples, cortex (Ct), trigeminal ganglia (TG), trigeminal nucleus caudalis (Vc) and periaqueductal grey (PAG) were harvested, flash frozen in liquid nitrogen and stored at -80°C until preparation. On the day of preparation, samples were placed in ice-cold lysis buffer (20 mM Tris-HCl, 50 mM NaCl, 2 mM MgCl₂·6H₂O, 1% v/v NP40, 0.5% v/v sodium deoxycholate, 0.1% v/v SDS; pH 7.4) supplemented with protease and phosphatase inhibitor cocktail (BiMake, B14002, and B15002). All subsequent steps were performed on ice or at 4°C. The samples were sonicated, then centrifuged at 15,000xg for 10 minutes. The supernatant was collected from the samples and BCA Assay was performed to determine the protein content (Pierce™ BCA Protein Assay Kit, Thermo Scientific, 23223).

Western immunoblotting

Total protein (10 µg) from the tissue supernatant was loaded on TGX precast gels (10% Criterion™, BioRad) and then transferred to nitrocellulose membranes (Amersham™ Protran™, GE Healthcare). After transfer, the membranes were blocked at room temperature for 1 h in blocking buffer (5% BSA in Tris-buffered saline with Tween 20 (TBST)). The following primary antibodies were diluted in blocking buffer: NHE1 (Abcam, ab67313, 1:500), and α-tubulin (Cell Signaling, 3873S, 1:20,000). The membranes were incubated in the diluted primary antibodies overnight at 4°C. The blots were then washed three times in TBST, incubated with secondary antibodies: GaM680 (LiCor, 926–68020), and GaR800 (LiCor, 926–32211) in 5%

milk in TBST for 1 h of rocking at room temperature, washed again, and imaged with a LiCor Odyssey infrared imaging system (LiCor, Lincoln, NE). Un-Scan-It gel version 6.1 scanning software (Silk Scientific Inc.) was used for quantification. To visualize multiple bands on the same blot, blots were stripped with One Minute® Plus Western Blot Stripping Buffer (GM Biosciences, GM6510). Protein expressions were corrected for the expression of the loading control (e.g. α -tubulin).

Culture and treatment of immortalized cell lines

bEnd.3 (CRL-2299, ATCC) cells were cultured in DMEM (Gibco, 11995–065), supplemented with 2 mM L-glutamine (ThermoScientific, 25030081), 10% fetal bovine serum (Gibco, 10082139), and penicillin (100 UI/mL)-streptomycin (100 μ g/mL) (Invitrogen, 15140122). 24 hours before KCl pulse, the media of bEnd.3 cells were changed to astrocyte-conditioned media harvested from confluent C8-D1A flasks. C8-D1A (CRL-2541, ATCC) and C8-B4 (CRL-2540, ATCC) cells were maintained in DMEM (Gibco, 11995–065), supplemented with 10% fetal bovine serum (Gibco, 10082139), and penicillin (100 UI/mL)-streptomycin (100 μ g/mL) (Invitrogen, 15140122). All cell lines were cultivated at 37°C in a humidified 5% CO₂/95% air atmosphere. All cell lines were treated with 60 mM KCl for 5 minutes, which is a typical condition to evoke potassium-triggered spreading depolarization in live brain slices [142]. Samples for subsequent analysis (subcellular fractionation, whole cell lysate, and immunocytochemistry) were harvested at 5 and 30 minutes after KCl pulse or aCSF application.

Isolation of cortical microvessels

Rat cortical microvessels were isolated as previously described [143, 144]. Briefly, rats were anesthetized with intraperitoneal injection of 80:10 mg/kg ketamine:xylazine, decapitated and the brains placed in ice-cold buffer A (136.9 mM NaCl; 2.7 mM KCl; 1 mM CaCl₂; 1.5 mM

KH₂PO₄, 8.1 mM Na₂HPO₄; 0.5 mM MgCl₂; 5 mM glucose; 1 mM sodium pyruvate, pH7.4) supplemented with Roche EDTA-free Complete Protease Inhibitor cocktail, Sigma protease inhibitor cocktail and 2 mM phenylmethylsulfonyl fluoride. All subsequent steps were performed on ice or at 4°C. After removal of the choroid plexis and meninges, three rat brains were pooled and homogenized in 20 ml of buffer A using a Potter-Elvehjem homogenizer with 20 strokes at moderate speed followed by 8 strokes in a glass Dounce homogenizer by hand. Homogenate was mixed with 30% Ficoll in buffer A and centrifuged for 20 min at 5800 × g in a Sorvall SS-34 rotor. The pellet was resuspended in 10 ml buffer A supplemented with 1% BSA using 2 strokes with the Potter-Elvehjem homogenizer. The suspension was then filtered through a 300 µm mesh filter and microvessels collected on a 40 µm mesh filter. Microvessels retained on the 40 µm mesh filter were resuspended in buffer A with 1% BSA and pelleted by centrifugation (10 min at 1500 × g). The pellet was washed twice in buffer B (20 mM Tris-HCl; 250 mM sucrose; 1 mM CaCl₂; 1 mM MgCl₂, pH 7.8) supplemented with Roche EDTA-free Complete Protease Inhibitor cocktail, Sigma protease inhibitor cocktail and 2 mM phenylmethylsulfonyl fluoride, and collected by centrifugation for 10 min at 2170 × g. The microvessel pellet was stored at -80°C until further use.

***In vitro* uptake experiments**

Functional implications of monolayer integrity or lack thereof were assessed *in vitro* as luminal to abluminal transport/uptake of select compounds. bEnd.3 cells were seeded at a density of 6.0×10^4 cells/cm² on the luminal side of collagen-coated filter membranes (0.4 µm pore polyester membrane) of 24-well tissue culture inserts (Costar, 3470). The tissue culture inserts were incubated at 37°C (5% CO₂) for 4–5 days. One day before experiment, astrocyte (C8-D1A cells)-conditioned media was added to the abluminal side of the inserts and incubated overnight

in the humidified incubator at 37°C (5% CO₂). On the day of experiment, zonisamide (10 nM) was added to the luminal side of inserts 30 min before KCl pulse. ¹⁴C-sucrose (PerkinElmer, NEC100XOO1MC) was applied to the luminal side to monitor the paracellular uptake. In a separate set of experiments, ³H-sumatriptan (American RadioLabeled Chemicals, ART1619) was used to determine *in vitro* uptake of a clinically relevant compound. Both radiolabeled compounds were added to luminal side at 0.25 µCi/ml concentration. The radioactivity of samples from the abluminal side was measured for disintegrations per minute (dpm; 1450 LSC and Luminescence Counter; PerkinElmer) at 5 and 30 minutes after aCSF or KCl-pulse (60 mM, 5 min) (aCSF or KCl was added to the abluminal side when radioligands were applied). For each individual experiment, 3–4 inserts/group with cells and three inserts without cells were assayed. The radioactivity in the inserts without cells at both time-points were two-three times higher compared to the inserts with cells, indicating the existence of barrier. All experiments were carried out in triplicate, using 3–4 trans-well inserts/group.

Data analysis and statistics

GraphPad Prism 7.0 software (GraphPad Software) was used for statistical analysis. Unless otherwise stated, the data were expressed as mean ± SEM. Periorbital allodynia measurements were assessed using a repeated measure two-way ANOVA to analyze differences between treatment groups over time with either a Bonferroni or Tukey test applied *post hoc*. Molecular studies were compared by unpaired t-test or one-way ANOVA, as indicated. Differences were considered significant if $p \leq 0.05$ to give 80% power to detect at 20% difference and prevent a type II error (GPower3.1).

2.1.3 Results

2.1.3.1 Loss of functional NHE1 activity facilitates sumatriptan uptake in vitro

In this experiment, we wanted to examine the role of NHE1 on the abluminal uptake of the popular antimigraine agent sumatriptan, ³H-sumatriptan was used in order to track transport across the blood endothelial barrier (BEB). The transport of ³H-sumatriptan across the bEnd.3 mouse cell monolayer was significantly increased during the KCl pulse (**Figure 5A**; aCSF: 115.3±7.2% of vehicle-treated vs. KCl: 142.2±6.2% of vehicle-treated, $p = 0.01$, one-way ANOVA, Tukey post-test, $n = 18/\text{group}$, $F(4,76) = 26.98$). No significant differences were observed 6–30 min post aCSF or KCl however (Fig 9B; aCSF: 96.4±4.1% of vehicle-treated vs. KCl: 96.0±3.9% of vehicle-treated, $p > 0.99$, one-way ANOVA with Tukey post-test, $n = 11-13/\text{group}$). Unexpectedly, inhibition of NHE1 with zoniporide significantly enhanced the abluminal uptake of ³H-sumatriptan during KCl-pulse (**Figure 5A**; KCl: 142.2±6.2% of vehicle-treated vs. KCl+zoniporide: 186.4±6.3% of vehicle-treated, $p < 0.0001$, one-way ANOVA with Tukey post-test, $n = 13/\text{group}$, $F(4,76) = 26.98$). These results suggest that manipulation of pH via NHE1 may be a strategy to selectively enhance blood to CNS uptake of sumatriptan to increase therapeutic efficacy.

Figure 5

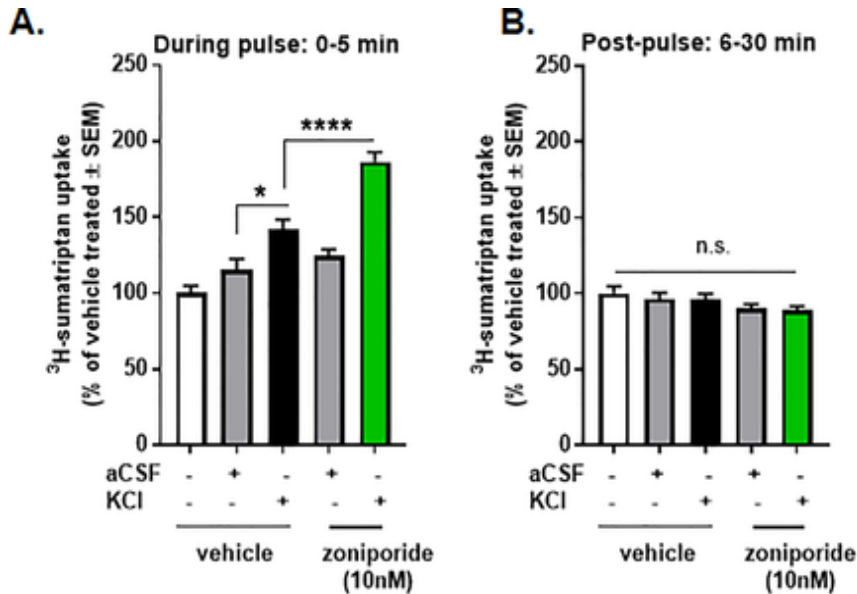


Figure 5. NHE1 inhibition enhanced KCl induced transport of sumatriptan *in vitro*. (A) ^3H -sumatriptan uptake during a 5 min KCl or aCSF pulse with or without pretreatment of zoniporide (10nM). All data represent % of vehicle treated \pm SEM (n = 13–18). (B) ^3H -sumatriptan uptake post-pulse with or without pretreatment of zoniporide. All data represent % of vehicle treated \pm SEM (n = 11–13). All data represent % of wild-type naïve \pm SEM (n = 9–13). * p<0.05, ** p<0.01, **** p<0.0001 as assessed by one-way ANOVA. n.s. = non-significant. (Liktor-Busa et al., Functional NHE1 expression is critical to blood brain barrier integrity and sumatriptan blood to brain uptake; 2020)

2.1.3.2 NHE1 inhibition with zoniporide causes periorbital allodynia but enhances sumatriptan efficacy after cortical injection of KCl in vivo

To examine the effects of NHE1 inhibition in our model of allodynia associated CSD rats were treated with zoniporide (1 mg/kg, IP) at 10 min before cortical KCl or aCSF injection (**Figure 6A**). Pretreatment with zoniporide did not alter the facial allodynia induced by KCl (**figure 6 B and C**) (AUC- KCl: 11.96 ± 2.02 vs. KCl+zoniporide: 13.6 ± 3.13 , $p = 0.97$, one-way ANOVA with Tukey post-test, $n = 5-6/\text{group}$, $F(3,20) = 7.033$). However, systemic administration of zoniporide to aCSF control rats induced facial sensitivity statistically indistinguishable from cortical KCl (AUC- KCl: 11.96 ± 2.02 vs. aCSF+zoniporide: 13.51 ± 2.04 , $p = 0.98$, one-way ANOVA with Tukey post-test, $n = 5-6/\text{group}$, $F(3,20) = 7.33$) (**figure 6 B and C**). These results show systemic NHE1 inhibition in absence of injury may induce periorbital allodynia in female rats.

To test whether pH manipulation via NHE1 inhibition is a useful strategy to enhance antiallodynic efficacy of sumatriptan following cortical KCl injections as suggested by the in vitro results, rats were treated with specific NHE1 inhibitor zoniporide (5mg/kg IP,) or saline (1mL/kg, IP) 10 min before the cortical KCl injection (0.5 μ L, 1M, $t = -30$ min). After induction of periorbital allodynia, sumatriptan (0.6mg/kg, SC, $t = 0$ min) was administered (**Figure 7A**). Zoniporide pretreatment significantly enhanced sumatriptan reversal of cortical KCl induced periorbital allodynia 30 min after sumatriptan administration as compared to post-baseline (zoniporide + KCl + sumatriptan pBL vs. 30 min, $p = 0.03$, two-way ANOVA with Tukey's post-test, $n = 5-10/\text{group}$, $F(6,78) = 6.536$) and saline pretreatment (zoniporide + KCl + sumatriptan 30 min vs. saline + KC l+ sumatriptan 30 min, $p = 0.03$, two-way ANOVA with Bonferroni's post-test, $n = 5-10/\text{group}$, $F(6,78) = 6.536$) (**Figure 7B**).

Figure 6

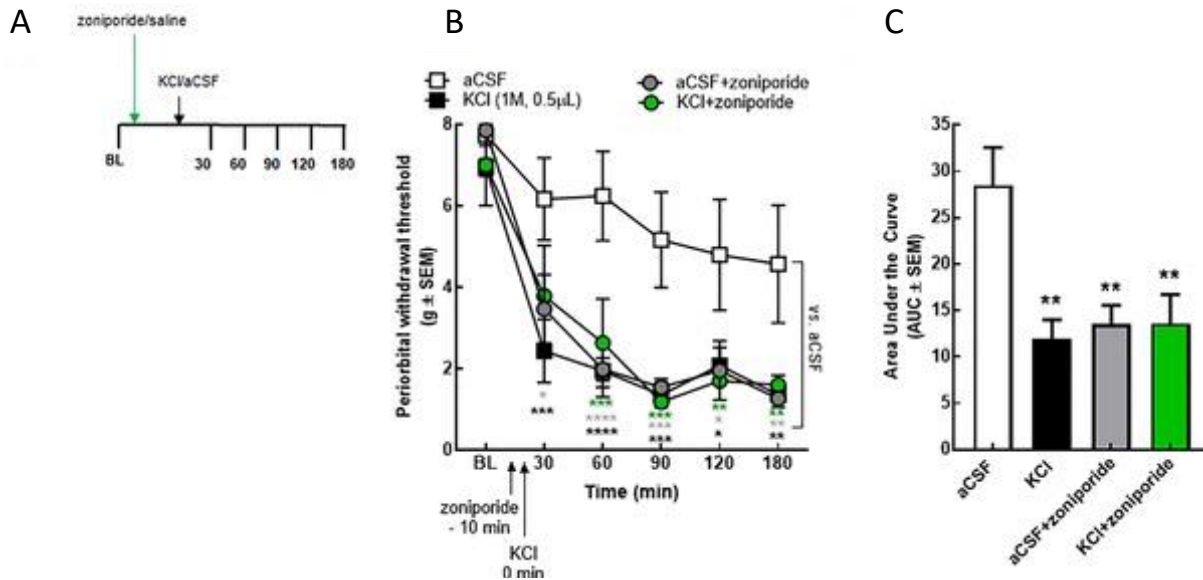


Figure 6. Systemic inhibition of NHE1 by zoniporide induced periorbital allodynia alone

(A) Timeline of the zoniporide-KCl/aCSF combination treatments. **(B)** Periorbital withdrawal threshold determined by von Frey test in rats injected with cortical KCl (0.5 µL, 1M) or aCSF (0.5 µL) with zoniporide (1 mg/kg, IP) or saline (1mL/kg, IP). Values are the mean ± SEM (n = 5–6). * p<0.05, ** p<0.01, *** p<0.001, and **** p<0.0001 compared to aCSF-treated as assessed by two-way ANOVA. **(C)** The area under the curve for the animals treated with aCSF/KCl ± zoniporide. Values are the mean ± SEM (n = 5–6). ** denotes significantly different (p<0.01) compared to aCSF-treated as assessed by one-way ANOVA [145]. (Liktor-Busa et al., Functional NHE1 expression is critical to blood brain barrier integrity and sumatriptan blood to brain uptake; 2020)

Figure 7

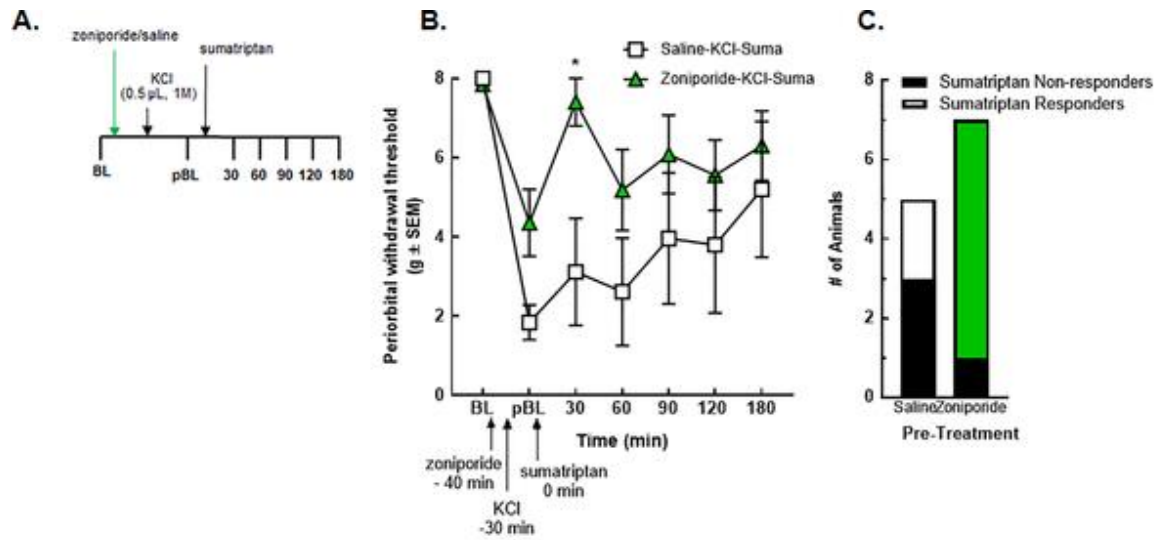


Figure 7. Systemic inhibition of NHE1 by zoniporide influenced the overall efficacy of sumatriptan. (A) Timeline of the zoniporide-sumatriptan combination treatments. (B) Periorbital withdrawal threshold determined by von Frey test in rats treated with zoniporide (5 mg/kg, IP) or saline (1mL/kg, IP) in combination with sumatriptan (0.6 mg/kg, SC) and cortical KCl injection (0.5 μ L, 1M). Values are the mean \pm SEM (n = 5–10). * denotes significantly different ($p < 0.05$) compared to post-baseline or saline-treated as assessed by two-way ANOVA. (C) Number of the sumatriptan responder and non-responder animals. Values are the mean \pm SEM (n = 5–6). * $p < 0.05$, ** $p < 0.01$, *** $p < 0.001$, and **** $p < 0.0001$ compared to aCSF-treated as assessed by two-way ANOVA. (Liktor-Busa et al., Functional NHE1 expression is critical to blood brain barrier integrity and sumatriptan blood to brain uptake; 2020).

2.1.3.3 Total expression of NHE1 was decreased in cortex and PAG samples at 90 min after dural manipulation.

The results of NHE1 inhibition alone increasing facial sensitivity as well as the previous recording of pH changes during cortical spreading depression [52, 53, 146, 147], we wanted to assess if NHE1 detection was reduced following cortical injection of KCl. The total amount of NHE1 protein detection in areas directly (i.e. occipital cortex) and indirectly (i.e. periaqueductal grey, PAG) affected by CSD [142, 148].

In cortex samples, WB detection of total NHE1 was significantly decreased at 90 min after post KCl injection (**Figure 8A**; naïve: 101.1 ± 4.5 , aCSF: 111.1 ± 11.7 , KCl: 83.2 ± 1.8 ; $n = 3$, loaded in duplicate, aCSF vs. KCl, $p = 0.04$, one-way ANOVA with Tukey post-test, $F(2,8) = 2.800$). Reduced detection of NHE1 was also observed in the PAG samples at the same time-point (**Figure 8B**; naïve: 100.0 ± 10.9 , aCSF: 85.6 ± 7.9 , KCl: 47.3 ± 6.1 ; $n = 3$, loaded in duplicate, aCSF vs. KCl, $p = 0.016$, one-way ANOVA with Tukey post-test, $F(2,15) = 10.14$). This data indicates the expression of NHE1 could be impaired in regions engaged by CSD events.

Figure 8

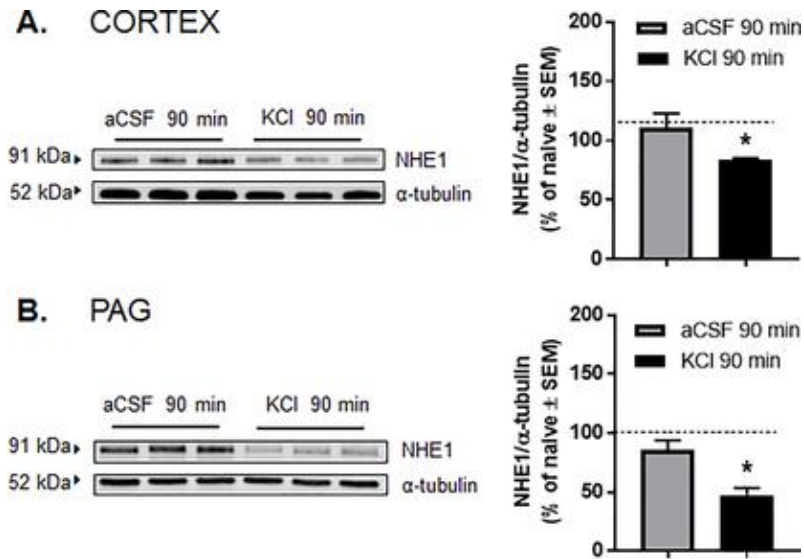


Figure 8. Total expression of NHE1 was decreased in cortex and PAG samples at 90 min after dural manipulation. (A and B) Representative immunoblots indicating NHE1 and α -tubulin as a loading control in pain nuclei engaged in spreading depression, namely cortex (A), PAG (B) Samples were harvested 90 min after cortical aCSF or KCl injections. All data represent the % of naïve relative expression \pm SEM (n = 3, loaded in duplicate). The dashed line indicates the relative expression of NHE1 in naïve samples. No significant differences were observed between naïve and aCSF-treated samples. * Denotes significantly different (p<0.05), as assessed by one-way ANOVA. (Liktor-Busa et al., Functional NHE1 expression is critical to blood brain barrier integrity and sumatriptan blood to brain uptake; 2020)

2.1.4 Conclusion

There is research showing changes in pH can influence vascular tone and angiogenesis (i.e., intracellular acidosis is associated with vasodilation) [149]. Several experimental papers provided evidence for a vascular-neuronal cross talk, a bi-directional communication between endothelium and neurons. Mason and Russo, in their review article suggest a new theory of vascular activation of nervous system underlying migraine pathophysiology as well [150]. The role of NHE1 in the development of various diseases in the brain [151], such as cerebral ischemia-induced neuronal injury has been defined, the work in our lab has demonstrated for the first time that NHE1 can modulate pain processing underlying headache associated facial allodynia in rats, with a special emphasis of drug delivery across the BBB which may contribute to increased efficacy as of a migraine therapeutic. The protective role of NHE1 suggest that normalization of pH homeostasis by targeting NHE1 function or surface expression could be a unique therapeutic approach to enhance efficacy of existing therapeutics for migraine.

2.2 Sumatriptan Blood to Brain Uptake post KCl Insult is Mediated by OATP In Vitro, but not In Vivo

2.2.1 Introduction

CSD is not only associated with migraine with aura but also with other neurologic pathologies. Although the role of CSD in these pathologies is not well understood it may affect pharmacodynamics and pharmacokinetics of drugs used for these diseases. The efficacy of treatment for these neurological diseases also relies on therapeutics reaching the CNS. Similarly, it may be vital for migraine therapeutics as well. As such it is imperative to understand how CSD events alter drug uptake to effectively treat patients. CSD event could impair the protective function of the blood brain barrier (BBB) as well as change its physiologic regulating properties. Mechanistically, CSD events are driven by increases in extracellular potassium [152] leading to breakdown of the ionic gradients that activate neuronal, glial, and vascular endothelial cells to change cerebral blood flow leading to dysregulation of the NVU and neurovascular coupling [153]. Whether CSD events impact solute carrier (SLC) transporter functional expression and drug transport is not known.

The organic anion transporting polypeptides (OATPs), transporters of the SLC superfamily, are localized on endothelial and epithelial cells throughout the body and are involved in the uptake of xenobiotics [154]. Human OATP1A2 has a dense population in the brain and is believed to be involved in drug uptake from the blood to the brain [154]. Oatp1a4, the rodent ortholog of human OATP1A2, is located on the luminal and abluminal side of the blood brain barrier [154]. OATP1A2 activity is potentially increased during pathological states based on studies done in preclinical models. For example, during inflammation or hypoxia/reoxygenation, Oatp1a4 functional expression levels are reportedly increased possibly allowing for increased activity of the transporter [155, 156]. Although expression of Oatp1a4 is

higher than its human counterpart in general this evidence suggests that the pathological regulation of Oatp1a4 may be involved in enhancing blood-to-brain uptake of Oatp1a4 substrates and may be clinically relevant in humans.

OATPs have a broad range of chemical substrates such as statins and neuro-steroids [154]. In humans, the anti-migraine medication sumatriptan is thought to be transported into the brain via OATP1A2 [157]. Under normal physiological conditions CNS uptake of sumatriptan is believed to be limited as a knock-in OATP1A2 mouse model showed no change in sumatriptan uptake[158]. However, following CSD induction by cortical KCl injection, sumatriptan levels were increased in the brainstem of rats, which suggested the involvement of a transporter mediated processes [7]. Whether the CSD pathology impacts the blood to brain ratio of the prototypical triptan drug remains relatively unknown at this point.

Optimal therapeutic treatment relies on effective drug uptake across the BBB, a comprehensive understanding of how CSD impacts active transport at the BBB has implications for drug delivery. In this study, we investigated how high abluminal potassium levels in vitro and potassium chloride (KCl)-induced CSD events impact in vivo impact Oatp1a4 functional expression as well as the blood-to-brain uptake of sumatriptan, a prototypical migraine treatment.

2.2.2 Methods and Materials

Drugs and reagents

All drugs and reagents were obtained from Sigma-Aldrich (St. Louis, MO) unless otherwise specified. Oatp1a4 was quantified using SLCO1A2 Antibody-middle region Aviva Systems Biology (ARP43899_P050, San Diego, CA).

Animals

Female Sprague Dawley rats were obtained from Envigo (Indianapolis, IN) at 200-250g and housed in a climate-controlled facility with a 12-hour light and dark cycle and *ad libitum* food and water. The dural cannulation was performed during the day using the International Association for the Study of Pain and NHI policies, and the rats were housed individually after the surgery.

Culture and treatment of immortalized cell lines

bEnd.3 cells (CRL-2299, ATCC) were cultured in DMEM (Gibco, 11995-065), supplemented with 2mM L-glutamine (ThermoScientific, 25030081), penicillin (100UI/ml)-streptomycin (100µg/ml) (Invitrogen, 15140122), and 10% fetal bovine serum (Gibco, 10082139). The media of bEnd.3 cells was changed to astrocyte-conditioned media (ACM), collected from confluent flasks of C8-D1A cells, 24hr before treatment. Dulbecco's Modified Eagle Medium (DMEM, Gibco, 11995-065), penicillin (100UI/ml)-streptomycin (100µg/ml) (Invitrogen, 15140122), and 10% fetal bovine serum (Gibco, 10082139) were used to grow the C8-D1A (CRL-2541, ATCC) cells. All cells were grown in 5% CO₂/95% air at 37°C. The bEnd.3 cells were treated with either 3mM (physiological level), 60mM (CSD level) [142], or 90mM (highest possible physiological level) KCl in astrocyte conditioned media (ACM), artificial cerebrospinal fluid (aCSF) in ACM, or just ACM. The cells received KCl treatment for 5-minutes and were then harvested at either 5-minute or 30-minute timepoints. The samples for

western immunoblotting were centrifuged at 12,000rpm, 4°C for 10-minutes. The supernatant was pipetted into a separate tube and a Bicinchoninic acid (BCA) assay (Pierce™ BCA Protein Assay Kit, Thermo Scientific, 23223) was performed.

Western immunoblotting

Samples were loaded in TGX precast gels (10% Criterion™, BioRad) to have a total protein content of 10µg of protein in each well. The transfer was performed on a nitrocellulose membrane (Amersham™ Protran™, GE Healthcare). Blocking of the membrane was done with 5% Bovine Serum Albumin (BSA) in Tris-buffered saline with Tween 20 (TBST) for 1hr at room temperature. Primary antibody was prepared in blocking buffer with a 1:500 dilution for the Oatp1a4 antibody (ARP43899_P050I, Aviva Systems Biology, San Diego, CA) and 1:20,000 for α -tubulin (3873S, Cell Signaling Technology, Danvers, MA). Membranes were incubated overnight in the primary antibody at 4°C and then three 5-minute TBST washes were performed before incubating in secondary for 1h at room temperature on a rocker. The secondary antibody was made in 5% milk in TBST and the antibodies G α M680 (LiCor, 926-68020) and G α M800 (LiCor, 926-32211) were diluted to 1:10,000. After secondary antibody incubation, three more washes in TBST were performed and then the membranes were developed using a LiCor Odyssey infrared imaging system (LiCor, Lincoln, NE). The scans were analyzed using the Un-Scan-It gel version 6.1 scanning software (Silk Scientific Inc. Orem, UT), after contrast adjustment (Image J) to the whole blot to quantify the pixels of the bands. The Oatp1a4 expression was normalized to α -tubulin expression.

Immunocytochemistry

bEnd.3 cells were grown on collagenated glass coverslips to confluence. bEnd.3 cells were then washed with phosphate buffer saline (PBS) twice before fixing them with 1%

Paraformaldehyde (PFA) for 15-minutes. Next cells were incubated at room temperature in 10% BSA in PBS for one hour. Following three PBS washes, the cells were incubated in primary Oatp1a4 antibody (ARP43899_P0501, Aviva Systems Biology, San Diego, CA) at a 1:100 dilution in blocking buffer, overnight in a 4°C room. After washing with PBS five more times, the cells were incubated in secondary antibody, AlexaFlourTM555 (ThermoScientific, A34055), at a 1:500 dilution in blocking buffer for 1 hour at room temperature. The coverslips were mounted after additional PBS washes using Prolong Gold Antifade with DAPI (ThermoScientific, P36941) mounting media and were then dried and sealed. The images of the slides were captured with an Olympus microscope (BX61) and CoolSNAP HQ. The corrected total cell fluorescence (CTCF) was calculated as the Integrated Density – (Area of selected cell X Mean fluorescence of background readings) for 15 cells/slide, 5 background readings/slide and 3-4 slides per condition from values determined in FIJI (Image J) as described (<https://theolb.readthedocs.io/en/latest/imaging/measuring-cell-fluorescence-using-imagej.html>).

***In vitro* uptake experiments**

bEnd.3 mouse cells (CRL-2299, ATCC) were cultured on collagen coated trans-well inserts (Sigma-Aldrich, CLS3401-48EA) with 150 µl bEnd.3 media for growth facilitation at 37°C incubated for 4 days. The abluminal (deep well) section on the trans-wells were filled with 600 µl ACM at inoculation to create an *in vitro* model of the blood brain barrier. 30-minutes prior to the experiment, the luminal wells were treated with 1µM Estrone-3-sulfate (E3S) or vehicle (saline) and then incubated at 37°C. ACM containing 3mM and 60mM KCl and equivalent volume of aCSF (145 mM NaCl, 2.7 mM KCl, 1 mM MgCl₂, 1.2 mM CaCl₂, and 2 mM Na₂HPO₄, pH 7.4) was prepared for pulsing the bEnd.3 cells on a separate plate in the abluminal section of the wells. 1.5 mM sumatriptan succinate was prepared in DMEM media.

After 30-minutes, E3S containing media was removed and replaced with media containing 1.5 mM sumatriptan succinate. The wells were then added to the aCSF and KCl pulsing plate for 5-minutes. Once the time course was completed, 600 μ l of the collected abluminal media was placed in 2mL vials for read on high performance liquid chromatography (HPLC). Each well received one individual vial for a total of three for triplicate of each condition on a single plate.

Dural cannulation

The dural cannulation protocol used was previously defined [7] Rats were anesthetized by injecting ketamine:xylazine:acepromazine (45:5:2 mg/kg) intraperitoneally, checking for no whisker movement and toe pinch reflex. The rats were prepped by shaving the surgical site on the top of the head, cleaning it with chlorhexidine three times, and giving eye ointment and an injection of saline and gentamicin. A stereotaxic (Stoelting Co.) was used to secure the rats and the skin was cut 1.5-2cm to expose the skull. The skull was cleaned and cauterized until it was dry and visible. The guide cannula (D/V: -0.5mm from top of skull, 22 GA; Plastics One, C313G) was placed so that the pinprick and KCl would be -6.5mm A/P and -3mm M/L from the bregma, using a hand drill (DH-0 Pin Vise; Plastics One) to make a 0.66-1mm deep hole being careful not to puncture the dura. Two stainless-steel screws (Small Parts, MPX-080-3F-1M) were drilled in triangulation with the guide cannula using the same hand drill and at a 1mm depth. Then dental acrylic was used to seal the exposed skull and keep the guide cannula, which was also secured with glue, in place with the screws. The guide cannulas received dummy cannulas (Plastics One, C313DC). Rats were given a week to recover in single housed cages. The cannula's position and dural damage was assessed postmortem; subjects with improper placement, dural damage outside of injection point, or gross abnormalities were excluded from analysis.

Cortical injections and treatment with E3S

E3S was dissolved in saline and administered intraperitoneally (10mg/mL, 1mL/kg) 30-minutes before the cortical KCl injection. A Hamilton injector (30 GA, #80308 701 SN, Hamilton Company) was used to inject 0.5 μ l of aCSF (145mM NaCl, 2.7mM KCl, 1mM MgCl₂, 1.2mM CaCl₂, and 2mM Na₂HPO₄, at a pH of 7.4) or 1M KCl, which provides a final concentration of 60mM at the injection site, into the guide cannula 1.0mm past the dura and into the occipital cortex (V1M region).

***In situ* Brain Perfusion**

In situ perfusion studies were carried out in female Sprague-Dawley rats (200-250 g) as previously described by our group at 30-minutes and 90-minutes post aCSF/KCl injection [156, 159, 160]. Briefly, rats were anesthetized with ketamine/xylazine and heparinized (10,000 U/kg i.p.). Body temperature was maintained at 37°C using a heating pad. The common carotid arteries were cannulated with silicone tubing connected to a perfusion circuit then perfused with an erythrocyte-free modified mammalian Ringer's solution (117 mM NaCl, 4.7 mM KCl, 0.8 mM MgSO₄, 1.2 mM KH₂PO₄, 2.5 mM CaCl₂, 10 mM D-glucose, 3.9% (w/v) dextran (MW. 60,000), and 1.0 g/L bovine serum albumin (type IV), pH 7.4), warmed to 37°C and oxygenated with 95% O₂/5% CO₂. Evan's blue dye (55 mg/L) was added to the perfusate to serve as a visual marker of BBB integrity. Perfusion pressure and flow rate were maintained at 95-105 mmHg and 3.1 mL/minute respectively. Both jugular veins were severed to allow for drainage of the perfusate. Using a slow-drive syringe pump (0.5 mL/minute per hemisphere; Harvard Apparatus, Holliston, MA), ³H-sumatriptan (0.25 μ Ci/ml) was added to the inflowing perfusate. Following a 10-minute perfusion, the rats were decapitated, and the brains was removed. The meninges and choroid plexus were excised, and cerebral hemispheres were sectioned and homogenized. TS2

tissue solubilizer (1 mL) was added to each tissue sample and the samples were allowed to solubilize for 2 days at room temperature. To eliminate chemiluminescence, 100 μ l of 30% glacial acetic acid was added, along with 2 mL Optiphase SuperMix liquid scintillation cocktail (PerkinElmer, Boston, MA). Samples were measured for radioactivity on a model 1450 liquid scintillation counter (PerkinElmer).

Tissue collection

Rats were injected intraperitoneally with ketamine:xylazine (80:10mg/kg) to anesthetize them and then a transcardial perfusion was performed with cold 0.1M phosphate buffer saline at a rate of 3.1ml/minute. The rats were guillotined, the brains carefully extracted, and the V1M portion of the occipital cortex (V1M cortex), trigeminal nucleus caudalis (Vc), and periaqueductal grey (PAG) were collected. The left and right sides of the cortex and Vc were harvested separately. Samples were flash frozen in liquid nitrogen, and then were stored in a -80°C freezer until further processing. The samples were sonicated in cold lysis buffer (20mM Tris-HCl, 50mM NaCl, 2mM MgCl₂x6H₂O, 1% v/v NP40, 0.5% v/v sodium deoxycholate, 0.1% v/v SDS; pH 7.4) with protease and phosphatase inhibitors (BiMake, B14002, and B15002). Samples were kept on ice during the process and centrifuged at 4°C and 15,000xg for 10-minutes. After collection of the supernatant, a BCA assay (PierceTM BCA Protein Assay Kit, Thermo Scientific, 23223) was performed to determine the protein content.

Data Analysis and Statistics

Statistical Power analyses were conducted *a priori* to determine the minimum number of biological replicates required to give 80% power to detect a 20% difference and prevent a type II error using GPower3.1 Statistical analysis was performed with GraphPad Prism 7.0 and 8.3.1. Data are shown as mean \pm SEM. Western blot (WB) and corrected total cell fluorescence

(CTCF) data were assessed using an unpaired T-test. Transport, tissue, and in situ brain perfusion assays were compared by two-way ANOVA with a Tukey post-hoc. Statistical significance was considered when $p \leq 0.05$.

2.2.3 Results

2.2.3.1 Oatp1a4 in bEnd.3 endothelial cells dynamically facilitate sumatriptan uptake during CSD progression in vitro

Human OATP1A2 transport confirmed that bEnd.3 mouse cells express the homologous rodent Oatp1a4 protein in the physiological and pathological levels of K^+ . Immunocytochemistry (**Figure 9, A and B**) and WB (**Figure 9 C and D**) confirmed the presence of Oatp1a4 in bEnd3 cells. Oatp1a4 localization within bEnd.3 cells after KCl exposure was assessed by immunocytochemistry with corrected total cell fluorescence calculated (**Figure 9 A**). As compared to treatment for 5 minutes with aCSF or 3mM KCl, high abuminal KCl (60mM) not change the total cell fluorescence (**Figure 9B**, $p=0.85$). As compared to aCSF, application of KCl (60mM, 5-minutes) did not change total protein detection by WB 5-minutes or 30-minutes after pulse (**figure 9, C and D**; $p=0.24$). Together these data suggest that bEnd.3 murine brain endothelial cells express oatp1a4 and that this expression and localization is not altered after brief exposure to elevated K^+ levels as compared to controls.

Figure 9

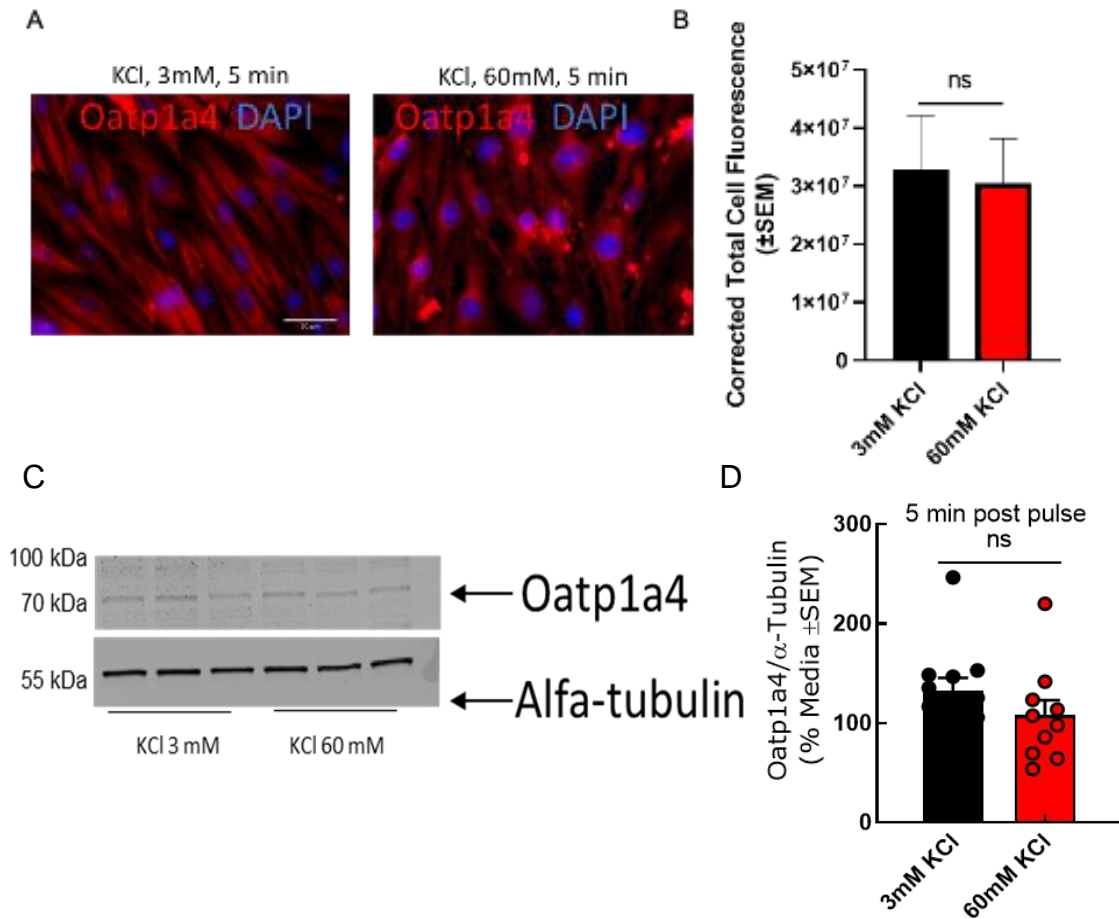


Figure 9. Localization and Expression of Oatp1a4 in mouse brain endothelial cells under physiological KCl and CSD KCl concentration. (A) Immunocytochemistry of b.End3 mouse cells of Oatp1a4 post 5-minute exposure to DMEM media containing 3mM or 60mM KCl concentrations; (B) analyzed using unpaired T-test on corrected total cell fluorescence (CTCF), no significance observed ($p=0.85$)($n=3$). Western blot of Oatp1a4 in b.End3 mouse cells 5 minutes post exposure to DMEM media containing 3mM or 60mM KCl concentrations, data expressed as percent Oatp1a4 of alpha tubulin, data assessed using unpaired T-test, no significance observed ($p=0.24$)($n=3$). Localization experiments (A/B) were performed by Vani Verkhovsky, and expression experiment (C/D) were performed by Dr. Erika Liktov-Busa.

Prior studies using humanized mice expressing OATP1A2 revealed no difference in the uptake of sumatriptan over time in a normal physiological state [158]. However, no studies have been performed evaluating Oatp1a4 transport during exposure to high extracellular potassium in vitro. Having established that bEnd.3 mouse cells express Oatp1a4 and show no change in localization or expression, we wanted to know if sumatriptan uptake across the brain endothelial barrier during and after an abluminal pulse with KCl (60mM) would be altered under the influence of an OATP inhibitor (E3). bEnd.3 mouse endothelial cells were treated with 1.5 mM sumatriptan succinate for 5-minutes in the luminal well both during (concurrent; **Figure 10A, B** and **Figure 11A, B**) or at 5-minutes after the KCl or aCSF exposure on the abluminal side of the trans-well. When sumatriptan succinate was applied during the 5- minute KCl (60 mM) exposure sumatriptan transport across the trans-well monolayer was increased (**Figure 10B**); this returned to control levels 30min post KCl pulse. In the presence of the OATP inhibitor E3S (30-min pretreatment), sumatriptan transport was reduced to equal aCSF levels (**Figure 10B**) suggesting a role for oatp1a4 in sumatriptan uptake when abluminal K⁺ is elevated *and* sumatriptan is present.

Comparatively, when sumatriptan succinate was applied 5-minutes after the 60mM KCl exposure (**Figure 11B**), neither the physiological 3mM nor the high extracellular 60mM levels of KCl significantly enhancement of sumatriptan transport (**Figure 11B**); oatp1a4 inhibition did not change this observation. These data indicate that sumatriptan blood to brain transport across bEnd.3 cell monolayers is mediated by Oatp1a4 during times when abluminal potassium concentrations are high and sumatriptan is present, but not after the pulse.

Figure 10

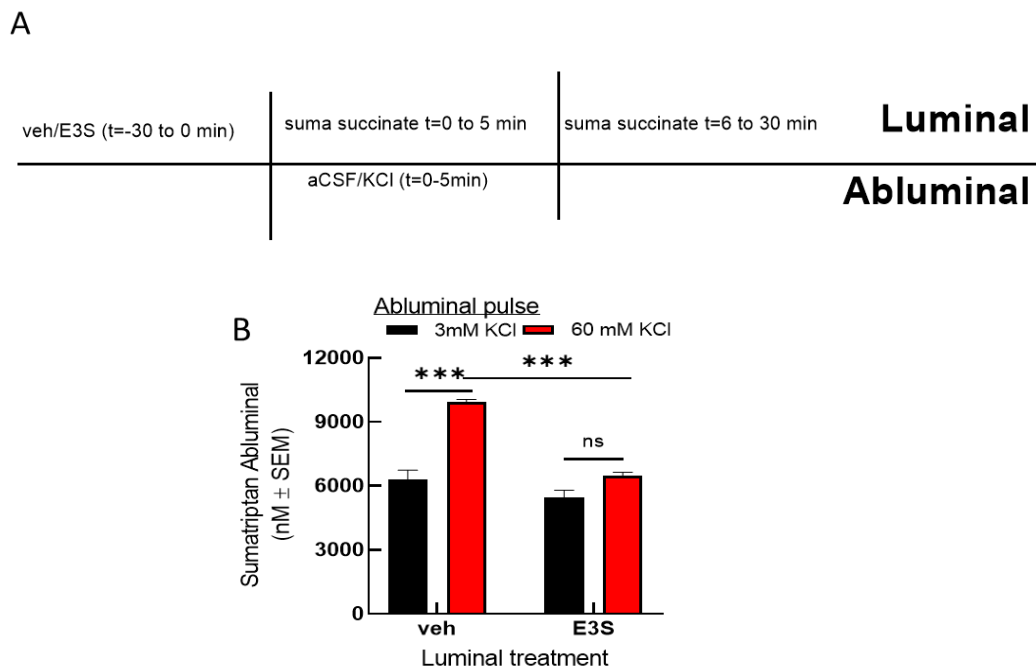


Figure 10. Suma succinate crossing from luminal to abluminal compartments of in vitro endothelial barrier. (A) Timeline of experimental treatment. (B) Amount of suma succinate present in media located in abluminal well of trans-well plate in 0-to-5-minute collection; *, **, ***, **** = $p < 0.05$, 0.01 , 0.001 , and 0.0001 vs. veh and vs. veh 60mM vs. E3S 60mM at same time point by 2 Way ANOVA with a Tukey post-hoc ($n=3$).

Figure 11

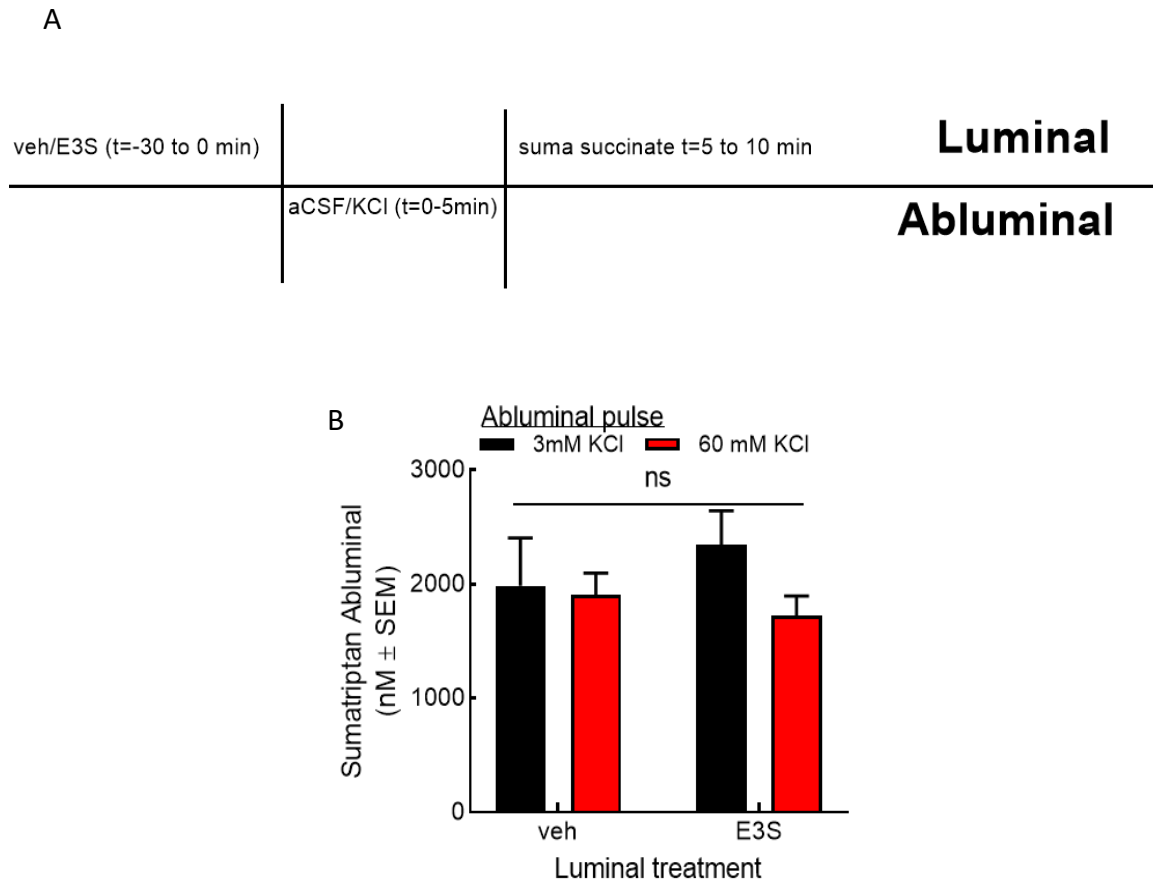


Figure 11. Suma succinate crossing from luminal to abluminal compartments of in vitro endothelial barrier. (A) Timeline of experimental treatment. **(B)** collection of suma succinate treatment in abluminal well post 5-minute exposure to 3mM or 60mM KCl DMEM media, collection taken after 5-minutes suma succinate exposure in luminal well; no significance observed between groups (n=3).

2.2.3.2 Oatp1a4 transport of sumatriptan during CSD in vivo

Previously, our lab showed sumatriptan uptake occurred in the cerebral cortex 90-minutes after cortical injection of KCl, but not aCSF [7]. To investigate whether sumatriptan uptake in vivo is associated with Oatp1a4 in this model of CSD, in situ brain perfusions were performed. Rats were treated with vehicle (1 mL/kg) or Estrone-3-sulfate (E3S, 10 mg/kg) intraperitoneally (I.P.) 30-minutes prior to the cortical injection of 0.5 μ of 1M KCl and the in-situ brain perfusion with ³H-sumatriptan performed either 30- or 90-minutes after cortical KCl injection in animals (**Figure 12A, B**). In animals pretreated with vehicle, ³H-sumatriptan levels in the cortex (F_{time} (1,7)= 11.86; p=0.0108) and brainstem (F_{time} (1,5)=23.48, p<0.0046) were significantly higher compared to historical aCSF data [7], with levels in both regions statistically higher 30-minutes post-injection as compared to 90-minutes (**Figure 12A, B**). Pretreatment with E3S in the 30- minute or 90-minute timepoints did block ³H-sumatriptan uptake in either the cortex or brainstem. The data suggest that parenchymal sumatriptan uptake during CSD occurs in a time-dependent manner but not via oatp1a4.

Figure 12

Figure 12. ³H-sumatriptan uptake in cortex and brainstem of rats post cortical injection of KCl with or without Oatp1a4 inhibitor. (A) sumatriptan detection in cortex 30- and 90- minutes after cortical KCl; (B) sumatriptan uptake in brainstem 30- and 90- minutes post cortical KCl injection; *, **, ***, **** = p < 0.05, 0.01, 0.001, and 0.0001 vs. veh and vs. veh 90-minutes vs. E3S 90- min by 2 Way ANOVA with a Tukey post-hoc (n=6-8).

2.2.3.3 CSD induction regulates Oatp1a4 in vivo in a regionally and time-dependent manner

The final experiment asked whether oapt1a4 expression was altered by cortical injection of KCl in the V1M cortex and brainstem containing the trigeminal brainstem complex. Tissue was harvested for WB detection of Oatp1a4 at 30-, 90-, and 180-minutes after CSD induction by cortical injection of KCl (**Figure 13A, B**). In these regions, Oatp1a4 was detectable at each time-point. Cortical injection of KCl significantly reduced Oatp1a4 detection was significantly reduced in the V1M cortex (**Figure 13A**) and brainstem (**Figure 13B**) as compared to aCSF. By 90-minutes after KCl injection, Oatp1a4 detection was significantly increased in the V1M cortex (**Figure 13A**; $F_{\text{time} \times \text{treatment}}(4, 24) = 40.26; p < 0.001$) and reduced in the brainstem (**Figure 13B**; $F_{\text{time} \times \text{treatment}}(F(1.206, 11.45) = 31.07; p < 0.0001)$). These data indicate that Oatp1a4 expression as detected by WB could be regulated during CSD events in a time and region dependent manner.

Figure 13

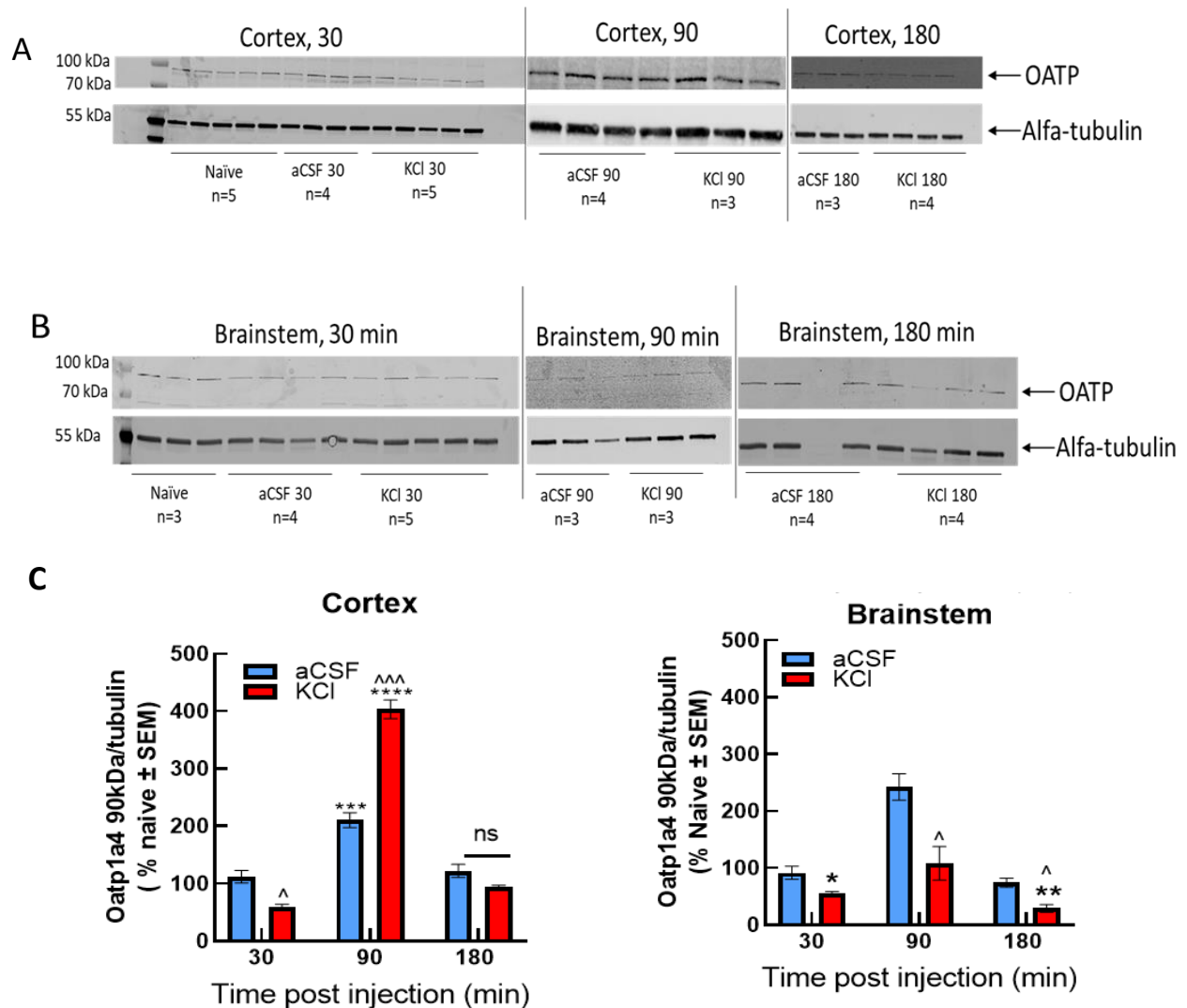


Figure 13. Expression of Oatp1a4 in cortex and brainstem at timepoints post cortical injection of KCl or aCSF. (A) Western blots of Oatp1a4 in rat cortex, data expressed as ratio of Oatp1a4/alpha tubulin to naïve tissue (n=3-5). (B) Western blots of Oatp1a4 in rat brainstem, data expressed as ratio of Oatp1a4/alpha tubulin to naïve tissue. (C) Western blot quantification; *, **, ***, **** = $p < 0.05, 0.01, 0.001, \text{ and } 0.0001$ vs. naïve ^, ^^, ^^, ^^ = $p < 0.05, 0.01, 0.001, \text{ and } 0.0001$ and vs. aCSF by use of unpaired T- test. Experiment performed by Dr. Erika Liktör-Busa.

2.2.4 Conclusions

Oatp1a4 and its human ortholog, OATP1A2, in the physiological brain may be regulated genetically (i.e., small nucleotide polymorphisms), epigenetically, or altered by sex, age, post-translational modification (e.g., glycosylation), and/or changes in the microenvironment [154, 161-163]. In pathological events leading to an increase in extracellular K^+ , such as stroke hypoxia, or inflammation can regulate Oatp1a4 functional expression at the blood brain barrier, this can impact the brain uptake of therapeutics [14, 156, 161, 164]. We now show that events with sub-clinical presentation like CSD, an electrical event associated with migraine, can actively regulate temporal and regional Oatp1a4 expression. Despite dynamics of oatp1a4 detection, these alterations did not result in meaningful changes in sumatriptan transport in vivo.

**CHAPTER 3: INHIBITION OF HSP90 PRESERVES
BLOOD-BRAIN BARRIER INTEGRITY AFTER
KCL INDUCED CORTICAL SPREADING
DEPRESSION VIA CLAUDIN-5 UPREGULATION**

3.1 Introduction

Primary and secondary headache disorders, like migraine, medication overuse headache (MOH), stroke, and traumatic brain injury, have been associated with a pathophysiological phenomenon termed cortical spreading depression (CSD) [165]. Mechanistically, CSD events are driven by increases in extracellular K^+ that induce depolarizing waves of activity spreading across the cortex, followed by a prolonged period of suppressed activity (i.e., depression) [166]. Direct cortical dysfunction, including breakdown of ionic gradients, leads to neuronal, glial, and vascular activation which can lead to dysregulation of the NVU [19]. Transient opening of the blood brain barrier (BBB) to small molecules has been reported during CSD events resulting from changes to cerebral blood flow and dysregulated neurovascular coupling [7, 167]. These events over time can both affect drug delivery and cause brain pathologies such as ischemia; this can lead to other major disease states detrimental to the health and function of a person's brain. HSP chaperones have been proposed to play a role in BBB integrity [168]. Although publications mainly report protective effects of HSPs in certain types of neurodegenerative diseases like Parkinson's and Huntington's disease, contrasting results have been reported [169]. Increased expression of HSP70 and 90 are linked to reductions in BBB integrity and/or neuroinflammation in autism spectrum disorders, cancers (e.g., glioblastoma, meningioma), amyotrophic lateral sclerosis (ALS), Alzheimer's Disease (AD), intracerebral hemorrhage, and stroke [168]. Given the overlap between the neurological diseases mentioned above and the reduced blood brain barrier integrity caused by CSD events previously reported, we hypothesized that HSP90 plays a role in CSD-induced transient paracellular leak of the blood brain barrier. In this study, pharmacological inhibition of HSP90 by application of 17-AAG was used in vitro (e.g., blood endothelial barrier -BEB) and an in vivo model with an intact BBB. We measured barrier integrity using trans endothelial electric resistance (TEER) across a monolayer

of rodent brain endothelial cells (bEnd.3), a sucrose uptake assay, and in situ brain perfusion using female Sprague Dawley rats.

3.2 Methods and Materials

Cell Culture

The bEnd.3 (CRL-2299, ATCC) cell line was used for in vitro experiments, cultured as described in Liktor-Busa et al. [145]. Cells were treated with 60 mM KCl for 5 minutes, which is a typical condition to evoke potassium-triggered spreading depolarization in live brain slices [142]. 10 mM 17-AAG (Fisher Biosciences) was made up in 100% DMSO then diluted in DMEM to 1 μ M concentration and applied apically to bEnd.3 cells for 24 hours prior to KCl exposure. This dose and incubation time was established in our previous work [170].

Proteomic Analysis

bEnd.3 cells were treated with either artificial cerebrospinal fluid (aCSF) or KCl (60mM) for 5 min, then lysed and soluble protein extracted. 200 μ g of harvested cell lysate supernatant was separated on a 10% SDS-PAGE gel and stained for total protein with Bio-Safe Coomassie G-250 Stain. Lanes from the gel were separated, cut into six slices, and underwent trypsin digestion; the resulting peptides were purified by C18 desalting performed as described [171]. High performance liquid chromatography-electrospray ionization tandem mass spectrometry (HPLC-ESI-MS/MS) was performed in positive ion mode on an Orbitrap Fusion Lumos tribrid mass spectrometer (Thermo) fitted with an EASY-spray source (Thermo). NanoLC was performed according to protocol published by Kruse et al.[171] Tandem mass spectra were extracted from files in Xcalibur 'RAW' and ProteoWizard 3.0 msConvert script was used to assign charge states with default parameters. Mascot (Matrix Science, ver 2.6.0) software was used with default probability cut off score settings to search fragment mass spectra against the

Mus musculus database in SwissProt_2018_01 (16965 entries). The search variables used were as follows: 10 ppm mass tolerance for precursor ion masses and 0.5 Da, for product ion masses, trypsin digestion, maxima of two missed tryptic cleavages, variable modifications of phosphorylation of threonine, tyrosine, and serine, and oxidation of methionine. Scaffold software (Proteome Software, ver 4.8.7) was used to cross correlate Mascot search results with X! Tandem software. Significance value was set at $p \geq 0.05$. Targeted evaluation for Hsp90, 70, and co-chaperones was performed.

Ion intensity-based label free quantification was performed using Progenesis QI for proteomics software (Nonlinear Dynamics, ver 2.4). .raw files were imported and converted into two dimensional maps with y axis defined as time, and x axis defined as m/z which was then followed by selection of a reference run for alignment. The aligned runs were then used to create an aggregate data set containing all peak information from all samples, after which data pool was narrowed down to only +2, +3, and +4 charged ions for further analyses. The top 8 most intense precursors of a given feature were grouped into a peak list of fragment ion spectra and exported in Mascot generic file (.mgf) and searched against the *Mus musculus* SwissProt_2018_01 database utilizing Mascot software. The following search variables were used: 10 ppm mass tolerance for precursor ion masses, and 0.5 Da for-product ion masses, trypsin digestion, maxima of two missed tryptic cleavages, variable modifications of oxidation of methionine and phosphorylation of serine, tyrosine, and threonine, 13C=1. The data was collected into a Mascot .xml file and imported into Progenesis allowing for assignment of peptides and proteins. Peptides with a Mascot ion score < 25 were not used for further analyses. Non-conflicting peptides and precursor ion abundance values were normalized using a reference run to perform protein quantification.

Trans endothelial electrical resistance (TEER)

TEER is an established method of evaluating endothelial cell barrier integrity which captures active and passive breaches in vitro [172]. TEER was assessed via two-electrode chopstick method (EVOM2), as described [100] at the following timepoints immediately post-pulse: 10, 20, 30, 60, 120, and 180 minutes after replacement of abluminal media.

Sucrose Transport

Functional implications of monolayer integrity or lack thereof were assessed in vitro as luminal to abluminal transport/uptake of ^{14}C -sucrose. Detailed description of uptake experiments is published by Liktor-Busa et al. [145].

Animals

Intact, female Sprague Dawley rats (200-250 g) were purchased from Envigo (Indianapolis, IN) and housed in a climate-controlled room on a regular 12/12 h light/dark cycle with lights on at 7:00 am with food and water available ad libitum. All procedures were performed during the 12-hour light cycle and according to the policies and recommendations of the International Association for the Study of Pain and the NIH guidelines for laboratory animals, and with IACUC approval from the University of Arizona (17-223). Dural cannulation and in situ brain perfusion were performed as previously described by Cottier et al. and Liktor-Busa et al. [7, 145]. CSD was induced by delivery of a focal injection of 0.5 μl of 1 M KCl through the guide cannula. Injection of aCSF into the cerebral cortex was used as vehicle control. Cortical injections were performed 24 h after dural application of 5 μL of vehicle (1% DMSO in aCSF) or 17-AAG (0.5 nmol) [100]. This dose and treatment time for 17-AAG in rodents was also established in our previous work [170].

Western Blot

Tissue was collected from rats as described in Liktov-Busa et al. [145]. Total protein (40 μ g) from tissue supernatant was loaded into TGX precast gels (4-20% CriterionTM, BioRad) and transferred to nitrocellulose membrane (AmershamTM ProtranTM, GE Healthcare). After Transfer, the membrane was blocked at room temperature for 1 hour in blocking buffer (5% dry milk in Tris-buffered saline with tween 20 (TBST)). The following primary antibodies were diluted in blocking buffer (5% BSA in TBST): Claudin-5 (ThermoFisher Scientific, 35-2500, 1:500), and α -tubulin (Cell Signaling, 3873S, 1:10,000). The membrane was incubated in diluted primary antibodies for 48 hours at 4°C. The membrane was washed three times in TBST for 5 minutes each then incubated with Goat α Mouse IRDye-680 (LiCor, 926-68072) in 5% milk in TBST for 1 hour rocking at room temperature. The membrane was washed again three times for five minutes each and imaged with an Azure Sapphire laser imager (Azure Biosystems). The Western image was produced using Azure Capture software and analyzed using Azure Spot Western Analysis software. Bands quantified using ImageJ FIJI software open access from NIH.

Statistics

GraphPad Prism 7.0 and 8.3.1 software (GraphPad Software) were used for statistical analysis; numbers needed for each experiment were determined using G.Power3.1 for 80% power to detect a 20% difference when alpha = 0.05. Unless otherwise stated, the data were expressed as mean \pm S.E.M. Groups were compared by unpaired t-test or one-way ANOVA with Tukey's post-test, as indicated. Differences were considered significant if $p \leq 0.05$.

3.3 Results

3.3.1 CSD-like Environments Increase HSP90a Expression in Brain Endothelial Cells In Vitro

Endothelial cells comprise the first layer of the BBB and are integral for the function of the NVU [173]. The first experiment assessed whether CSD-like concentrations of K⁺ changed expression of HSP90 proteins in bEnd.3 brain endothelial cells. Using an unlabeled proteomics technique and targeted analysis, data indicates that a 5 min exposure of high extracellular KCl (60mM) did not change protein expression of HSP70, or the inducible form, HSP72 (**Figure 14A**). However, HSP90a, but not HSP90b, was significantly increased after KCl stimulation (5 min, 60 mM) as compared to aCSF control (**Figure 14B**). In addition, the HSP90 co-chaperones, CDC37 and endoplasmin were detected, with significant increases observed in endoplasmin levels after KCl (**Figure 14C**). Together, these data indicate that high extracellular K⁺ in the abluminal side of brain endothelial cells can rapidly regulate HSP90 levels as well as its co-chaperone endoplasmin. These results further justified further examination of the role of HSP90 in CSD-induced barrier dysfunction.

3.3.2 Inhibition of HSP90 Prevents Paracellular Breaches of the BEB/BBB

In models of hypoxia and extreme insult, HSP90 has been implicated in BEB function by reorganizing tight junctions and adherens junctions [129, 168, 174-176]. Experiments two (**Figure 15**) and three (**Figure 16**) were designed to test global function by way of assessing BEB permeability. TEER, sucrose uptake, and in situ brain perfusion has been utilized in previous studies to assess barrier integrity [7, 170, 177]. The selective inhibitor of HSP90, 17-AAG, was used to pharmacologically assess the role of HSP90 in vitro and in vivo.

Figure 14

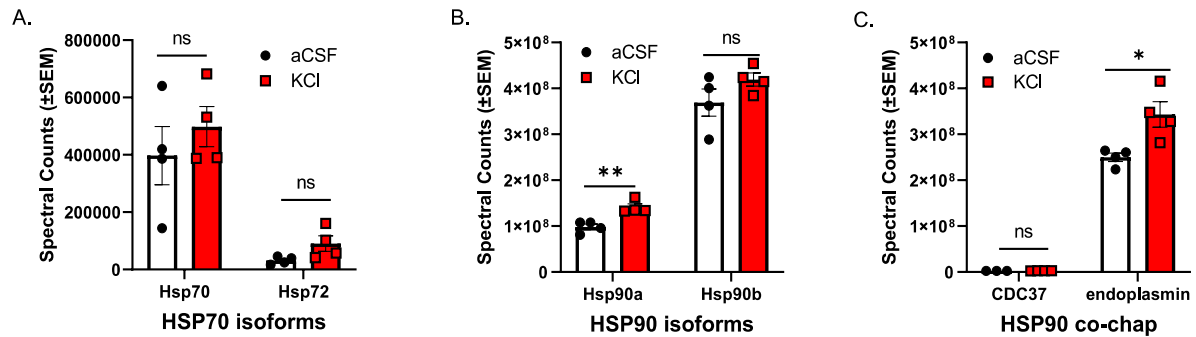


Figure 14. KCl stimulation increases HSP90a and the co-chaperone endoplasmin in murine brain endothelial cells. Proteomic Spectral counts for (A) HSP70 isoforms, (B) HSP90 isoforms, and (C) HSP90 co-chaperones detected by unlabeled proteomic approaches. * $p < 0.05$, ** $p < 0.01$, Two-way ANOVA, Sidak-Holms corrected T-test. $N = 4$ mean \pm SEM. (Palomino et. Al, Inhibition of HSP90 preserves blood-brain barrier, in submission)

Figure 15

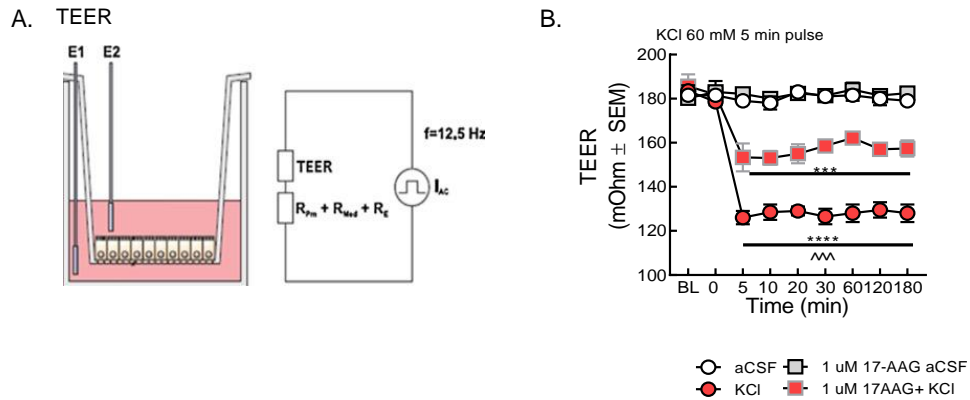


Figure 15. Selective inhibition of HSP90 with 17-AAG reduced 60mM KCl insult associated with CSD to blood-brain barrier leak in vitro. (A) Setup of probe in trans-well plate for measurement **(B)** TEER values were significantly reduced after KCl pulse (5 min, 60 mM) as compared to aCSF controls on the monolayer of bEnd.3 cells, suggesting loss of barrier integrity (KCl vs aCSF: *** $p < 0.001$, **** $p < 0.0001$, as tested by one-way ANOVA with Tukey's post-test). 24h preincubation with 17-AAG (1 μ M) attenuated the KCl-induced changes in TEER values (KCl + 17-AAG vs. KCl + vehicle: ^^ $p < 0.001$, assessed by one-way ANOVA, Tukey's post- test). Values are mean \pm SEM (n=3 in triplicate). (Palomino et. Al, Inhibition of HSP90 preserves blood-brain barrier; in submission).

3.3.3 17-AAG Prevents Paracellular Leak Induced by KCl In Vitro

Our previous studies have shown that 5-minute KCl exposure significantly reduced TEER values as compared to aCSF controls, indicating loss in of BEB resistance. To determine whether Hsp90 played a role in this reduction, bEnd.3 cells were preincubated with 17-AAG (1 μ M), a concentration previously utilized in vitro and in vivo [170] (**Figure 15B**). 17-AAG statistical limited the KCL-mediated reduction of TEER suggesting a role for Hsp90. Changes in TEER can reflect wither changes in paracellular integrity as well as expression of ion channels/transporters. To assess the role of Hsp90 in paracellular integrity breaches induced by KCl, 17-AAG was applied as above and the uptake of ¹⁴C-sucrose across the endothelial monolayer monitored. KCl exposure significantly increased the amount of ¹⁴C-sucrose detected in the abluminal chamber within the first 5 min after application (**Figure 16B**); this normalized by 30 min post KCl exposure (**Figure 16C**). 24-hour pretreatment with 17-AAG mitigated this movement of sucrose across the bEnd.3 cell monolayer in KCl treated cells, without altering sucrose movement in those exposed to aCSF, suggesting increased restoration or protection of a functional BEB.

Figure 16

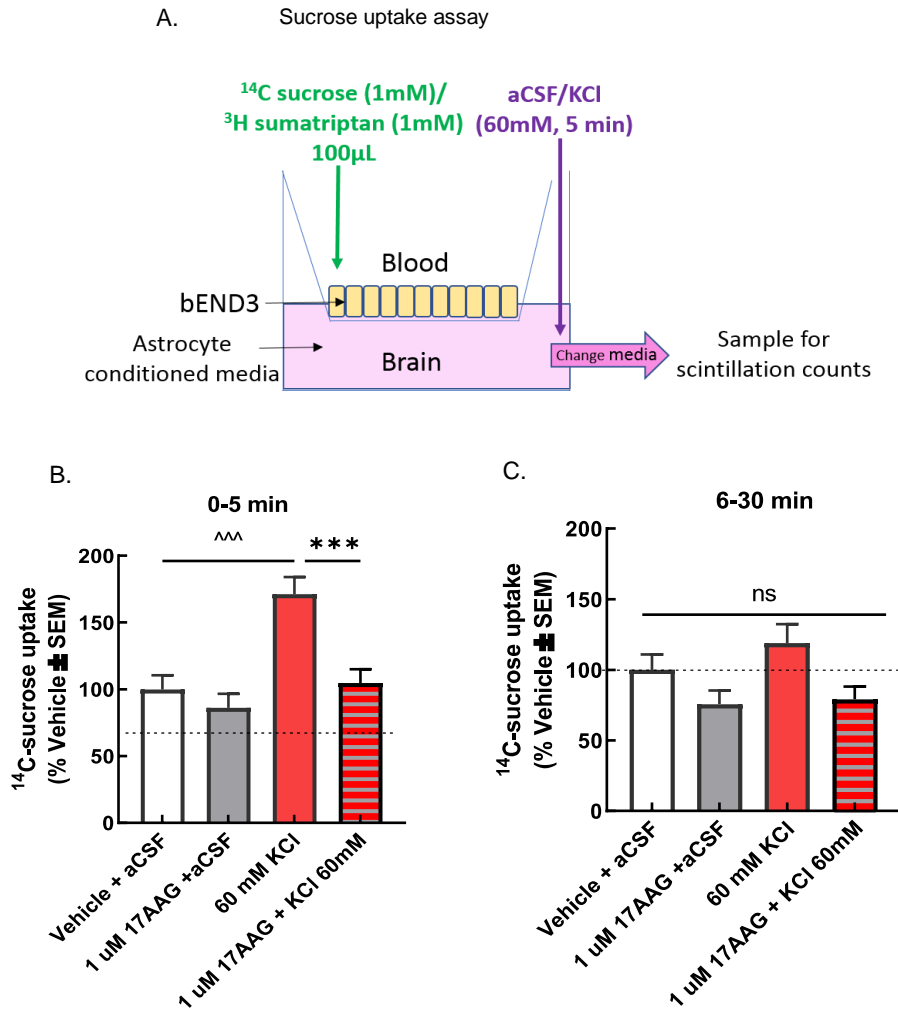


Figure 16. Selective inhibition of HSP90 with 17-AAG reduced 60mM KCl insult associated with CSD induced blood-brain barrier paracellular leak in vitro. (A) Setup of trans-well paracellular leak model. **(B)** ¹⁴C-sucrose transport was measured in trans-well, media in bottom well was collected after 5 and **(C)** 30 min. The amount of ¹⁴C-sucrose detected in the abluminal chamber was significantly increased after 5 min KCl exposure compared to aCSF controls, indicating reduced barrier integrity (KCl vs aCSF at 5 min: $^{^^^}p < 0.001$, as tested by one-way ANOVA with Tukey's post-test). No significant difference between KCl vs. aCSF was observed

after 30 min. Treatment with the HSP90 inhibitor 17-AAG (1 μ M, 24 h) prevented sucrose movement across the monolayer in KCl treated cells, but it did not influence sucrose permeability in aCSF-treated cells (KCl + 17-AAG vs. KCl + vehicle: *** $p < 0.001$, assessed one-way ANOVA with Tukey's post-test). Values are normalized to percent of vehicle \pm SEM (n=4, dotted line). (Palomino et. Al, Inhibition of HSP90 preserves blood-brain barrier, in submission)

3.3.4 17-AAG Increases Functional Expression of Claudin 5 Which May Prevent Paracellular Leak of the BBB In Vivo.

Given the in vitro data suggesting a role for Hsp90 in KCl mediated BEB paracellular leak, we next determined whether the inhibition of HSP90 reduced CSD induced transient leak in vivo (i.e., intact BBB). In situ brain perfusion was performed at 90 minutes after the induction of CSD by cortical KCl injection, the time of peak sucrose uptake in this model. As previously reported [7], cortical injection of KCl significantly increased ¹⁴C-sucrose uptake into the parenchyma at 90 min (**Figure 17B**) suggesting paracellular leak. Pre-exposure (24h) to 17-AAG onto dura (0.5 nmol, in vivo dose established in [170]) significantly reduced sucrose uptake at the same timepoint (**Figure 16B**) suggesting that in vivo HSP90 plays a role in paracellular breaches at the BBB during CSD events.

Previous reports have shown that HSP90 inhibition can restore tight junction proteins occludin and zona occluding 1 (ZO-1), an anchoring protein for claudin 5 as well as inhibit matrix metalloprotease 9 (MMP9) and upregulate TGF Beta expression; to date claudin 5 has not been investigated. Therefore, we wanted to observe whether inhibition of HSP90 with 17-AAG changed protein detection levels of the tight junction protein, claudin-5. Application of 17-AAG 24h prior to cortical KCl injection significantly increased Western blot detection of claudin 5 in the cortex and PAG 90 min after KCl injection (**Figure 18A, B**). Taken with the in-situ brain perfusion data, the observations indicate suggest that inhibition of HSP90 with 17-AAG restores BBB paracellular integrity by increasing functional expression of claudin 5 (**Figure 19**).

Figure 17

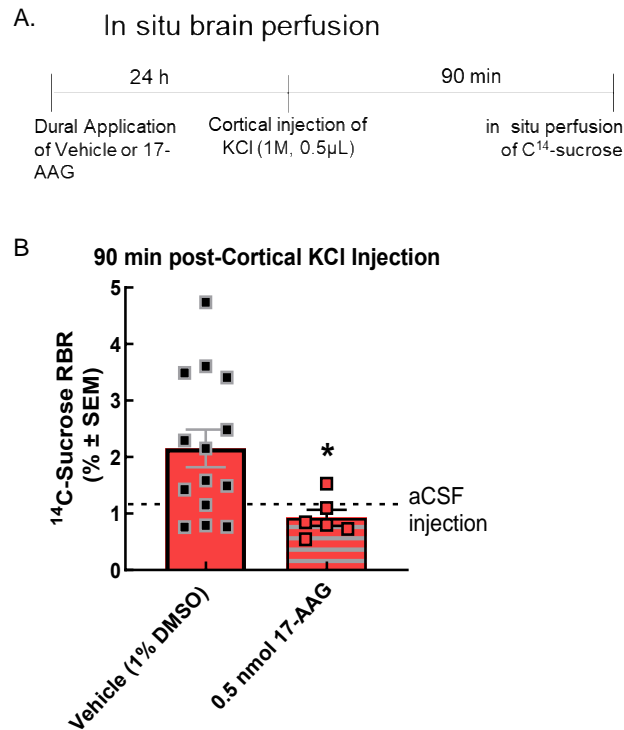


Figure 17. 17-AAG reduced cortical spreading depression associated blood-brain barrier leak in vivo. (A) Timeline of treatment, cortical injection, and perfusion (B) ¹⁴C-sucrose uptake was measured in whole cortex and presented in the brain to plasma ratio (RBR) after 10 min brain perfusion. The in-situ brain perfusion of female rats showed that dural application of 17-AAG (0.5 nmol) 24 h before cortical injections significantly reduced ¹⁴C-sucrose uptake, suggesting that HSP90 inhibition could prevent KCl-caused BBB leak. (KCl + 17-AAG vs. KCl + vehicle: *p<0.05, assessed unpaired t-test). Values are mean ± SEM (n=6-11). (Palomino et. Al, Inhibition of HSP90 preserves blood-brain barrier, in submission)

Figure 18

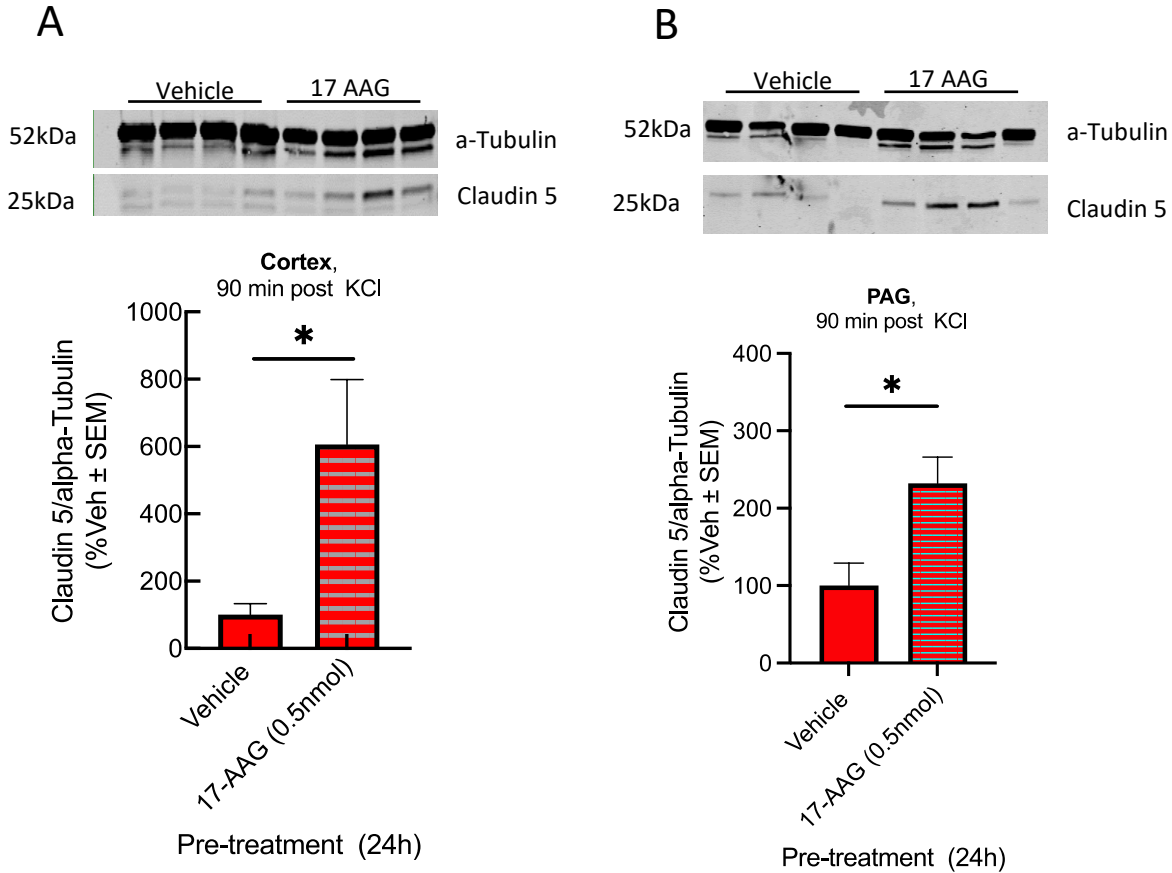


Figure 18. 17-AAG reduced cortical spreading depression associated blood-brain barrier leak in vivo. (A) Cortical tissue was harvested from rats pretreated with either vehicle or 17AAG on the dura mater and injected with KCl after 24 h. Detection of total protein for claudin 5 was significantly increased in tissue harvested from rats exposed to 17-AAG as compared to vehicle. N=4/treatment, Students T-test, $p < 0.05$ (Palomino et. Al, Inhibition of HSP90 preserves blood-brain barrier, in submission)

3.4 Conclusion

Current results suggest that inhibition of HSP90 with the selective HSP90 inhibitor 17-AAG reduces CSD associated BBB paracellular leak at the endothelial cell level both in vitro and in vivo via modulation of tight junction expression. Investigation of cellular and molecular mechanisms underlying this effect is warranted and requires future studies to develop new therapeutic approaches centered on concepts targeting HSPs as a treatment for stroke, headache/migraine, and other diseases where an impaired BBB is implicated. Variability in claudin 5 expression seen in the western blots of the cortex and PAG in vivo may as well as the grouping pattern seen in the in-situ perfusion of ^{14}C -sucrose uptake into the cortex may be attributed to hormonal changes. It is well documented that tight junction protein expression in females varies depending on hormone concentration levels relevant to their menstrual cycle. HSP90 protein is linked to the steroid hormone receptor and activity may also be affected in response to 17-AAG pretreatment. Future studies may include cycling the female rats and testing in each phase. The role of HSP90 during a CSD event could be related to post translational modifications of structural proteins which maybe relevant to maintaining tight junction expression at the cell surface.

Figure 19

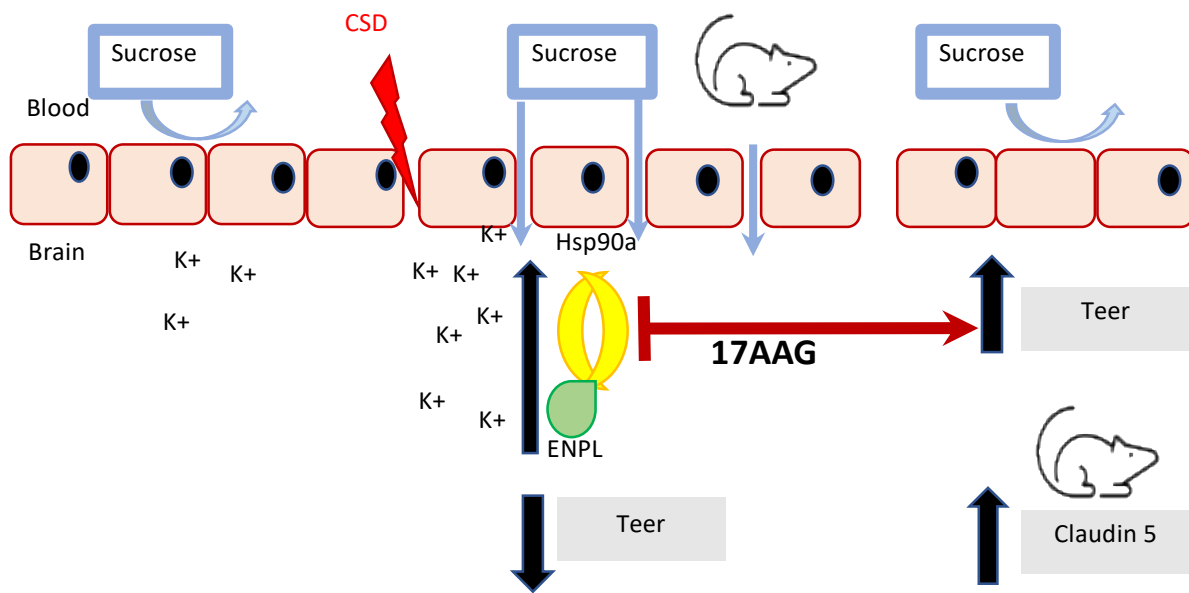


Figure 19. Summary of findings. Inhibition of HSP90 using 17AAG improves blood brain barrier integrity possibly through increased claudin 5 protein levels in the cortex. (Palomino et. Al, Inhibition of HSP90 preserves blood-brain barrier; in submission).

**CHAPTER 4: HSP90 INHIBITION MITIGATES
FACIAL ALLODYNIA IN A CSD MODEL
THROUGH MODULATION OF
ENDOCANNABINOID SYSTEM IN THE PAG.**

4.1 Introduction

Migraine with aura and headache associated secondary diseases such as stroke and traumatic brain injury have a limited options for adequate for pain relief. Preclinical studies utilizing HSP90 inhibitors have shown to be effective in modulating pain sensitization and inflammation associated with various disease states [122, 178]. Similarly, Recent studies have shown HSP90 inhibition with 17-AAG can regulate receptor signaling pathways which can alter pain behavior by enhancing morphine antinociception in the spinal cord [122, 123, 170]. Additionally, HSP90 may be a valuable and useful target to better understand mechanisms related to migraine pain [121].

One system relevant to migraine and which HSP90 has been linked is the endocannabinoids system. There is a study which suggests the co-chaperone of HSP90, AHA1, interacts with CB1R to traffic the receptor to the surface of the cell [179]. This could be of significance as there is evidence of the notion that Clinical Endocannabinoid Deficiency (CED) has a part in the pathophysiology of migraine pain [180-182]. Since HSP90 inhibition alleviates somatic pain, promotes morphine-mediated antinociception, and has been linked to the CB1R regulation, we hypothesized that HSP90 inhibition would mitigate CSD associated periorbital allodynia in a CBR dependent manner.

4.2 Methods and Materials

Drugs and reagents

7-(Allylamino)-17-demethoxygeldanamycin, 99% (17-AAG) (#AAJ66960MC) was purchased Alfa Aesar. SR141617 (Rimonabant) was purchased from Cayman Chemicals (Ann Arbor, MI).

Animals

Intact, female Sprague Dawley rats (200-250 g) were purchased from Envigo (Indianapolis, IN) and housed in a climate-controlled room on a regular 12/12 h light/dark cycle with lights on at 7:00 am with food and water available *ad libitum*. Animals were initially housed 3 per cages but individually housed after the dural cannulation. All procedures were performed during the 12-h light cycle and according to the policies and recommendations of the International Association for the Study of Pain and the NIH guidelines for laboratory animals, and with IACUC approval from the University of Arizona. Justification for animal numbers was consistent with NIH policy (NOT-OD-15-102), and experiments were randomized to blinded treatment groups to give 80% power to detect a treatment effect size of 20% compared to a baseline response of 5% at a significance level of 0.05 [142, 183, 184]. Numbers required to achieve statistical power were determined by G.Power3.1. Female rats were used as headache disorders affect females to males at a nearly 3:1 ratio [185, 186]. The stage of estrus cycle was not determined in this study.

Dural cannulation

Dural cannulation was performed as previously described [7, 139, 145]. Briefly, anesthesia was induced with intraperitoneal 45:5:2 mg/kg cocktail of ketamine:xylazine:acepromazine. Rats were placed in a stereotactic frame (Stoelting Co.), and a 1.5- to 2-cm incision was made to expose the skull. A 0.66- to 1-mm hole (Pinprick/KCl: -6 mm

A/P, -3 mm M/L from bregma) was made with a hand drill (DH-0 Pin Vise; Plastics One) to carefully expose, but not damage, the dura. A guide cannula (0.5 mm from top of skull, 22 GA, #C313G; Plastics One) was inserted into the hole and sealed into place with glue. Two additional 1 mm holes were made caudal to the cannula to receive stainless-steel screws (#MPX-080-3F-1M; Small Parts), and dental acrylic was used to fix the cannula to the screws. A dummy cannula (#C313DC; Plastics One) was inserted to ensure patency of the guide cannula. Rats were housed individually and allowed 6–8 d to recover. Cannula placement and dural integrity at screw placement was confirmed postmortem.

Cortical injections

Cortical injections were performed using a Hamilton injector (30 GA, #80308 701 SN, Hamilton Company) customized to project 1.0 mm into the beyond the dura into the occipital cortex. The injector was inserted through the guide cannula to deliver a focal injection of 0.5 μ l of 1 M KCl or artificial CSF (aCSF) into the cerebral cortex. aCSF was comprised of 145 mM NaCl, 2.7 mM KCl, 1 mM MgCl₂, 1.2 mM CaCl₂, and 2 mM Na₂HPO₄ (pH 7.4), and the solution was passed through a 0.2- μ m syringe filter before injection. Cortical injection was always considered at t = 0 min.

Pre-or postcortical injection treatments

17-AAG was applied onto the dura mater 24 hours before cortical injections at concentrations of 0.5 and 5 nmol utilizing the guide cannula in place for cortical injections. 17-AAG was dissolved in 100% DMSO to a concentration of 10 mM stock, then diluted to 0.5 nmol in saline for final concentration. The 5nmol concentration dose was made from the same 10 mM stock into DMSO-Tween80-saline (1:1:80, v/v/v). Rimonabant (SR141617A, 1mg/kg, 1mL/kg IP) or SR144528 (1mg/kg, 1mL/kg IP).

Periorbital mechanical allodynia

Periorbital allodynia was evaluated before ($t = 1, 2, 3,$ and 4 hours after 17-AAG treatment) and after cortical injection ($t = 30, 60, 90, 120, 180, 300, 360$ min) by an observer blinded to drug condition. Rats were grouped based on their postsurgical baseline to ensure equivalent pre-injection thresholds ($6-8$ g). Any rats exhibiting excessive postsurgical allodynia (threshold <6 g) were removed from the study. Rats were acclimated to testing box 1 h prior to evaluation of periorbital mechanical allodynia with calibrated von Frey filaments as previously described by Edelmayer and coworkers [140, 141]. Behavioral responses were determined by applying calibrated von Frey filaments perpendicularly to the midline of the forehead at the level of the eyes with enough force to cause the filament to slightly bend while held for 5 sec. A response was indicated by a sharp withdrawal of the head, vocalization, or severe batting at the filament with attempts to bite it. The withdrawal threshold was determined using a modified version of the Dixon up-down method

Tissue harvest

Rats were anesthetized with ketamine/xylazine mix as described above, then transcardially perfused with ice cold 0.1 M phosphate buffer at flowrates to not burst microvasculature (i.e., 3.1 ml/min). After decapitation, periaqueductal grey (PAG) were harvested, flash frozen in liquid nitrogen and stored at -80°C until further use

Membrane Preparation

Flash frozen tissue was thawed on ice, dounce homogenized in ice cold lysis buffer (20 mM HEPES, 1 mM MgCl_2 , 2 mM DTT, 10 units/ml benzodase) and centrifuged at $100,000 \times g$ for 45 min (Beckman Coulter rotor Ti55). The supernatant was discarded, and the pellet was resuspended in buffer HEPES (20 mM) supplemented with DTT (2 mM). Protein concentration

of samples was determined (DC protein assay, Bio-Rad) before aliquoting and flash freezing samples in liquid nitrogen. Samples were stored at -80 until further use.

Western- Immunoblotting

Samples were thawed on ice. Total protein (20 µg) from tissue supernatant was loaded into TGX precast gels (10% Criterion™, BioRad) and transferred to nitrocellulose membrane (Amersham™ Protran™, GE Healthcare). After Transfer, the membrane was blocked at room temperature for 1 hour in blocking buffer (5% dry milk in Tris-buffered saline with tween 20 (TBST)). The following primary antibodies were diluted in blocking buffer (5% BSA in TBST): beta actin (abcam ab6276, 1:2000), FAAH (abcam ab54615, 1:1000), AHA1 (abcam ab83036, 1:1000), Heat shock protein 90 (cell signaling, 1:5000), Heat shock protein 70 (cell signaling 48725, 1:7000), Cannabinoid Receptor 1 (abcam ab259323, 1:500), α -tubulin (Cell Signaling, 3873S, 1:10,000). The membrane was incubated in diluted primary antibodies for 48 hours at 4°C. The membrane was washed three times in TBST for 5 minutes each then incubated with Goat α Mouse IRDye-680 (LiCor, 926–68020) or Goat α Rabbit IRDye-800 (LiCor, 926-32211) in 5% milk in TBST for 1 hour rocking at room temperature. The membrane was washed again three times for five minutes each and imaged with an Azure Sapphire laser imager (Azure Biosystems). The Western image was produced using Azure Capture software and analyzed using Azure Spot Western Analysis software. Bands quantified using ImageJ FIJI software open access from NIH.

RT-qPCR on tissue

Total RNA was extracted from the tissue using RNeasy Mini Kit (No. 74104) from Qiagen (Germantown, MD) per the manufacturer's protocol, with final reconstitution of the RNA in nuclease-free water and storage at -80°C until analysis. The RNA was quantified using a

NanoDrop ND-1000 Spectrophotometer (ThermoFisher). Single-stranded complementary DNA (cDNA) was synthesized using high-capacity cDNA reverse transcription kit (27-874-06) from Fisher Scientific, following the manufacturer's protocol. The amplified cDNA was added to the RT² SYBR Green Master Mix (No. 330500; Qiagen) and gene specific primers. RT² qPCR primer assays (No. 330001; Qiagen) detected the expression of *CNR1*, CB1 gene, (PPR52793A) as well as *TUBA1a*, alpha tubulin gene all gene expression was normalized to alpha tubulin gene expression. The sequence for these was a 5' 3' primers designed to flank intronic sequences to identify genomic DNA contamination and was analyzed by Basic Local Alignment Search Tool (BLAST) to confirm target selectivity. The quantitative PCR (qPCR) was performed on the Lightcycler 96 Real-Time PCR System (Roche, Indianapolis, IN), using the thermal program: 95°C for 10 min, 45 cycles of 95°C for 15 sec, and 60°C for 1 min and a melt curve analysis. The melt curves were analyzed to confirm selectivity and supported by agarose gel electrophoresis. Cycle thresholds (Ct) normalized to GAPDH Ct generated relative gene expression of each target.

³⁵S-GTP γ S Coupling

The ³⁵S-GTP γ S coupling assay was also performed as in our previous work (e.g., [18,31,35]). Briefly, 10 μ g of cell membrane protein was combined with 0.1 nM of ³⁵S-GTP γ S (PerkinElmer, #NEG030H250UC) and concentration curves of PrNMI (see the figure legends for details) in a 200 μ L reaction volume in the presence of 100 μ M GDP. The reactions were incubated at 30 °C for 2 h; then, they were collected and read as above. The resulting data were normalized to stimulation caused by vehicle (0%) and baseline of each sample and fit to a 3-variable (Hill Slope = 1) agonist and antagonist model using GraphPad Prism 9.0.

Quantification of 2-AG and AEA by LC-MS

The brain samples for LC-MS were purified by organic solvent extraction, as described by Wilkerson et al. [187]. Briefly, tissues were harvested, snap-frozen in pre-weighted tubes, and stored at -80°C . On the day of processing, tissues were weighed and homogenized in 1 ml of chloroform/methanol (2:1 v/v) supplemented with phenylmethylsulfonyl fluoride (PMSF) at 1 mM final concentration to inhibit the degradation by endogenous enzymes. Dounce homogenizer was used for homogenization. Homogenates were then mixed with 0.3 ml of 0.7% w/v NaCl, vortexed, and then centrifuged for 10 min at $3200 \times g$ at 4°C . The aqueous phase plus debris were collected and extracted two more times with 0.8 ml of chloroform. The organic phases from the three extractions were pooled and internal standard was added to each sample. Mixed internal standard solutions were prepared by serial dilution of d^4 -AEA- and d^5 -2-AG- in acetonitrile. The organic solvents were evaporated under nitrogen gas. 6 ml of 30% glycerol in methanol per sample was added before evaporation. Dried samples were reconstituted with 0.2 ml of chloroform and mixed with 1 ml of ice-cold acetone to precipitate proteins. The mixtures were then centrifuged for 5 min at $1800 \times g$ at 4°C . The organic layer of each sample was collected and evaporated under nitrogen. Analysis of 2-AG and AEA was performed on an Ultivo triple quadrupole mass spectrometer combined with a 1290 Infinity II UPLC system (Agilent, Palo Alto, CA). The instrument was operated in electrospray positive mode with a gas temperature of 150°C at a flow of 5L/min, nebulizer at 15 psi, capillary voltage of 4500V, sheath gas at 400°C with a flow of 12L/min and nozzle voltage of 300V. Transitions monitored were 348.3 \rightarrow 287.3 and 62, 352.3 \rightarrow 287.4 and 65.9, 379.3 \rightarrow 287.2 and 269.2, and 384.3 \rightarrow 287.2 and 296.1 for AEA, d^4 -AEA, 2-AG, and d^5 -2-AG-. The first fragment listed was used for quantification and the second fragment was used for confirmation. The first 3 min of analysis time was diverted to

waste. Chromatographic separation was achieved using an isocratic system of 21% 1 mM ammonium fluoride and 79% methanol on an Acquity UPLC BEH C-18 1.7 μ 2.1x100 mm column (Waters, Milford, MA) maintained at 60°C. After each injection the column was washed with 90% methanol for one minute then re-equilibrated for 5 min prior to the next injection. Samples were maintained at 4°C. Mixed calibration solutions were prepared by serial dilution of AEA and 2-AG stock solutions in 80% C₂H₃N. Calibration curves were prepared for each analysis by adding 10 μ l internal standard solution to 20 μ l standard solution. Prior to sample analysis, 200 μ l of 80:20 C₂H₃N:H₂O was added to dried samples which were then vortexed and sonicated. The samples were centrifuged at 15,800 x g at 4°C for 5 min. Supernatant was transferred to autosampler vials and 5 μ l was injected for analysis.

PGE₂ ELISA

PGE₂ ELISA kit (Abcam, ab133021) was used according to manufacturer`s guidance. Tissue samples were weighed and homogenized in assay buffer supplemented with indomethacin at 10 μ M final concentration to block endogenous prostaglandin synthetase. The homogenized samples were centrifuged at 8000 x g at 4°C for 10 min. 100 μ L of the supernatant was applied in the immunoassay.

Statistical Analysis

GraphPad Prism 7.0, 8.3.1 and 9.3.1 software (GraphPad Software) were used for statistical analysis. Unless otherwise stated, the data were expressed as mean \pm S.E.M. Periorbital allodynia measurements were assessed using a repeated measure two-way ANOVA to analyze differences between treatment groups over time with a Bonferroni test applied *post hoc*. Molecular studies were compared by unpaired t-test or one-way ANOVA, as indicated. Differences were considered significant if $p \leq 0.05$.

4.3 Results

4.3.1 Cortical Spreading Depression Increases Expression of HSP90 in the PAG of Rats 90 Minutes Post KCl Injection

First, we determined if cortical injection of aCSF or KCl to induce CSD altered HSP90 expression in regions of the brain associated with CSD events, headache, or both; the cortex (Ct. V1M), PAG, and TG. Female rats were injected via dural canula with either a 0.5 μ L cortical injection of 1 M KCl to induce CSD or aCSF control[7], followed by tissue harvest at 30-, 90-, and 180-minute post cortical injection. Western blot detection of HSP90 protein was not changed by KCl injection in the Ct. V1M (CSD induction point) and TG (dural activation by injection) at any time point taken (**Figure 20 A and C**). In contrast, PAG detection of HSP90 was statistically higher 90 minutes post KCl injection as compared to aCSF control (**Figure 20 B**). Interestingly this time point is when peak facial allodynia is observed in this model in previous studies [7, 188].

Figure 20

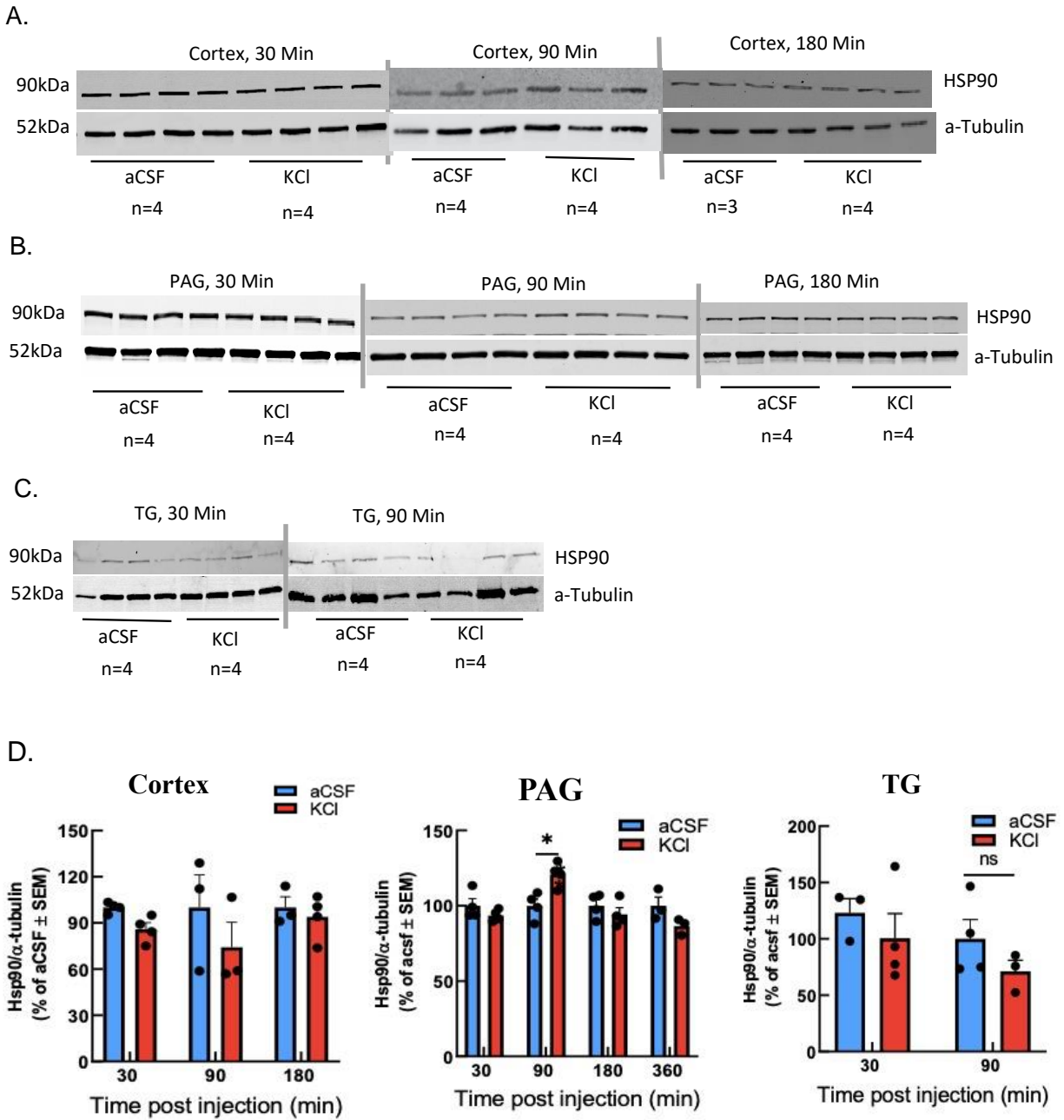


Figure 20. Total expression of HSP90 in key brain regions associated with CSD post cortical injection of aCSF or KCl. Brain tissue was harvested from regions of the brain associated with CSD pain for western blot at different timepoints post aCSF or KCl injection A) Western blot of Cortex 30-,90-, and 180-minutes post aCSF or KCl injection B) Western blot of PAG 30-,90-, 180-, and 360-minutes post aCSF or KCl injection. C) Western blot of TG 30- and 90-minutes post aCSF or KCl injection. D) quantification of western blot image; All data represent the % of aCSF relative expression \pm SEM (n = 4). No significant differences were observed in cortex or TG, there was significance observed at 90-minutes post KCl-treated samples when compared to aCSF in PAG showing increased HSP90 expression. *Denotes significantly different ($p < 0.05$), as assessed by one-way ANOVA.

4.3.2 Periorbital Allodynia Associated with Cortical Spreading Depression is Mitigated by 24-hour Pretreatment with HSP90 Inhibitor 17-AAG

Using the HSP90 inhibitor 17-AAG, we investigated the role of HSP90 in CSD-associated periorbital allodynia [7, 188]. 5 μ L of 0.5nmol of 17-AAG was applied to the dura (24h pre-KCl injection) [123, 170] and a 5 nmol suprathreshold dose. This route was chosen to limit systemic side effects and localize mechanism of action to the dura and brain since 17-AAG has been noted to cross the blood barrier [189, 190]. Since headache was a noted symptom of 17-AAG treatment by some patients in clinical trials for cancer [178], we wanted to assess facial allodynia of the rats up to 4 hours post 17-AAG application. Acute application of 0.5 or 5 nmol 17-AAG did not induce periorbital allodynia compared to vehicle groups (**Figure 21A**). The same animals were observed 24-hours post application of 17-AAG or vehicle before aCSF cortical injection, and no periorbital allodynia was observed (**Figure 21 B**). After aCSF injection,

animals receiving the suprathreshold dose of 17-AAG (5 nmol) developed significant periorbital allodynia, whereas the 0.5 nmol did not; these data suggest a dose dependent effect of the HSP90 inhibitor on facial tactile sensitivity (**Figure 21B**). Subsequent experiments using cortical KCl injections to induce CSD used the 0.5 nmol 17-AAG dose.

To determine whether HSP90 inhibition effectively mitigated CSD -associated allodynia, female rats were pretreated with either vehicle or 17-AAG (0.5 nmol) over the dura mater followed by CSD induction with 0.5 μ L of 1 M KCl 24- hours later. In control rats (vehicle-KCl), peak periorbital allodynia was induced by 90 minutes and lasted for 3 hours (**Figure 21C**). Pretreatment with 0.5 nmol 17-AAG significantly attenuated CSD associated periorbital allodynia 90 minutes after KCl injection (**Figure 21C**). Of the animals pretreated with 17-AAG, 4/10 (40%) were classified as sensitive to periorbital probing which was defined as having periorbital withdrawal thresholds < 6g at two or more consecutive timepoints within 120 minutes of the KCl injection (CSD induction); this was a significant reduction from vehicle pretreated animals 11/12 (91.6%) (**Figure 22C**). Together, these data suggest that HSP90 plays a role in cortical KCl induced periorbital allodynia.

Figure 21

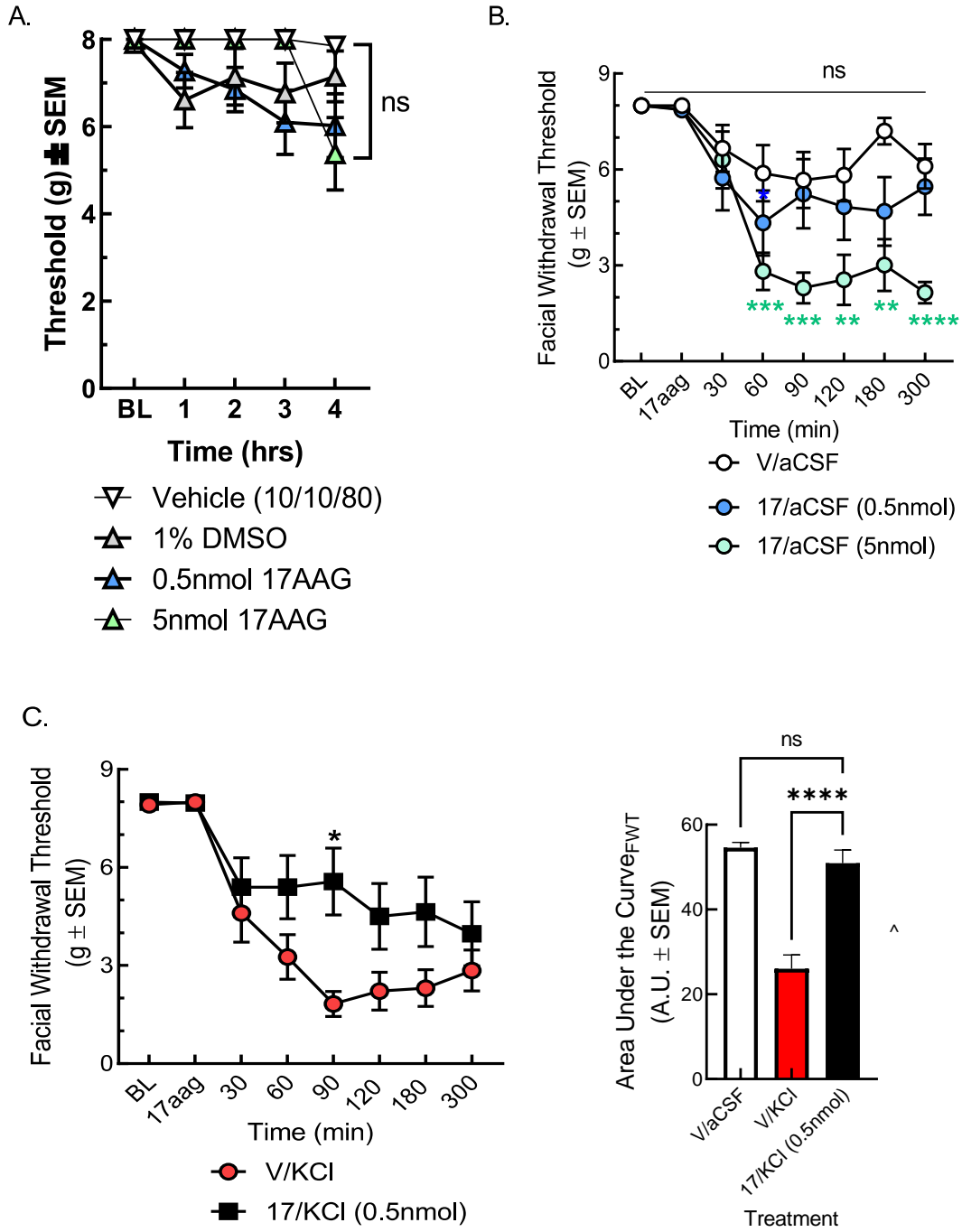


Figure 21. HSP90 inhibition with 17-AAG applied over dura mater alleviates frequency of periorbital allodynia. (A) injection of 17-AAG (0.5 nmol and 5 nmol) or vehicle (1% DMSO in saline or 1:1:8 DMSO/Tween 20/ saline) into canula over dura mater, periorbital Von Frey performed up to 4 hours; no significance (B) 24-hours post 17-AAG (0.5 nmol or 5 nmol) or vehicle application cortical aCSF (0.5 μ L) injected via dural canula, periorbital Von Frey performed up to 5 hours, significant reduction in periorbital threshold observed in 5 nmol 17-AAG/ aCSF group (C) 24-hours post 17-AAG (0.5 nmol) or vehicle (1%DMSO in saline) application cortical 1M KCl (0.5 μ L) injected via dural canula, periorbital Von Frey performed up to 5 hours, significant relief observed at the 90 minute time point in 17-AAG treated group. (D) area under the curve for 17-AAG/KCl vs V/KCl treated groups. Values are the mean \pm SEM (n = 8–10). * p<0.05, ** p<0.01, *** p<0.001, and **** p<0.0001 compared to V/aCSF-treated as assessed by two-way ANOVA; * denotes significantly different (p<0.05) compared to V/KCl group at 90 min timepoint as assessed by two-way ANOVA. Area under the curve analysis * p<0.05, ** p<0.01, *** p<0.001, and **** p<0.0001 compared to 17/KCl treated assessed by one-way ANOVA. Values are the mean \pm SEM (n = 9–11)

4.3.3 Effects of HSP90 Inhibitor 17-AAG on Periorbital Allodynia is Reversed by the Presence of CB1R Antagonist Rimonabant

Previous studies have shown that CB1R is chaperoned to the surface of cells by HSP90 co-chaperone AHA1[191-193]. Given this information, and the fact that CED maybe a critical factor in migraine pain [99, 180], we asked whether the effect of mitigating periorbital allodynia by the HSP90 inhibitor 17-AAG related to CB1R activity. To determine if CB1R has a role in the responders to 17-AAG attenuation of CSD related periorbital allodynia by KCl cortical injection, a separate set of animals were pretreated 24-hours before with 17-AAG as well as with the CB1R inverse agonist/antagonist, rimonabant (1mg/kg) 30 minutes before the KCl cortical injection. Rimonabant increased the number of animals meeting the sensitive inclusion criteria (8/10, 80%) as compared to 17-AAG alone (4/10, 40 %). Further analysis of the majority response/ treatment group showed that blockade of CB1R eliminated the benefit of 17-AAG pretreatment at 90 minutes post KCl injection over the duration of the experiment (**Figure 22A and B**). These data suggest that the pain-relieving effects of HSP90 inhibition during CSD induction works in part by CB1R modification or activity.

Figure 22

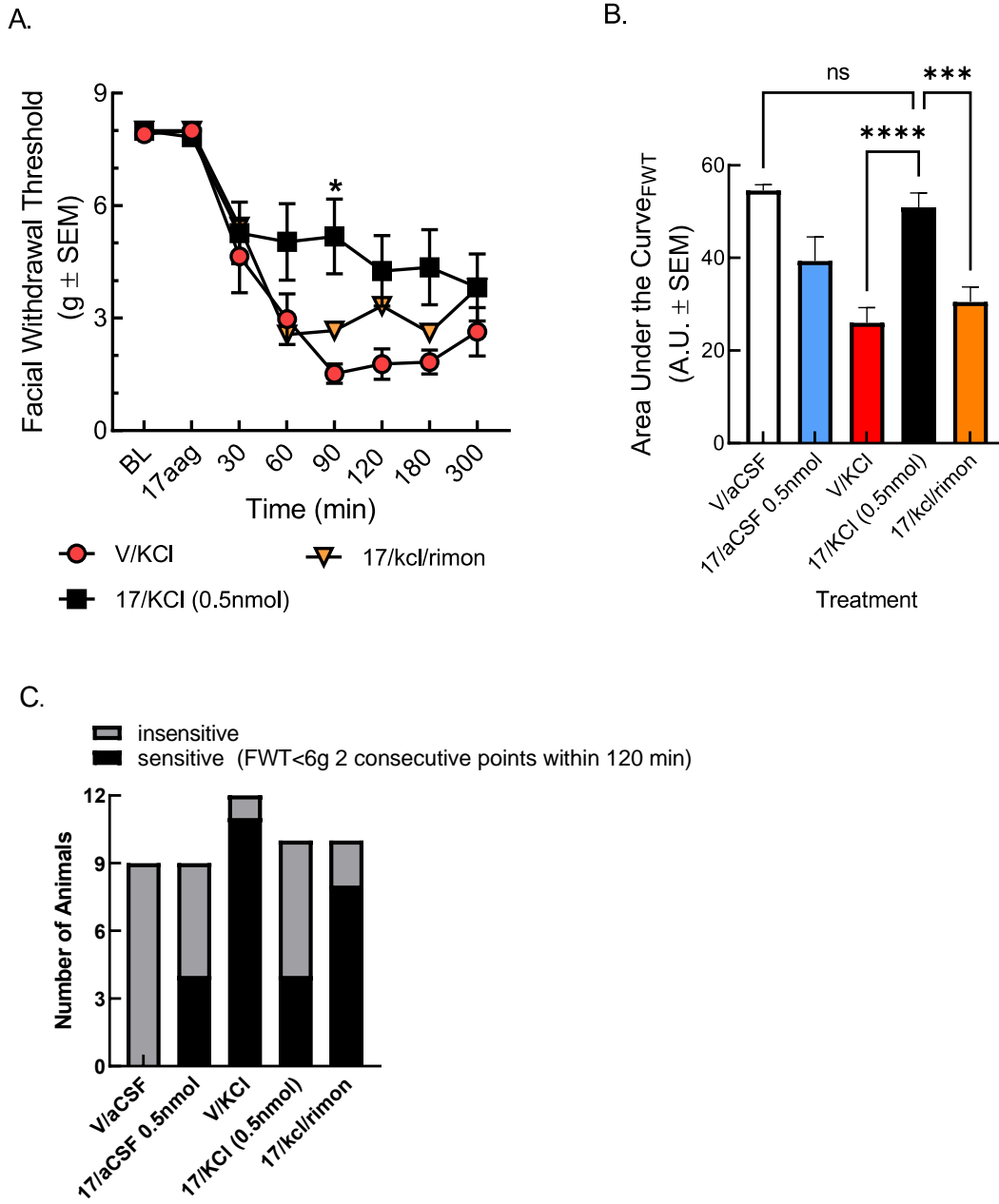


Figure 22. I.P. Injection of CB1R antagonist/ inverse agonist rimonabant blocks antinociceptive effects of 24-hour pretreatment with 17-AAG. (A) 24-hours pre-injection with 17-AAG (0.5 nmol) or vehicle (1%DMSO in saline) followed by rimonabant (1mg/kg) pre-injection 30 minutes before cortical 1M KCl (0.5 μ L) injection via dural canula, periorbital Von Frey performed up to 5 hours; (B) Area under the curve comparing all groups; (C) Number of the KCl and aCSF responder and non-responder animals with various treatments. For facial withdraw threshold values are the mean \pm SEM (n = 9–11). * Denotes significantly different (p<0.05) compared to V/KCl-treated as assessed by two-way ANOVA. Area under the curve analysis * p<0.05, ** p<0.01, *** p<0.001, and **** p<0.0001 compared to 17/KCl treated assessed by one-way ANOVA. Values are the mean \pm SEM (n = 9–11).

4.3.4 Expression Levels of CB1R and AHA1 Were Not Increased in the PAG of Rats 90 Minutes Post KCl or aCSF Injection in Either Vehicle or 17-AAG Pretreated Groups

Since the behavior with HSP90 inhibition and rimonabant pretreatment before KCl injection suggests CB1R activity may play a role in periorbital allodynia associated with CSD, we wanted to investigate CB1R tone as well as AHA1 expression [179] As we originally observed a significant increase of HSP90 protein in the PAG of female rats 90 minutes post KCl injection, we processed and analyzed PAG tissue from female rats pretreated with vehicle or 0.5 nmol 17-AAG 24-hours before CSD induction with KCl, as well as vehicle-KCl or vehicle-aCSF controls. Real time qPCR showed that levels of CNR1 transcript, normalized to aCSF control, were not significantly different between aCSF and KCl vehicle controls. However, 17-AAG did statistically reduce transcript as compared to vehicle in cortical KCl groups ($p=0.051$) (**Figure 23A**). Western blot detection of CB1R and AHA1 protein showed no significant change between 17-AAG and vehicle groups or when compared to aCSF control (**Figure 23B&C**). Despite a change in transcript levels, the lack of change in protein levels of CB1R or AHA1 suggested there may be a change in receptor activity or function.

Figure 23

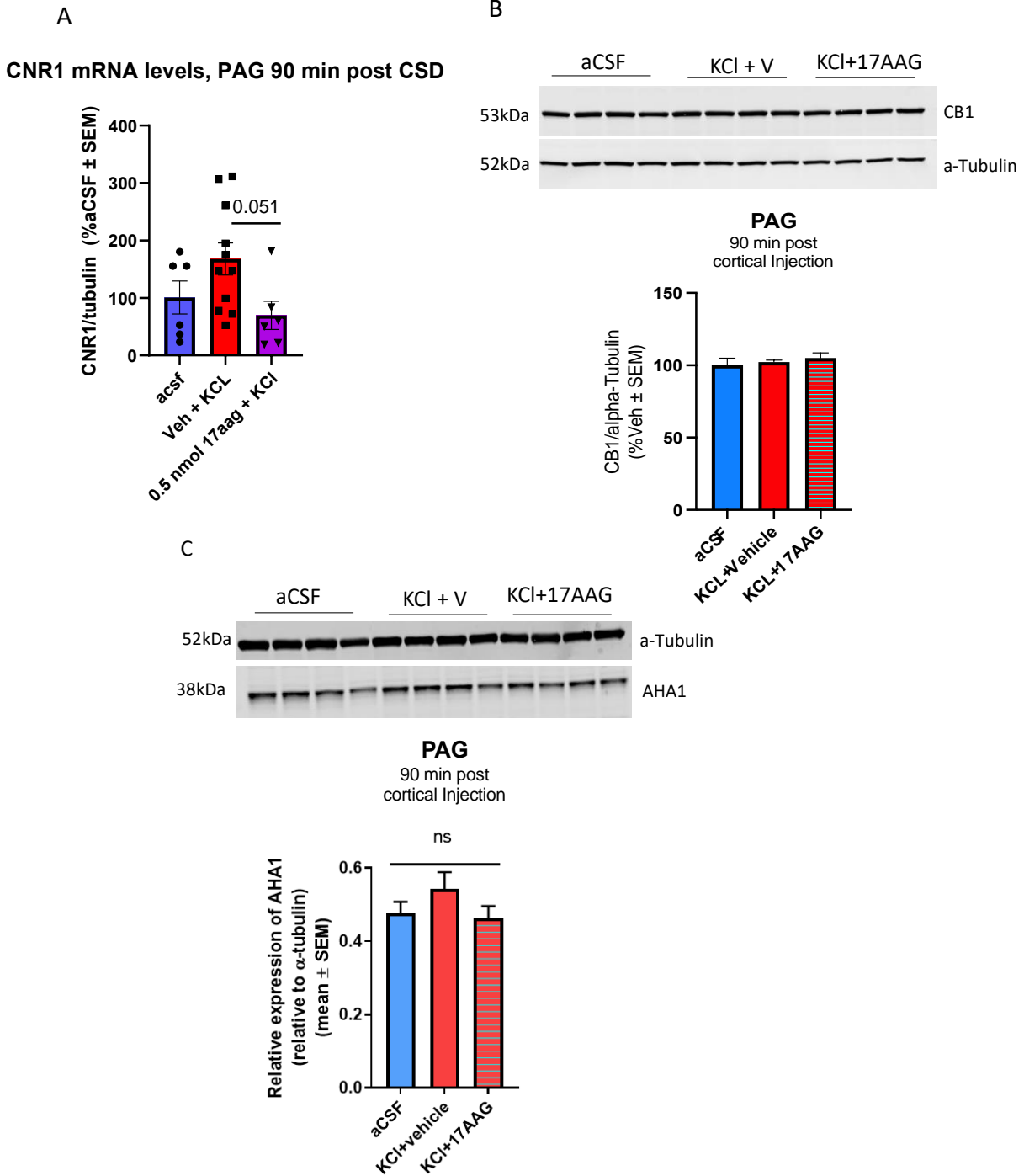


Figure 23. CNR1 mRNA transcript and CB1R along with AHA1 protein levels assessed in 17-AAG pretreated PAG tissue. Brain tissue was harvested from PAG region of the brain after 24-hour pretreatment with 0.5 nmol 17-AAG and 90 minutes post cortical injection of aCSF or 1M KCl (0.5 μ L) **A)** RT-qPCR detection of mRNA transcript for CNR1 which encodes for CB1R; no significant observed between groups as assessed by one-way ANOVA (n=6-11) **B)** Western blot for CB1R protein levels of PAG tissue 90 minutes post aCSF/KCl cortical injection and 24-hour pretreatment with 17-AAG (0.5 nmol) or vehicle (1%DMSO); no significance observed as assessed by one-way ANOVA(n=4). **C)** Western blot for AHA1 protein levels of PAG tissue 90 minutes post aCSF/KCl cortical injection and 24-hour pretreatment with 17-AAG (0.5 nmol) or vehicle (1%DMSO); no significance observed as assessed by one-way ANOVA quantification of western blot image; All data represent total expression of protein/ a tubulin relative expression \pm SEM (n = 4).

4.3.5 GTP γ S Binding in 24-hour Pretreated 17-AAG or Vehicle Rat PAG Tissue 90 Minutes Post KCl or aCSF Injection Using Specific CB1R Agonist PrNMI Reveal Rightward Shift in Potency

To determine if CB1 receptor function in the PAG as changed by HSP90 inhibition a GTP γ S binding assay was performed using PrNMI, a CB1R agonist shown to have high affinity [194, 195]. Female rats were pretreated with 17-AAG or vehicle 24-hours before KCl injection and PAG was harvested 90 minutes post KCl injection. Tissue was also harvested from aCSF control as well as KCl injected rats alone 90 minutes post cortical injection. We performed the assay in agonist mode and antagonist mode side by side utilizing the same sample membrane preparations. For agonist mode with PrNMI (**Figure 24A**), both KCl ($EC_{50} = 0.73\mu\text{M}$) and vehicle KCl ($EC_{50} = 0.88\mu\text{M}$) induced a rightward shift in potency as compared to aCSF ($EC_{50} = 0.31\mu\text{M}$) (**Figure 24B**). Interestingly, we observed further right-ward shift in potency in the group pretreated with 17-AAG ($EC_{50} = 2.1\mu\text{M}$) (**Figure 24B**). There was no significant change in efficacy observed across groups (**Figure 24B**). Antagonist mode using rimonabant (**Figure 24C and D**), confirmed the specificity of PrNMI to CB1R. The right ward shift in potency caused by the pretreatment of 17-AAG suggests the CB1 receptor system in the PAG is being desensitized and/or occupied leading to less receptor availability for functional activity.

Figure 24

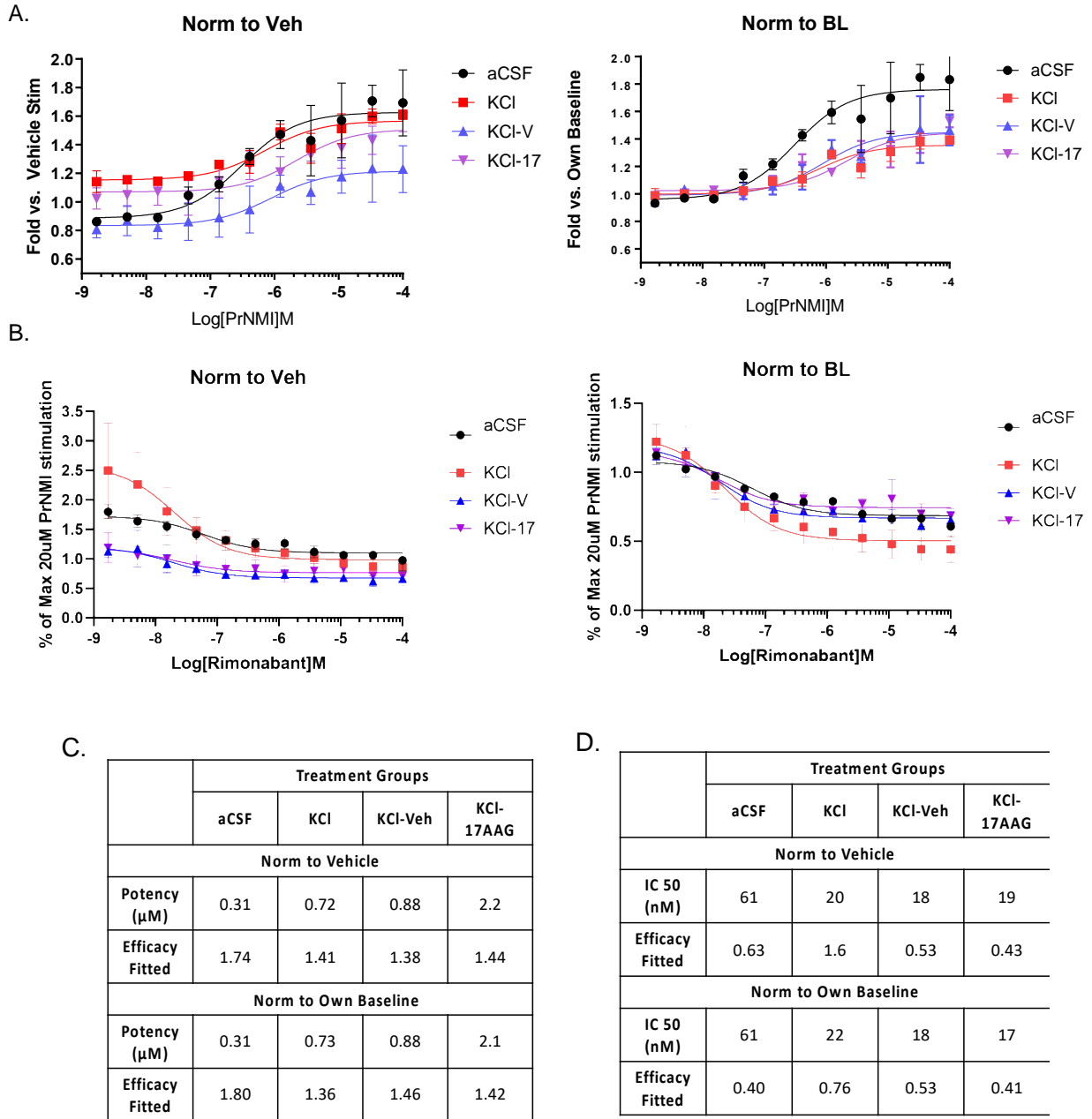


Figure 24. ³⁵S-GTP γ S coupling assay using PrNMI for CB1R functionality and CB1R competitive antagonist rimonabant with agonist PrNMI to validate CB1R specificity in PAG tissue 90 min post acsf/KCl injection and with vehicle or 17-AAG pretreatment. (A). CB1R specific compound PrNMI used in agonist mode and **(B)** specific compound PrNMI used along with antagonist rimonabant in antagonist mode on PAG tissue harvested 90 minutes post cortical aCSF or KCl injection as well as vehicle (1%DMSO in saline) or 17-AAG (0.5 nmol) 24-hour pretreatment followed by KCl injection and harvest 90 minutes after. PrNMI is a full CB1R agonist, which was used at increasing concentration up to 100 μ M producing curves using the ³⁵S-GTP γ S assay (see Methods). N = 3 independent experiments performed, with summary curves shown. **(C)** Potency (EC50) and efficacy (EMAX) were calculated separately for each experiment and reported as the mean \pm SEM. PrNMI showed decreased potency in KCl groups and a further decrease in the 17-AAG pretreated KCl group but not change in efficacy, suggesting receptor system could be desensitized and there may be a loss in the receptor pool, or they are occupied causing a competitive antagonist effect. **(B)** PrNMI is a full CB1R agonist, which was used at 20 μ M concentration and rimonabant, a competitive antagonist/inverse agonist, specific for CB1R was used at multiple increasing concentrations to produce curves using the ³⁵S-GTP γ S assay (see Methods). N = 3 independent experiments performed, with summary curves shown. **(D)** Potency (IC50) and efficacy (EMAX) were calculated separately for each experiment and reported as the mean \pm SEM. Rimonabant decreased stimulation by PrNMI at increasing concentrations showing that it was competing away PrNMI at the CB1R validating PrNMI specificity.

4.3.6 CSD Affects Endocannabinoid Lipid Levels in a Region-specific Manner 90 Minutes Post KCl, and 24-hour Pretreatment with 17-AAG Increases AEA Lipid Levels in PAG 90 Minutes Post KCl Injection

The GTP γ S functional assay suggests decrease receptor function activity which could be due to a change in the levels of endogenous lipid neurotransmitters 2-AG and AEA. The tissue samples harvested 90 minutes post KCl or aCSF cortical injection were subject to lipid extraction process to be analyzed via liquid chromatography/mass spectrometry combination (LCMS). Cortical injection of KCl significantly and selectively reduced 2-AG levels within the PAG but not the Ct. V1M, TG, or trigeminal nucleus caudalis (Vc) (**Figure 25A**). AEA levels were unchanged in any region (**Figure 25B**). 24-hour pretreatment with 0.5 nmol 17-AAG onto the dura mater did not restore 2-AG levels (**Figure 25C**), however AEA levels in the PAG 90 minutes post KCl injection were significantly increased compared to vehicle (**Figure 25D**). These results show that pretreatment with 0.5 nmol 17-AAG increases endogenous lipid AEA levels in the PAG 90 minutes post KCl injection.

Figure 25

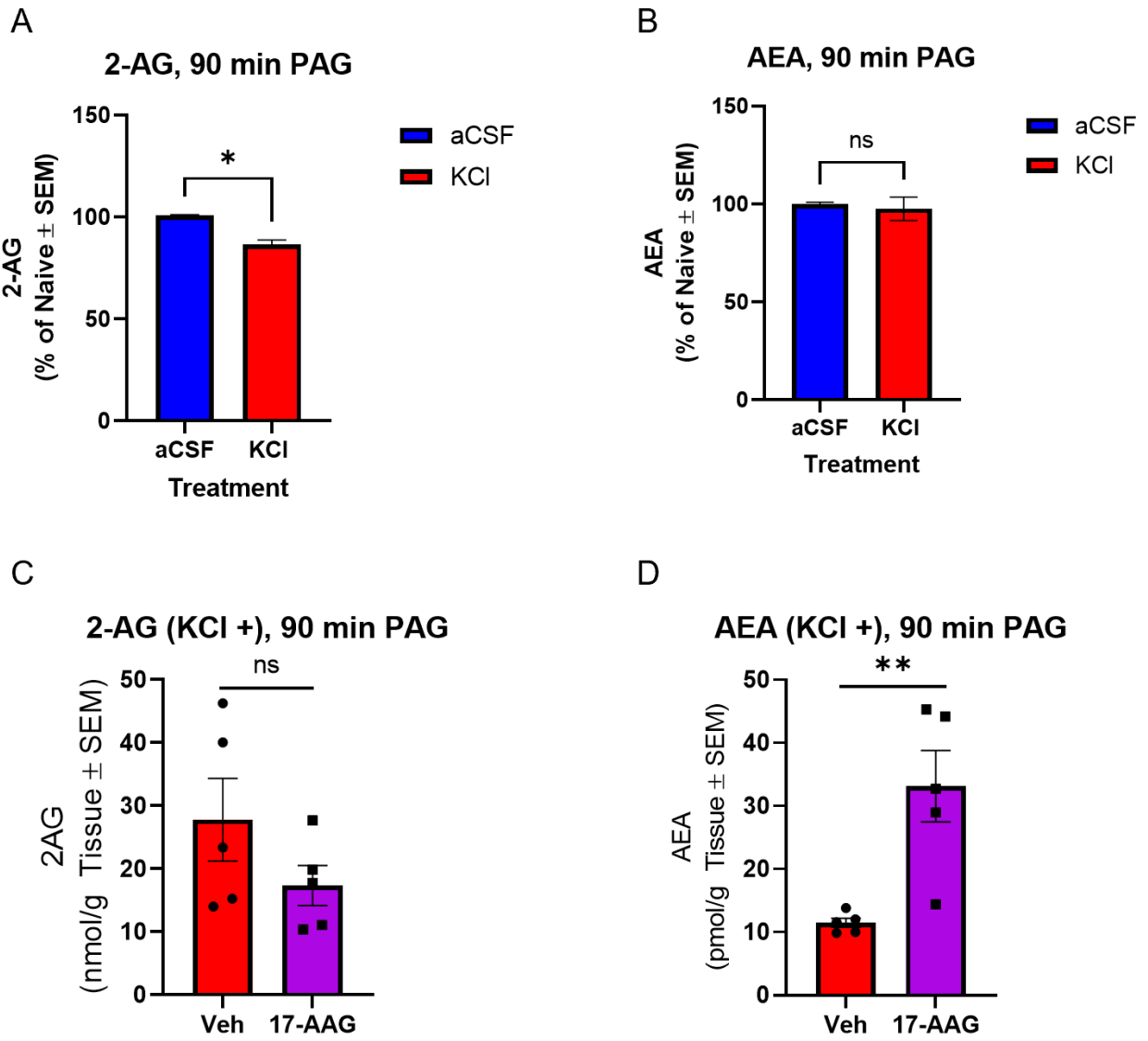


Figure 25. Reduction in 90-minute PAG tissue of eCB levels after CSD in female rats, 17-AAG pre-treatment increases eCB levels in CSD induced rats. (A) Tissue samples were collected at different time-points 90 minutes after cortical injections. (A) Decreased level of 2-AG was detected only in PAG at 90 min after KCl injection as compared to aCSF (2-AG: aCSF vs KCl $p=0.0196$ as assessed by unpaired t-test. (B) AEA levels were not significantly different between aCSF and KCl groups in this region. (AEA: aCSF vs KCl 90 min: $p=0.3331$), Values are expressed as % of naive \pm SEM ($n=3-6$ /condition). ns=non-significant. $*p<0.05$ aCSF vs. KCl. (C) 2-AG levels were not significantly different in vehicle (1%DMSO)/KCl treated female rats compared to 24-hour pretreated 17-AAG (0.5 nmol) treated group as assessed by unpaired t-test. (D) Significant increase of AEA levels were detected in 24-hour 17-AAG (0.5 nmol) pretreated KCl group compared to vehicle (1% DMSO) pretreated KCl group 90 min post cortical injection. Values are expressed as total concentration of eCB \pm SEM ($n=5$ /condition). ns=non-significant

4.3.7 FAAH but not HSP70 Expression in Rat PAG 90 Minutes Post KCl Induction is Affected by 17-AAG Pretreatment

The next experiments were designed to understand how AEA levels were elevated after application of 17AAG. AEA levels are primarily controlled by the degradative enzyme FAAH, in the PAG. As compared to aCSF, KCl injection alone significantly reduced detection of FAAH protein in the PAG by ~ 43%. 17AAG pretreatment significantly and further reduced FAAH levels to 70% of aCSF controls (**Figure 26B**).

In addition to regulation of absolute levels, 17-AAG application is reported to upregulate heat shock protein 70 (HSP70) which, in turn can increase intracellular lipid trafficking, including AEA [99, 196]. In tissue harvested from female rats pretreated with 17-AAG (0.5 nmol) or vehicle followed by injection of KCl for CSD induction, 90 minutes post KCl injection, no difference was observed across groups in protein detection levels of HSP70 (**Figure 26A**). These data indicate that HSP70 expression is not changed in the PAG by 17-AAG application. Together these data suggest that 17AAG increases AEA levels via a FAAH inhibition but not through HSP70.

Figure 26

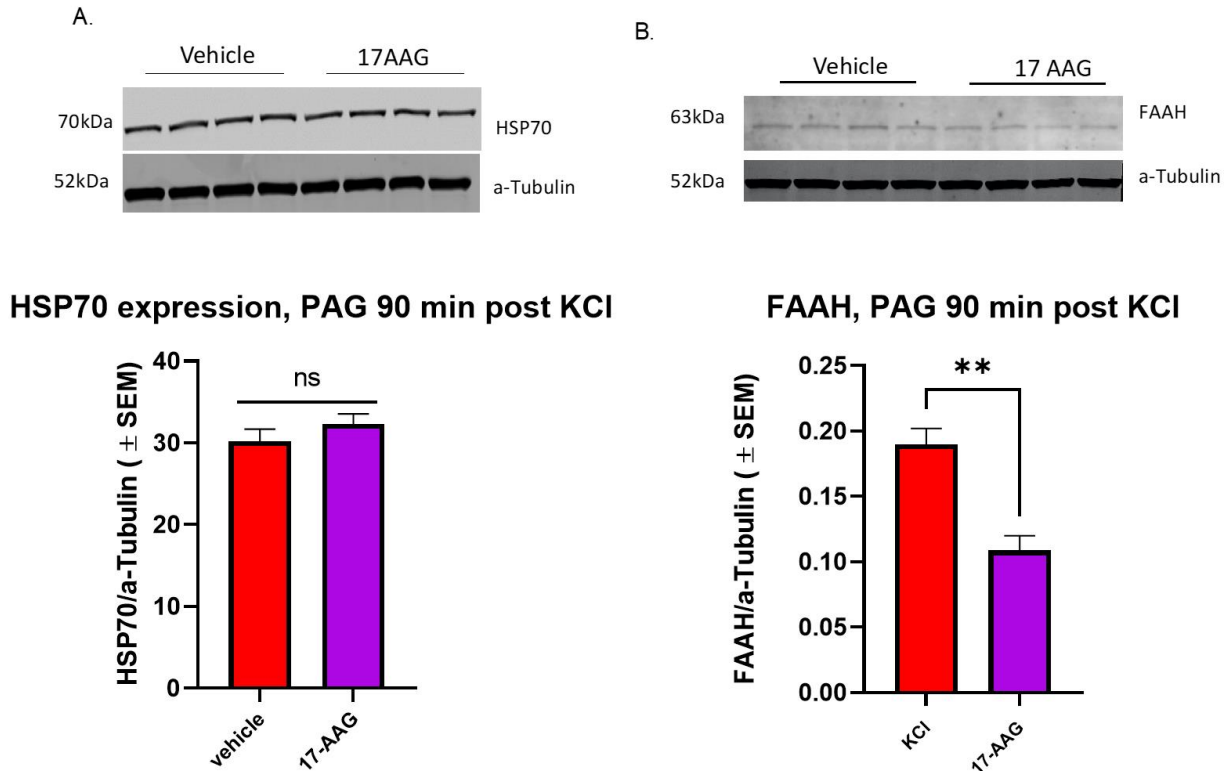


Figure 26. FAAH and HSP70 protein levels assessed in PAG of 17-AAG pretreated female rats followed by KCl induced CSD. Brain tissue was harvested from PAG region of the brain after 24-hour pretreatment with 0.5 nmol 17-AAG and 90 minutes post cortical injection of aCSF or 1M KCl (0.5 μ L). **(A)** Western blot for HSP70 protein levels of PAG tissue 90 minutes post aCSF/KCl cortical injection and 24-hour pretreatment with 17-AAG (0.5 nmol) or vehicle (1%DMSO); no significance observed as assessed by one-way ANOVA(n=4). **(B)** Western blot for FAAH protein levels of PAG tissue 90 minutes post aCSF/KCl cortical injection and 24-hour pretreatment with 17-AAG (0.5 nmol) or vehicle (1%DMSO); significant reduction of FAAH detection observed. * * $p<0.01$ veh/KCl vs. 17-AAG/KCl as assessed by one-way ANOVA quantification of western blot image; All data represent total expression of protein/ a tubulin relative expression \pm SEM (n = 4).

4.3.8 CSD Induction Promotes Neuroinflammation in the PAG in a Time Dependent Manner

Given our previous results showing that 2-AG levels are reduced in the PAG in animal models of headache at times of peak periorbital allodynia [116], we investigated whether CSD induction by cortical injection of KCl altered PGE2 and neuroinflammation within the PAG. We measured PGE2 by ELISA and neuroinflammation biomarkers by Western blot. PGE2 levels in the PAG were similar between aCSF and KCl injected samples 90 min after cortical injection; notably PGE2 levels were higher in samples taken 180 min after cortical KCl injection versus aCSF controls (**Figure 27A**). The microglial marker, Iba-1, was statistically higher in PAG samples from KCl rats as compared to aCSF injected controls within 30 min of injection and remained elevated for 180 min (**Figure 28A**). The astrocyte marker, GFAP, was increased by 90 min (**Figure 28B**) in PAG from KCl injected rats and remained higher 180 min post-injection ($p=0.03$) as compared to aCSF rats; there was not statistical interaction between time and injury ($F(2,8) = 2.734, p=0.13$). Together, these results indicate that CSD induction produces time-dependent neuroinflammation within the PAG.

Figure 27

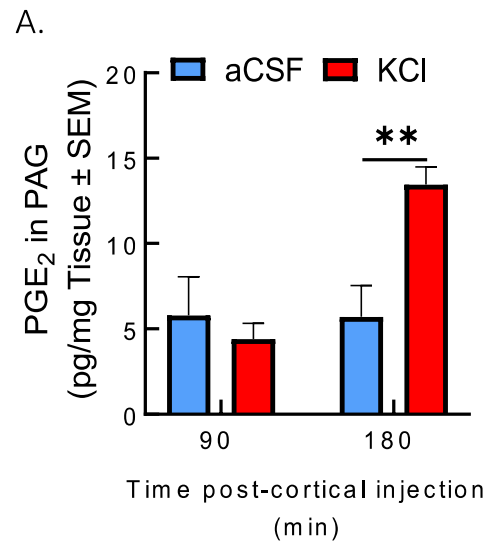


Figure 27. Elisa for prostaglandin E2 in PAG tissue collected post CSD induction. Brain tissue was harvested from PAG region of the brain 90- and 180- minutes post cortical injection of aCSF or 1M KCl (0.5 μ L). (A) Elisa for PGE₂ lipid levels in PAG, there was no significant difference between aCSF and KCl injection 90 min post; However, there was a significant increase 180 minutes post KCl injection. (two-way RM ANOVA time x cortical injection $F(1,8)=10.08$, Bonferroni post-hoc $p=0.009$). (n=2-4/condition) * $p<0.05$, ** $p<0.01$, KCl vs. aCSF as assessed by two-way ANOVA with Bonferroni post-test

Figure 28

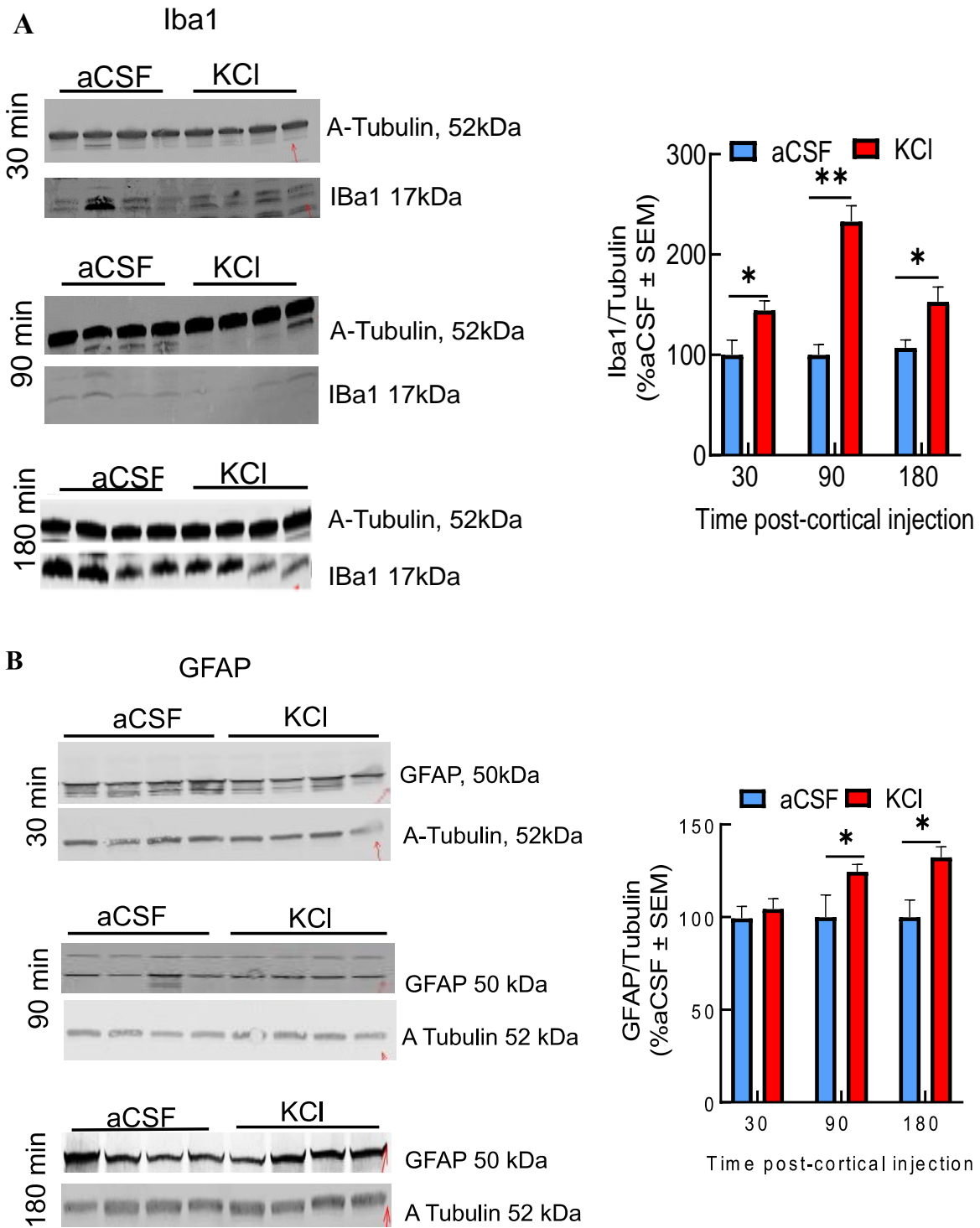


Figure 28. Neuroinflammatory associated markers increased post CSD. Neuroinflammatory markers Iba1 and GFAP were measured in PAG samples harvested at 30, 90, and 180 min after cortical injection of KCl or aCSF by Western immunoblotting (A, B) Relative expression of Iba1 in PAG was significantly increased at 30, 90, and 180 min after injection of KCl compared to aCSF control (two-way RM ANOVA time x cortical injection $F(1,8)=10$). Data are expressed as % of aCSF control \pm SEM (n=3-4/condition). The expression of GFAP was elevated at 90 and 180 min post-KCl compared to aCSF control (two-way RM ANOVA injury $F(1,6)=8.773$, $p=0.025$; $p=0.044$). Data represent % of aCSF control \pm SEM (n=3-4/condition). Experiment performed by Dr. Erika Liktor-Busa

4.4 Conclusion

The studies above support a role for HSP90 in periorbital allodynia associated with CSD induction via dysregulation of the endocannabinoid system within the PAG specifically. Pharmacological inhibition of HSP90 with 17-AAG influences changes in AEA levels to alleviate headache like behaviors in a rodent model. The role of HSP90 in facial pain related to CSD may be to facilitate post translation activity such as phosphorylation of the enzyme FAAH. Increasing activity of FAAH can lead to increased AEA breakdown. There was also a significant increase of PGE2 measured through ELISA observed post KCl injection suggesting an increase of neuroinflammation in the PAG post CSD induction. PGE2 is a metabolite of AEA breakdown suggesting FAAH activity. Western blot data from tissue taken from the PAG showed a significant increase in protein detection of Iba1 and GFAP associated with microglial cells and astrocytes which are known inflammatory mediators in the brain suggesting increased activity of lipid hydrolysis enzymes. These novel observations support a role for HSP90 in migraine pain and development of new therapeutic approaches targeting HSP90 or its associative chaperones to treat headache disorder

Figure 29

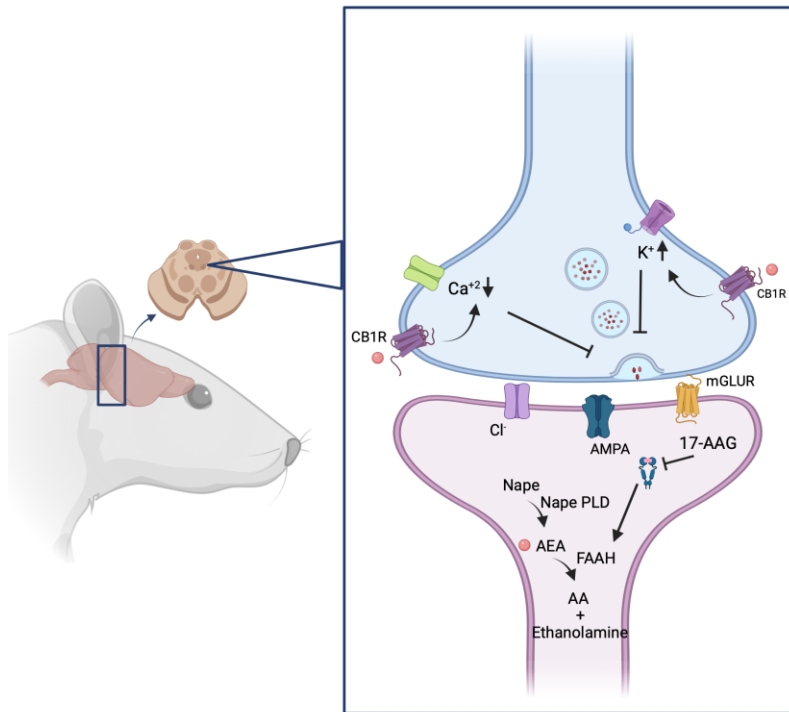


Figure 29. Summary of HSP90 interaction to increase AEA in PAG. Brain tissue was harvested from PAG region of the brain after 24-hour pretreatment with 0.5 nmol 17-AAG and 90 minutes post cortical injection of 1M KCl (0.5 μ L). There was a rightward shift in potency of CB1R function indicating desensitization implicating increased use of the receptor. There was increased AEA levels in 17-AAG treated animal tissues compared to vehicle post 90 minutes post CSD induction. There were reduced levels of FAAH enzyme protein levels suggesting HSP90 may facilitate its activity and consequently HSP90 inhibition interferes with its function decreasing its activity.

**CHAPTER 5: ENDOGENOUS 2-AG LEVELS IN
THE BRAIN INFLUENCE FACIAL ALLODYNIA
AND BLOOD-BRAIN BARRIER INTEGRITY**

5.1 2-AG Levels in the Brain Influence Facial Allodynia and Blood-brain Barrier Integrity

5.1.1 Introduction

The endocannabinoid system (ES) plays an essential role in both central and peripheral pain processing [197]. Anandamide (AEA) and 2-arachidonoylglycerol (2-AG), the two main endocannabinoid lipids, are produced by N-acyl phosphatidylethanolamine phospholipase D (NAPE-PLD) and diacylglycerol lipases (DAGLs). Both AEA and 2-AG differentially activate the G protein-coupled cannabinoid receptors, CB1R and CB2R [105]. AEA is predominantly hydrolyzed by fatty acid amide hydrolase (FAAH). Monoacylglycerol lipase (MAGL) and α,β -hydrolase domain containing 6 (ABHD6) enzymes are responsible for hydrolysis of 2-AG [105].

Currently there is evidence supporting Clinical Endocannabinoid Deficiency (CED) as playing a role in the pathophysiology of functional pain disorders, including migraine [99, 180, 182, 198]. For example, AEA levels and FAAH activity are reduced in the cerebrospinal fluid of patients suffering from chronic manifestation of migraine or medication overuse headache [199-201]. While increasing AEA tone was a promising therapeutic approach to reduce migraine [182], the recent failure of a FAAH inhibitor (BIA 10-2474) in Phase I human clinical trials has questioned the safety of this approach [202-204]. Initial evidence using the non-selective MAGL inhibitor (URB602) in a rodent model of migraine induced by the administration of nitroglycerine proposes that targeting MAGL might reduce migraine triggered pain [99]. Yet targeting the hydrolysis of 2-AG via ABHD6 has been understudied to date.

Based on this premise and our data showing a reduction in PAG 2-AG levels, we set out to define the efficacy of ABHD6 inhibitors in a migraine with aura model involving CSD induction on periorbital allodynia and the associated receptor mechanisms; studies also investigated the role of 2AG reduction on BBB integrity under CSD like conditions.

5.1.2 Methods and Materials

Drugs and reagents:

Ketamine/xylazine was purchased from Sigma-Aldrich (St. Louis, MO) and isoflurane from VetOne. (IL, USA). MJN110, KT-182, SR141617 (Rimonabant), and SR144528 were purchased from Cayman Chemicals (Ann Arbor, MI). All other chemicals, unless noted were purchased from Sigma-Aldrich (St. Louis, MO).

Animals

Adult, intact, female Sprague Dawley rats (200-250 g) were purchased from Envigo (Indianapolis, IN) and housed in a climate-controlled room on a regular 12/12 h light/dark cycle with lights on at 7:00 am with food and water available *ad libitum*. Animals were initially housed 3 per cages but individually housed after the dural cannulation. All procedures were performed during the 12-h light cycle and according to the policies and recommendations of the International Association for the Study of Pain and the NIH guidelines for laboratory animals, and with IACUC approval from the University of Arizona. Justification for animal numbers was consistent with NIH policy (NOT-OD-15-102), and experiments were randomized to blinded treatment groups to give 80% power to detect a treatment effect size of 20% compared to a baseline response of 5% at a significance level of 0.05 [142, 184]. Numbers required to achieve statistical power were determined by G.Power3.1. Female rats were used as headache disorders affect females to males at a nearly 3:1 ratio [185, 186, 205]. The stage of estrus cycle was not determined in this study.

Dural cannulation

Dural cannulation was performed as previously described [7, 139, 145]. Briefly, anesthesia was induced with intraperitoneal 45:5:2 mg/kg cocktail of ketamine:xylazine:acepromazine. Rats were placed in a stereotactic frame (Stoelting Co.), and a

1.5- to 2-cm incision was made to expose the skull. A 0.66- to 1-mm hole (Pinprick/KCl: -6 mm A/P, -3 mm M/L from bregma) was made with a hand drill (DH-0 Pin Vise; Plastics One) to carefully expose, but not damage, the dura. A guide cannula (0.5 mm from top of skull, 22 GA, #C313G; Plastics One) was inserted into the hole and sealed into place with glue. Two additional 1 mm holes were made caudal to the cannula to receive stainless-steel screws (#MPX-080-3F-1M; Small Parts), and dental acrylic was used to fix the cannula to the screws. A dummy cannula (#C313DC; Plastics One) was inserted to ensure patency of the guide cannula. Rats were housed individually and allowed 6–8 d to recover. Cannula placement and dural integrity at screw placement was confirmed postmortem.

Cortical injections

Cortical injections were performed using a Hamilton injector (30 GA, #80308 701 SN, Hamilton Company) customized to project 1.0 mm into the beyond the dura into the occipital cortex. The injector was inserted through the guide cannula to deliver a focal injection of 0.5 μ l of 1 M KCl or artificial CSF (aCSF) into the cerebral cortex. aCSF was comprised of 145 mM NaCl, 2.7 mM KCl, 1 mM MgCl₂, 1.2 mM CaCl₂, and 2 mM Na₂HPO₄ (pH 7.4), and the solution was passed through a 0.2- μ m syringe filter before injection. Cortical injection was always considered at t = 0 min.

Pre-or postcortical injection treatments

KT-182, the selective ABHD6 inhibitor, was injected intraperitoneally (2mg/kg, IP) 3 h before (t = -3h) or 30 min after (t = +30min) cortical injection of KCl. KT-182 was dissolved in ethanol-cremaphore-saline (1:1:18, v/v/v). Rimonabant (1mg/kg, IP) or SR144528 (1mg/kg, IP) were administer 30 min before KT-182 in receptor dependency studies.

Periorbital mechanical allodynia

Periorbital allodynia was evaluated before and after cortical injection ($t = 30, 60, 90, 120, 180, 360$ min, and 24 h) by an observer blinded to drug condition. Rats were grouped based on their postsurgical baseline to ensure equivalent pre-injection thresholds (6-8 g). Any rats exhibiting excessive postsurgical allodynia (threshold <6 g) were removed from the study. Rats were acclimated to testing box 1 h prior to evaluation of periorbital mechanical allodynia with calibrated von Frey filaments as previously described by Edelmayer and coworkers [140, 141]. Behavioral responses were determined by applying calibrated von Frey filaments perpendicularly to the midline of the forehead at the level of the eyes with enough force to cause the filament to slightly bend while held for 5 sec. A response was indicated by a sharp withdrawal of the head, vocalization, or severe batting at the filament with attempts to bite it. The withdrawal threshold was determined using a modified version of the Dixon up-down method

***In situ* Brain Perfusion**

In situ perfusion studies were carried out in female Sprague-Dawley rats (200-250 g) as previously described by our group at 120 minutes post vehicle or LEI106 (40mg/kg) I.P. injection [188]. Briefly, rats were anesthetized with ketamine/xylazine and heparinized (10,000 U/kg i.p.). Body temperature was maintained at 37°C using a heating pad. The common carotid arteries were cannulated with silicone tubing connected to a perfusion circuit then perfused with an erythrocyte-free modified mammalian Ringer's solution (117 mM NaCl, 4.7 mM KCl, 0.8 mM MgSO₄, 1.2 mM KH₂PO₄, 2.5 mM CaCl₂, 10 mM D-glucose, 3.9% (w/v) dextran (MW. 60,000), and 1.0 g/L bovine serum albumin (type IV), pH 7.4), warmed to 37°C and oxygenated with 95% O₂/5% CO₂. Evan's blue dye (55 mg/L) was added to the perfusate to serve as a visual marker of BBB integrity. Perfusion pressure and flow rate were maintained at 95-105 mmHg and 3.1 mL/minute respectively. Both jugular veins were severed to allow for drainage of the

perfusate. Using a slow-drive syringe pump (0.5 mL/minute per hemisphere; Harvard Apparatus, Holliston, MA), ^{14}C -sucrose (0.5 $\mu\text{Ci/ml}$) was added to the inflowing perfusate. Following a 15-minute perfusion, the rats were decapitated, and the brains was removed. The meninges and choroid plexus were excised, and cerebral hemispheres were sectioned and homogenized. TS2 tissue solubilizer (1 mL) was added to each tissue sample and the samples were allowed to solubilize for 2 days at room temperature. To eliminate chemiluminescence, 100 μl of 30% glacial acetic acid was added, along with 2 mL Optiphase SuperMix liquid scintillation cocktail (PerkinElmer, Boston, MA). Samples were measured for radioactivity on a model 1450 liquid scintillation counter (PerkinElmer).

Cell Culture

The bEnd.3 (CRL-2299, ATCC) cell line was used for in vitro experiments, cultured as described in Liktor-Busa et al. [145]. Cells were treated with 100 mM KCl for 5 minutes, which is a typical condition to evoke potassium-triggered spreading depolarization in live brain slices [142]. 1 mM LEI106 was made up in 10% DMSO, 10% tween 20, and 80 % saline then diluted in DMEM to 300 μM concentration and applied apically to bEnd.3 cells for 15 minutes prior to KCl exposure or TEER readings.

Trans endothelial electrical resistance (TEER)

TEER is an established method of evaluating endothelial cell barrier integrity which captures active and passive breaches in vitro [172]. TEER was assessed via two-electrode chopstick method (EVOM2), as described [100] at the following timepoints immediately post-pulse: 10, 20, 30, 60, 120, 180 minutes and 24 hours after replacement of abluminal media.

Tissue harvest

Rats were anesthetized with ketamine/xylazine mix as described above, then transcardially perfused with ice cold 0.1 M phosphate buffer at flowrates to not burst microvasculature (i.e., 3.1ml/min). After decapitation, periaqueductal grey (PAG) were harvested, flash frozen in liquid nitrogen and stored at -80°C until further use

Membrane Preparation

Flash frozen tissue was thawed on ice, dounce homogenized in ice cold lysis buffer (20 mM HEPES, 1 mM MgCl₂, 2 mM DTT, 10 units/ml benzonase) and centrifuged at 100,000 x g for 45 min (Beckman Coulter rotor Ti55). The supernatant was discarded, and the pellet was resuspended in buffer HEPES (20mM) supplemented with DTT (2 mM). Protein concentration of samples was determined (DC protein assay, Bio-Rad) before aliquoting and flash freezing samples in liquid nitrogen. Samples were stored at -80 until further use.

Western- Immunoblotting

Samples were thawed on ice, 25 µg of protein was loaded on a 10% pre-cast polyacrylamide gel (Mini-PROTEAN TGX™, Biorad) and then transferred to a PVDF membrane (Immobilon-PSQ, Sigma Aldrich). After transfer, membranes were blocked with 5% milk in tris-buffered saline with 0.05% TWEEN-20 (TBST) for one hour at room temperature. Following blocking, membranes were incubated overnight at 4°C in primary antibodies (ABHD6 (g, MAGL (ab77398, Abcam) diluted in blocking buffer. The membranes were then washed three times with TBST, incubated with secondary antibodies (goat-anti-mouse IgG-HRP and donkey anti-goat secondary IgG-HRP (Santa Cruz)) for one hour at room temperature, then washed with TBST three more times. Membranes were then incubated in enhanced chemiluminescent substrate (SuperSignal West Femto Maximum Sensitivity Substrate, ThermoFisher Scientific) for one minute at room temperature and detected using Chemidoc MP

(Bio-Rad). The membranes were stained with Ponceau S (G Biosciences) to obtain total protein. Analysis was done using ImageJ.

Statistical Analysis

GraphPad Prism 7.0 and 8.3.1 software (GraphPad Software) were used for statistical analysis. Unless otherwise stated, the data were expressed as mean \pm S.E.M. Periorbital allodynia measurements were assessed using a repeated measure two-way ANOVA to analyze differences between treatment groups over time with a Bonferroni test applied *post hoc*. Molecular studies were compared by unpaired t-test or one-way ANOVA, as indicated. Differences were considered significant if $p \leq 0.05$.

5.1.3 Results

5.1.3.1 Inhibition of 2-AG degradation by ABHD6 prevents and reverses CSD induced periorbital allodynia in CBR -independent and -dependent manners, respectively

The first investigation asked whether ABHD6 played a functional role in the induction of CSD associated periorbital allodynia, using the brain-penetrant inhibitor KT-182 [206]. Dosing with KT-182 (2 mg/kg, IP) 3h before cortical KCl injection significantly prevented the development of facial tactile allodynia for up to 360 min (**Figure 30A**). Application of CB1R or CB2R antagonist did not block these effects (**Figure 30B & C**). In the reversal paradigm, KT-182 (2mg/kg, IP) dosed 30 min after CSD induction by cortical KCl significantly reversed established periorbital allodynia (**Fig 31A**). This effect was significantly attenuated by both CB1R antagonism with SR141617 (1 mg/kg, IP) and SR144528 (1 mg/kg, IP), respectively at discrete time points (**Figure 31B**); the dominating effect was by CB1R (**Figure 31C**). Together, these data suggest that ABHD6 activity controls CSD associated cephalic allodynia through both CBR-dependent and independent mechanisms.

Figure 30

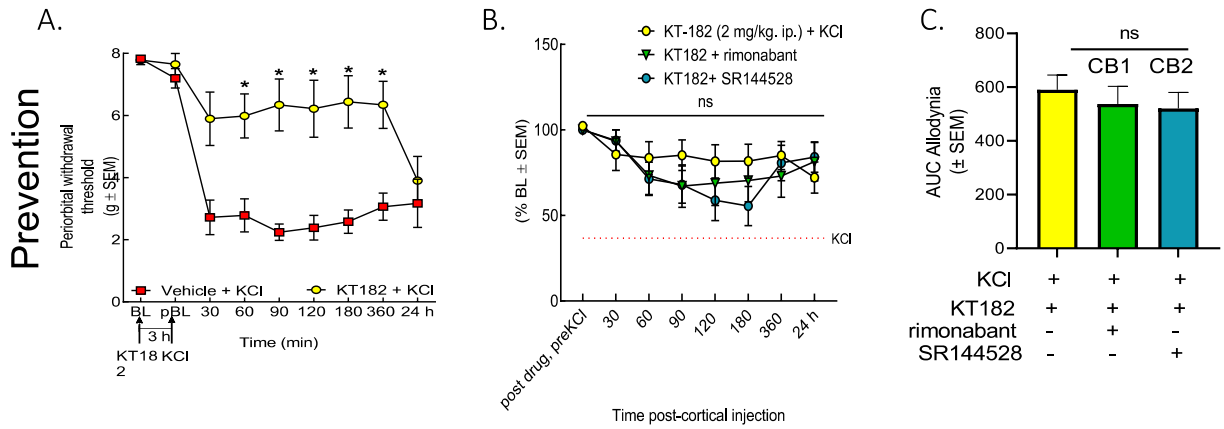


Figure 30. Pharmacological inhibition of ABHD6 during CSD prevention paradigm.

Periorbital withdrawal threshold determined by von Frey test in female rats injected with cortical KCl (0.5 μ L, 1M) in combination with KT182 (2 mg/kg, ip), an ABHD6 inhibitor or MJN110 (10 mg/kg, ip), a MAGL inhibitor in prevention paradigm. **(A)** 3-hour pre-injection of KT182 prevented CSD-induced periorbital allodynia at different time-points as compared to vehicle controls (KCl + vehicle vs. KCl + KT-182: 30 min: $p=0.081$; 60 min: $p=0.026$, 90 min: $p=0.013$; 120 min: $p=0.033$, 180 min: $p=0.018$, 360 min: $p=0.027$, as assessed by two-way ANOVA(time x treatment) with Bonferroni post-hoc analysis, $F(8,135)=5.838$); **(B)** Neither SR144528 nor Rimonabant significantly blocked this effect. **(C)** representative graph of area under the curve for graph B.

Figure 31

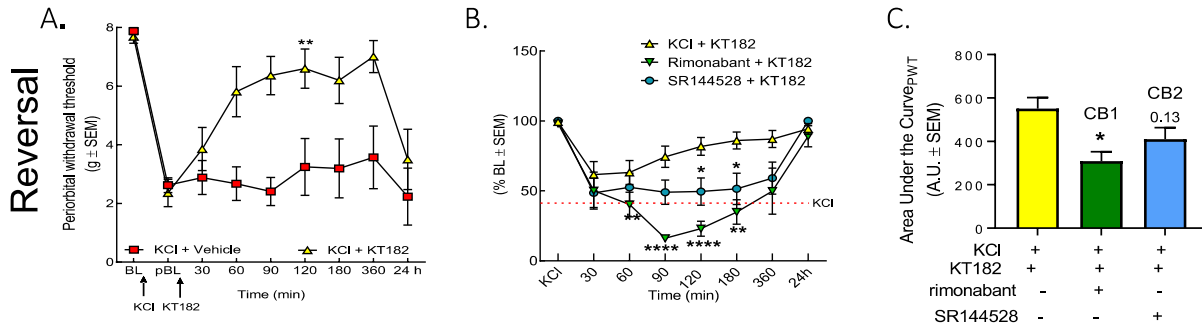


Figure 31. Pharmacological inhibition of ABHD6 during CSD reversal paradigm.

Periorbital withdrawal threshold determined by von Frey test in female rats injected with cortical KCl (0.5 μ L, 1M) in combination with KT182 (2 mg/kg, ip), an ABHD6 inhibitor or MJN110 (10 mg/kg, ip), a MAGL inhibitor in reversal treatment paradigm. **(A)** Injection of KT182 in reversal treatment paradigm alleviated periorbital allodynia caused by cortical KCl at 60, 90, 120, 180, and 360 min (KCl+vehicle vs. KCl+KT182, 60 min: $p=0.092$, 90 min: $p=0.003$, 120 min: $p=0.14$, 180 min: $p=0.334$, 360 min: $p=0.168$, as assessed by two-way ANOVA (time x post-treatment with Bonferroni post-test, $F(8,104)=4.162$ $p=0.002$). **(B and C)** ABHD6 reversal of CSD periorbital allodynia was blocked by SR144528 and Rimonabant within the first 180 min **(C)** area under curve for graph B. Values are the mean \pm SEM ($n=9$ /condition). ns=non-significant, * $p<0.05$, ** $p<0.01$, *** $p<0.001$, KCl+vehicle vs. KCl+treatment, as assessed by two-way ANOVA with Bonferroni post-test.

5.1.3.2 2-AG could have a role in maintenance of blood-brain barrier in vivo

Previous research in our lab focused on how CSD affects blood-brain barrier as it can affect central sensitization as well as drug delivery and efficacy [7, 188]. To understand if 2-AG affects blood brain barrier we utilized TEER which is a screening technique for brain endothelial barrier permeability [188]. Using a compound which has induced headache through 2-AG depletion, LEI106, we grew a bEnd.3 monolayer in a 12 well trans-well plate and applied LEI106 (300 μ M) or vehicle (1:1:8 DMSO/tween20/saline) 15 min before TEER measurements in the luminal well as high a dose was applied in vivo to induce headache like pain in animals[188]. We also applied the inhibitor in the presence of 100 mM KCl to observe any possible additive effects. 100 mM KCl was applied in control wells as a positive control to open the BEB (Figure #A). We observed that LEI106 significantly reduced TEER in comparison to vehicle at the 2–3-hour timepoint alone (**Figure 32A**). There was also no additive effect observed with LEI106 in the presence of high extracellular KCl (100 mM).

To investigate this effect further we injected female rats with vehicle (1:1:8 DMSO/tween20/saline) or LEI106 (40mg/kg) I.P. and performed in situ brain perfusions with ¹⁴C-sucrose for 15 minutes 120 minutes post I.P. injection of vehicle or LEI106 where peak reduction in periorbital allodynia was observed [188]. We harvested and compared sucrose uptake in 3 regions of the brain associated with headache, cortex, PAG, and medulla (Vc). Sucrose uptake was significantly increased in the PAG region in animals treated with LEI106 compared to vehicle, but not in cortex or medulla (**Figure 32B**). This data suggests 2-AG could be important in maintaining BBB integrity in the PAG during headache.

Figure 32

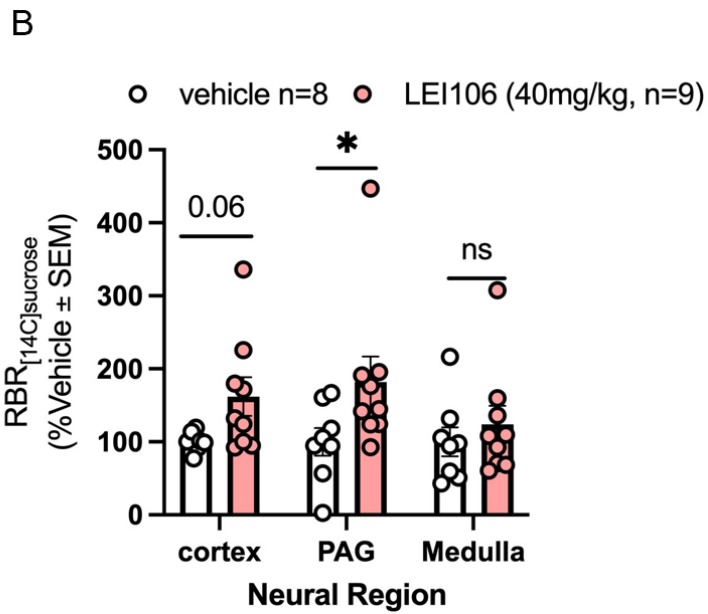
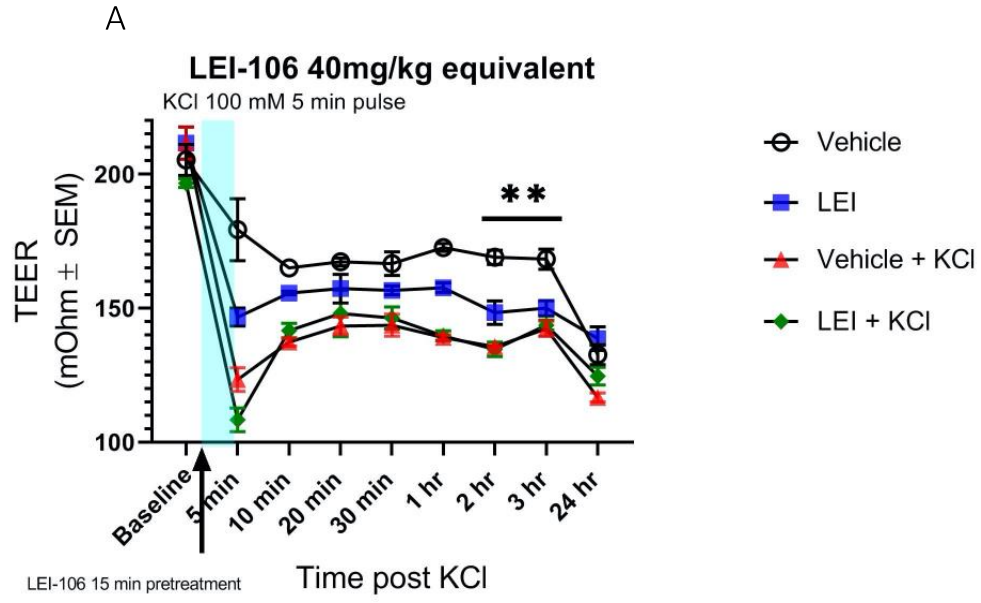


Figure 32. Inhibition of DAGL α with LEI106 compromises blood brain barrier integrity.

LEI106, a DAGL alpha inhibitor was applied 15 min before TEER in conjunction with KCl to observe effects of decrease 2-AG levels on BEB integrity (A) TEER values were significantly reduced after KCl pulse (5 min, 100 mM) and KCl + LEI 106 as compared to aCSF (vehicle) controls, additionally LEI106 significantly reduced TEER 2-3 hours post application, on the monolayer of bEnd.3 cells, suggesting loss of barrier integrity (KCl vs aCSF and LEI106 vs. aCSF): ** $p < 0.01$, as tested by two-way ANOVA with Tukey's post-test). (B) ^{14}C -sucrose uptake was measured in whole cortex, PAG, and medulla and presented the brain to plasma ratio (RBr) after 15 min brain perfusion. The in situ brain perfusion of female rats showed that I.P. injection of LEI106 (40mg/kg) significantly increased ^{14}C -sucrose uptake into the PAG alone ($p = 0.02$), suggesting that 2-AG in the PAG may have a role in BBB maintenance. (LEI106 vs. vehicle (1:1:8 DMSO/tween20/saline): * $p < 0.05$, assessed unpaired t-test). Values are mean \pm SEM (n=8-9).

5.1.3 Conclusion

In this study we utilized CB1 and CB2 receptor antagonists in the presence of an ABHD6 inhibitor to discern the role of these receptors in ameliorating headache pain associated with CSD., ABHD6 inhibitor KT182 significantly prevented periorbital allodynia independent of CBR activation, whereas reversal of established periorbital allodynia with KT-182 required CB1R primarily. Lastly, 2-AG may have a role in BBB maintenance as LEI106, a DAGL α inhibitor, at high dose reduced TEER values of a BEB in vitro. In situ brain perfusions using ^{14}C -sucrose to assess paracellular permeability revealed LEI106 significantly increased sucrose uptake in the PAG but not cortex or medulla.

5.2 Assessing Blood-brain Barrier Integrity in a Chronic Morphine Medication Over-use Headache Model

5.2.1 Introduction

Chronic morphine use is normalized in the treatment of some chronic pain conditions, and an ongoing aspect of the opioid epidemic. Long-term use of opioids is associated with increased abuse liability, development of analgesic tolerance, opioid induced hyperalgesia, and medication overuse headache. About 60 million people worldwide are affected by medication overuse headache altogether (MOH), and is one of the top 20 causes of disability [2]. MOH is defined by the ICHD-3 as the frequent intake of headache medication in a person with a primary headache disorder for more than 3 months and as a result has a headache occurring 15 or more days per month [2]. Headaches caused by chronic opioid use in patients not suffering from a primary headache is usually not diagnosed as MOH according to the ICHD-3 definition. Opioids are not typically prescribed for treatment of headache or migraine since it does not provide pain relief for these pathologies and contributes to MOH. One study on the effects of chronic morphine on BBB in rats, showed no change in P-glycoprotein (p-gp), a BBB transporter, expression and there was no paracellular leak in the cortex or hippocampus when using brain in situ with ¹⁴C- sucrose[207]. However, the effect of chronic morphine induced headache pain and how it affects blood-brain barrier integrity, specifically tight junctions, in other regions such as the PAG is not well explored. In this study, we use both in vitro and in vivo approaches to determine the effects of chronic morphine on paracellular permeability of the BEB/BBB.

5.2.2 Methods and Materials

Cell Culture

The bEnd.3 (CRL-2299, ATCC) cell line was used for in vitro experiments, cultured as described in Liktor-Busa et al. [145]. Cells were treated with 60 mM KCl for 5 minutes, which is a typical condition to evoke potassium-triggered spreading depolarization in live brain slices [142]. 10 mM was made up in saline then diluted in DMEM to 35 μ M concentration and applied apically to bEnd.3 cells for 15 minutes or 24 hours prior to KCl exposure.

Trans endothelial electrical resistance (TEER)

TEER is an established method of evaluating endothelial cell barrier integrity which captures active and passive breaches in vitro [172]. TEER was assessed via two-electrode chopstick method (EVOM2), as described [100] at the following timepoints immediately post-pulse: 10, 20, 30, 60, 120, 180 minutes and 24 hours after replacement of abluminal media.

Animals

Intact, female Sprague Dawley rats (200-250 g) were purchased from Envigo (Indianapolis, IN) and housed in a climate-controlled room on a regular 12/12 h light/dark cycle with lights on at 7:00 am with food and water available *ad libitum*. Animals were initially housed 3 per cages but individually housed after the dural cannulation. All procedures were performed during the 12-h light cycle and according to the policies and recommendations of the International Association for the Study of Pain and the NIH guidelines for laboratory animals, and with IACUC approval from the University of Arizona. Justification for animal numbers was consistent with NIH policy (NOT-OD-15-102), and experiments were randomized to blinded treatment groups to give 80% power to detect a treatment effect size of 20% compared to a baseline response of 5% at a significance level of 0.05 [142, 184]. Numbers required to achieve statistical power were determined by G.Power3.1. Female rats were used as headache disorders

affect females to males at a nearly 3:1 ratio [185, 186]. The stage of estrus cycle was not determined in this study.

Continuous morphine infusions

All animals received a constant systemic exposure of either morphine or vehicle starting 7 d before and continuing throughout electrophysiological recordings. Morphine was administered by subcutaneous implants of Alzet osmotic minipumps (model 2001) that released morphine sulfate (60 mg/ml) at a rate of 1 μ l/h across 7 d. Subcutaneous implantation of placebo pellets or a saline-filled osmotic minipump served as controls. Implants were performed under isoflurane anesthesia. In all studies the experimenter was blind to the treatment of the animal.

Periorbital mechanical allodynia

Periorbital allodynia was evaluated before and after cortical injection (t = 30, 60, 90, 120, 180, 360 min, and 24 h) by an observer blinded to drug condition. Rats were grouped based on their postsurgical baseline to ensure equivalent pre-injection thresholds (6-8 g). Any rats exhibiting excessive postsurgical allodynia (threshold <6 g) were removed from the study. Rats were acclimated to testing box 1 h prior to evaluation of periorbital mechanical allodynia with calibrated von Frey filaments as previously described by Edelmayer and coworkers [140, 141]. Behavioral responses were determined by applying calibrated von Frey filaments perpendicularly to the midline of the forehead at the level of the eyes with enough force to cause the filament to slightly bend while held for 5 sec. A response was indicated by a sharp withdrawal of the head, vocalization, or severe batting at the filament with attempts to bite it. The withdrawal threshold was determined using a modified version of the Dixon up-down method

***In situ* Brain Perfusion**

In situ perfusion studies were carried out in female Sprague-Dawley rats (200-250 g) after 7 days of continuous infusion with morphine see methods. Briefly, rats were anesthetized with ketamine/xylazine and heparinized (10,000 U/kg i.p.). Body temperature was maintained at 37°C using a heating pad. The common carotid arteries were cannulated with silicone tubing connected to a perfusion circuit then perfused with an erythrocyte-free modified mammalian Ringer's solution (117 mM NaCl, 4.7 mM KCl, 0.8 mM MgSO₄, 1.2 mM KH₂PO₄, 2.5 mM CaCl₂, 10 mM D-glucose, 3.9% (w/v) dextran (MW. 60,000), and 1.0 g/L bovine serum albumin (type IV), pH 7.4), warmed to 37°C and oxygenated with 95% O₂/5% CO₂. Evan's blue dye (55 mg/L) was added to the perfusate to serve as a visual marker of BBB integrity. Perfusion pressure and flow rate were maintained at 95-105 mmHg and 3.1 mL/minute respectively. Both jugular veins were severed to allow for drainage of the perfusate. Using a slow-drive syringe pump (0.5 mL/minute per hemisphere; Harvard Apparatus, Holliston, MA), ¹⁴C-sucrose (0.5 µCi/ml) was added to the inflowing perfusate. Following a 15-minute perfusion, the rats were decapitated, and the brains were removed. The meninges and choroid plexus were excised, and cerebral hemispheres were sectioned and homogenized. TS2 tissue solubilizer (1 mL) was added to each tissue sample and the samples were allowed to solubilize for 2 days at room temperature. To eliminate chemiluminescence, 100 µl of 30% glacial acetic acid was added, along with 2 mL Optiphase SuperMix liquid scintillation cocktail (PerkinElmer, Boston, MA). Samples were measured for radioactivity on a model 1450 liquid scintillation counter (PerkinElmer).

Statistical Analysis

GraphPad Prism 8.3.1 and 9.3.1 software (GraphPad Software) were used for statistical analysis. Unless otherwise stated, the data were expressed as mean ± S.E.M. Periorbital allodynia measurements were assessed using a repeated measure two-way ANOVA to analyze differences

between treatment groups over time with a Bonferroni test applied *post hoc*. Molecular studies were compared by unpaired t-test or one-way ANOVA, as indicated. Differences were considered significant if $p \leq 0.05$.

5.2.3 Results

5.2.3.1 Assessment of brain endothelial barrier exposed to acute and chronic morphine in vitro using trans-endothelial electrical resistance measurements and ^{14}C -sucrose

To determine whether the blood-endothelial barrier (BEB) was affected when exposed to morphine, we used trans-endothelial electrical resistance measurements (TEER). We grew bEnd.3 mouse cells in a 12 well trans-membrane plate with astrocyte conditioned media (ACM) in the abluminal well to enhance the BEB for increased TEER. We pretreated the luminal wells with a high dose of morphine (35 μM) or vehicle (saline) for both 15 minutes (acute) and 24-hours (chronic) before TEER measurements. We wanted to know how morphine would affect the BEB during a spreading depression event, so we included a KCl group in our experiment. Neither acute nor chronic exposure of 35 μM morphine in the luminal well significantly changed TEER as compared to the vehicle groups (**Figure 33 A, B and C**). Direct comparison of TEER values in KCl stimulated conditions after acute morphine, KCl reduced TEER significantly more than after chronic morphine exposure (**Figure 33D**). The data demonstrates that chronic morphine limits KCl induced TEER reductions as compared to acute treatment within the first 30 minutes, suggesting a compensatory mechanism (**Figure 33D**). Next, we assessed the paracellular permeability of the BEB with ^{14}C -sucrose and after chronic morphine exposure (**Figure 34**). We found that morphine alone did not increase paracellular permeability, but it did significantly reduce the damaging effects of high extracellular KCl ($p < 0.05$).

Figure 33

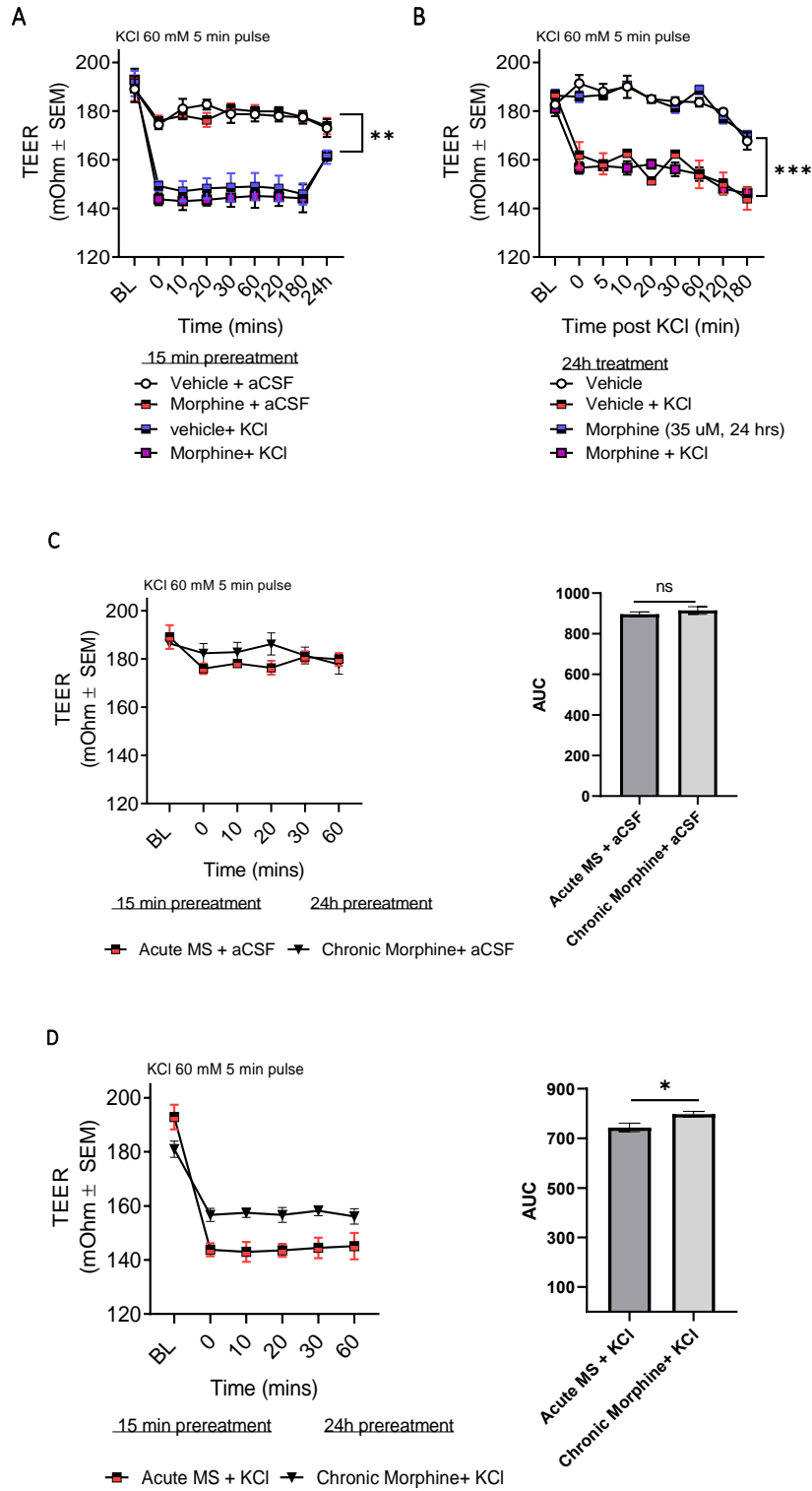


Figure 33. TEER measurement of acute and chronic morphine exposure on BEB in vitro.

A monolayer of bEnd.3 mouse cells was grown in a 12-well trans-well plate and treated with 35 μ M morphine 15 minutes and (acute) and 24-hours (chronic) before TEER measurements, 60 mM KCl was used as both a positive control as well as to observe if morphine exacerbates KCl effects on BEB. **(A)** TEER measurement taken 15 min after morphine treatment to luminal well, significance observed between aCSF and KCl treated groups **(B)** **(C)** TEER measurement taken 24 hours after morphine treatment to luminal well, significance observed between aCSF and KCl treated groups. ngs comparing aCSF groups treated with acute or chronic morphine, no significance observed. **(D)** TEER readings comparing KCl groups treated with acute or chronic morphine, there was a significant decrease in acute morphine group compared to chronic morphine group. * $p < 0.05$, ** $p < 0.01$, *** $p < 0.001$ as tested by two-way ANOVA with Tukey's post-test (n=3). AUC values assessed by unpaired t-test * $p < 0.05$. (n=3).

Figure 34

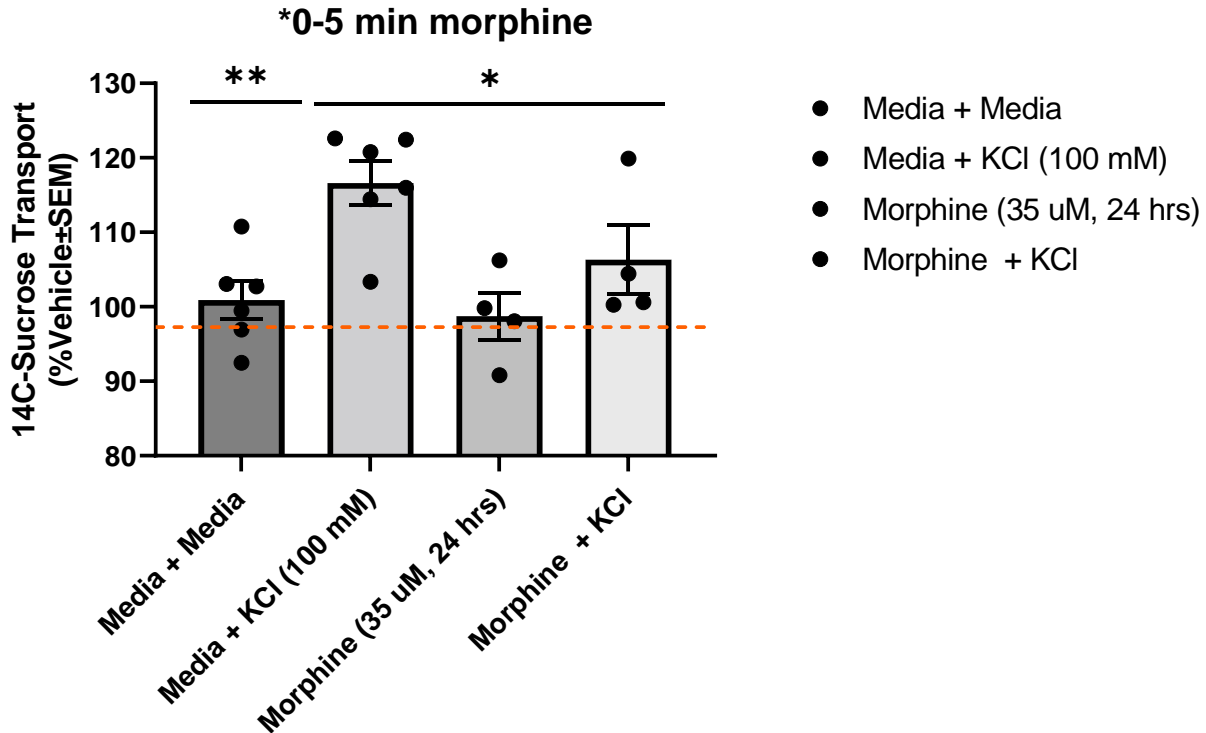


Figure 34. Chronic morphine exposure to blood endothelial barrier prevents paracellular leak caused by high extracellular KCl. A monolayer was grown in a 24 well transwell plate and used to assess sucrose transport across the BEB after 24-hour treatment with 35 μ M morphine. ¹⁴C-sucrose transport was measured in trans-well, media in bottom well was collected after 5 minutes (KCl vs aCSF at 5 min: $p < 0.001$, as tested by one-way ANOVA with Tukey's post-test). No significant difference between KCl vs. aCSF was observed after 30 min. Treatment with the HSP90 inhibitor 17-AAG (1 μ M, 24 h) prevented sucrose movement across the monolayer in KCl treated cells, but it did not influence sucrose permeability in aCSF-treated cells (KCl + 17-AAG vs. KCl + vehicle: $***p < 0.001$, assessed one-way ANOVA with Tukey's post-test). Values are normalized to percent of vehicle \pm SEM (n=3, dotted line). (Experiment performed by Aidan Levine)

5.2.3.2 Sustained infusion of morphine in rats induced significant periorbital allodynia

To further assess the effects of chronic morphine in the context of medication over-use headache, we utilized a morphine induced MOH model in which we implanted minipumps into female rats for seven days for sustained infusion of morphine (5mg/kg/d, SC) over seven days. On the seventh day we assessed periorbital allodynia and we noticed significant decrease in periorbital withdrawal threshold in the morphine group compared to vehicle, indicative of medication over-use headache similar to previous studies [208] (**Figure 35A**). Light stimulation had no significant change between the two groups (**Figure 35B**). This data suggest MOH can be induced by sustained morphine (5mg/kg/d) for seven days and can be used to assess blood-brain barrier integrity in vivo.

Figure 35

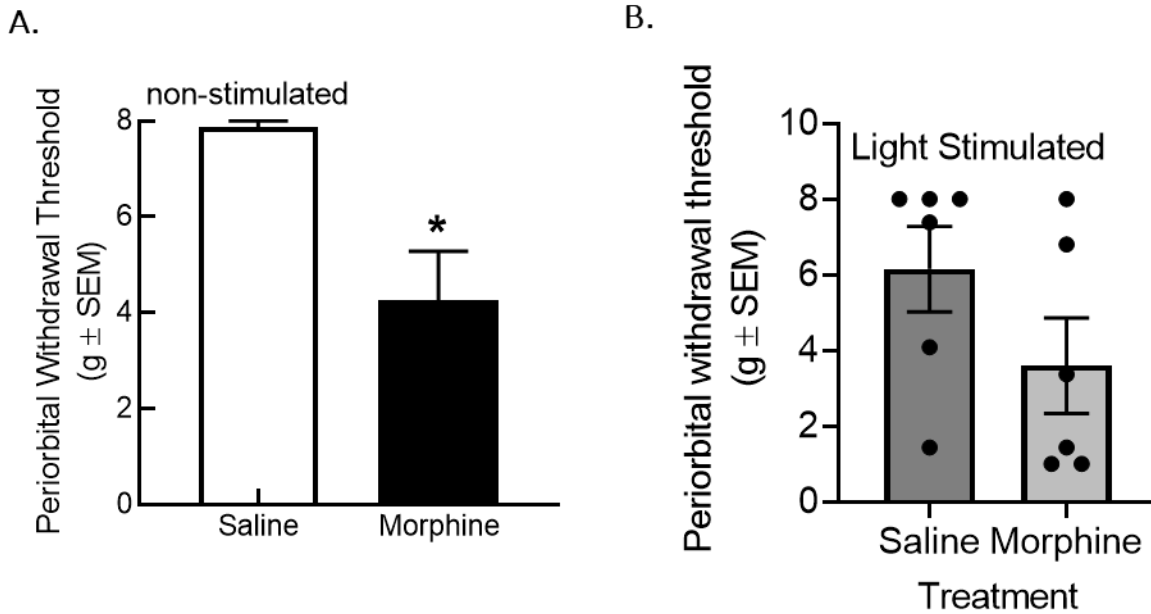


Figure 35. Assessment of periorbital allodynia after continuous infusion of morphine for seven days. Female rats were anesthetized using isoflurane, and an incision was made in the lower back above the left hind leg to insert an osmotic pump with morphine calculated to infuse morphine at 5mg/kg/d for seven days. **(A)** on the seventh day periorbital allodynia was assessed using von Frey, there was a significant reduction in facial withdrawal threshold in animals infused with morphine compared to the vehicle group. **(B)** To see if noxious stimulus could affect either group, we exposed all animals to heavy light stimulus for 30 minutes and repeated the Von Frey, there was no enhanced effect observed in the morphine group or vehicle group. Values expressed as mean \pm SEM * $p < 0.05$ as tested by one way-ANOVA($n=6$).

5.2.3.3 Assessment of blood-brain barrier integrity of morphine induced MOH in rats

Changes in electrical resistance can suggest but not confirm changes in paracellular permeability in vivo. To determine whether chronic morphine changes permeability of the blood-brain barrier in vivo, in situ brain perfusions with ^{14}C -sucrose were performed. Female rats receiving infusions of morphine (5mg/kg/d) for seven days were used for in situ perfusions. We observed significant blood to brain uptake of ^{14}C -sucrose in the periaqueductal grey (PAG), but not within the cortex or trigeminal brainstem complex (**Figure 36**). This data suggests that sustained morphine infusion promotes blood-brain barrier paracellular leak in a region-dependent manner.

Figure 36

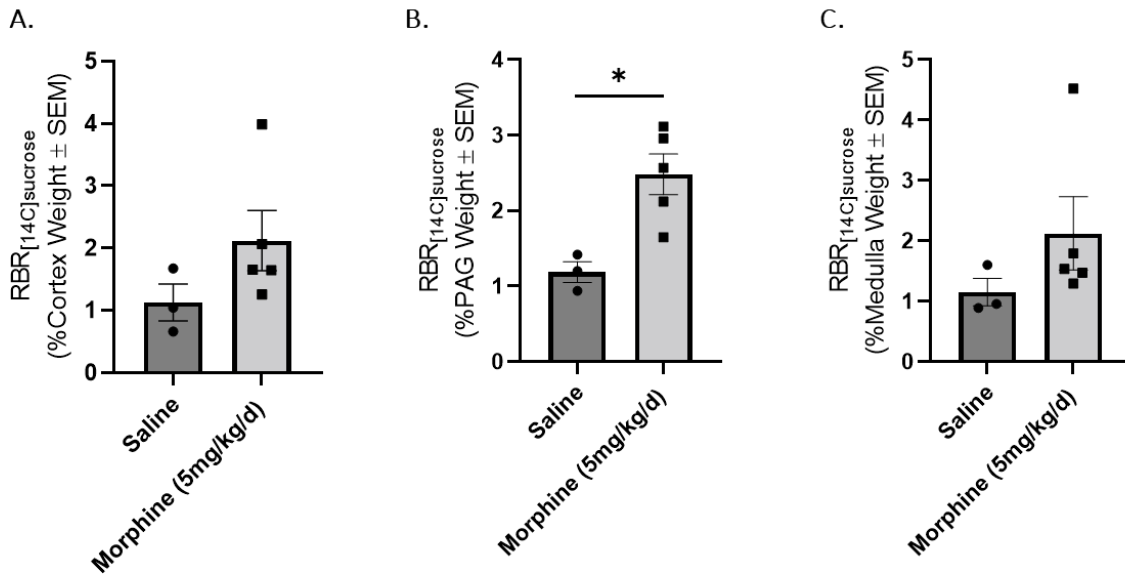


Figure 36. Assessment of blood-brain barrier integrity in morphine induced MOH model.

¹⁴C-sucrose uptake was measured in whole cortex, PAG, and medulla and presented the brain to plasma ratio (RBr) after 15 min brain perfusion in female rats after 7 days of continuous morphine and post periorbital assessment. (A) The in-situ brain perfusion of female rats showed that continuous morphine infusion (5mg/kg/d) significantly increased ¹⁴C-sucrose uptake into the PAG alone (B & C), and not the cortex or medulla containing the trigeminal brainstem complex suggesting chronic morphine affects BBB maintenance in the PAG. (Morphine vs. vehicle (saline): *p<0.05, assessed unpaired t-test). Values are mean ± SEM (n=3-6). n-values reflect outliers removed based on stats as well as evidence of blown vessels (by cortex values)

5.2.4 Conclusion

In this study we wanted to explore how morphine induced medication over-use headache affects the blood brain barrier. In our in vitro experiments utilizing TEER, we noticed there was no significant change with morphine application alone, nor was there an additive effect seen when KCl, related to spreading depression, was applied with morphine. There was a difference in TEER between chronic versus acute application of morphine on the BEB exposed to KCl. This could suggest there may be a compensatory mechanism in the chronic application in morphine which could lessen the effects of KCl. Moving forward, we utilized osmotic pumps to continuously infuse 5mg/kg/d of morphine into female rats for seven days similar to previous models used in MOH studies, [208] which caused periorbital allodynia in the rats. BBB integrity in regions of the brain associated with spreading depression and headache within situ brain perfusions using ¹⁴C-sucrose was only compromised within the PAG. This leak in the BBB may play a role in efficacy changes with headache therapeutics are in treating medication over-use headache and may be relevant in the role of opiates in central sensitization.

**CHAPTER 6 DISCUSSION AND CLOSING
STATEMENT**

Migraine affects many people as one of the 6th leading neurologically disabling diseases in the world [2]. Migraine with aura accounts for 30% of all migraineurs [4], however, patients who have had a stroke or traumatic brain injury (TBI) can also experience migraine with aura like symptoms as secondary result of their pathology adding to these numbers unofficially [2, 165, 209]. In addition, migraine with aura specifically, has been correlated with increased likelihood of stroke due to the constant ischemic stress which is believed to be due to multiple cortical spreading depression (CSD) events [165, 210, 211]. It is well known that both stroke and TBI impairs blood-brain barrier function[212, 213] and there have been extensive studies into therapeutics for these diseases to repair neurological damage. However, migraine with aura has only recently shown to be implicated in causing stroke and despite preclinical data suggesting BBB impairment from CSD events and migraine attacks there has been little research into neuroprotective mechanisms which can limit the stress on the neurovascular system.

Migraine with aura affects people world-wide and negatively impacts their quality of life in many aspects [4, 214, 215]. Migraine attacks are generally characterized by unilateral throbbing headache pain as well as sensitivity to visual, auditory, and mechanical afferent inputs [21, 98, 165, 216]. Migraine with aura adds other characteristics to the pathology with fully reversible symptoms within 5-60 minutes or presentation such as: visual and/or auditory disturbances, motor deficits, speech and/or language difficulties. The aura phase is then accompanied by headache [2]. The pain circuitry of migraine has generally been connected to stimulation of the trigeminovascular system which in the long term causes central sensitization which may facilitate the switch from episodic to chronic migraine as well as play a role in medication over-use headache (MOH) [63, 72, 217]. Currently, Migraine with aura can be treated with triptan and -ditan class drugs targeting the serotonergic system of the peripheral and

central nervous system as well as therapies reducing CGRP levels and action [94, 218, 219]. These medications have proved to be effective in some populations but give little insight into etiology or mechanism of migraine pain and sensitivity.

6.1 Spreading Depression Can Alter ASIC Transporter Function in the Cerebral Vasculature Improving Efficacy of Anti-migraine Therapeutics

Changes such as vascular dilation, depolarization of nociceptive afferents [60] and development of tactile allodynia [98] are linked to CSD events. Aside from blood flow, metabolic, and behavioral changes associated with CSD events there is also a dramatic failure of brain ion and pH homeostasis [220]. pH is a known regulator of BBB integrity that has documented effects on xenobiotic uptake [221]. The sodium-hydrogen antiporter (NHE) protein family is responsible for maintaining the homeostasis of intracellular pH in the central nervous system [61]. Migraine is currently managed by therapeutics such as triptans and CGRP antagonist, however these medications are not 100% effective in patients. Therefore, investigating regulation of the blood-brain barrier (BBB) by pH during and after a CSD event is imperative for therapeutic advancement.

Previous research data suggests that inhibition of specifically NHE1 of the NHE family has shown therapeutic potential in acute and inflammatory pain. These studies show a reduction in BBB breakdown and neurovascular damage after acute ischemic stroke in in vivo and in vitro models [130, 132, 138, 222]. In our lab we showed NHE1 inhibition increased sumatriptan movement across bEnd.3 monolayers early, but not late, post KCl exposure in vitro. This result suggests an alternative method of uptake for sumatriptan across the blood endothelial barrier (BEB). In vivo, the NHE1 inhibitor, zoniporide, potentiates the onset of sumatriptan anti-allodynic effect in rodents, further supporting the role of pH regulation in therapeutic efficacy

[145]. In addition to quicker response time to the drug, the number of responders to sumatriptan treatment was also increased in the zoniporide-treated group, and the control group mirrored the clinical percentage of sumatriptan sensitive patients [223], [220, 224, 225]. This could mean clinical variability in sumatriptan sensitivity may be associated with NHE1 expression and/or activity in the cerebral vasculature. There are differences observed in the efficacy of abortive drugs based on the phase of migraine in which they were administered, indicating changes in BBB associated components during the different phase of migraine [20].

Clinical reports using MRI and CT scans of migraine patients and animal models of spreading depression further support the hypothesis of compromised BBB integrity during migraine attack, which may affect drug delivery as well as central sensitization since transient openings can further disrupt ion homeostasis and pH [28, 220, 221, 224-226]. Although inhibition of NHE1 had a positive effect in conjunction with sumatriptan administration, the result of increased periorbital sensitivity induced by a single, systemic dose of zoniporide alone calls into question the overall positive effect of NHE1 inhibition as a therapy for migraine with aura and associative disease states. Interestingly, NHE1 has been studied in the context of pain and has proved to have a protective role in acute and chronic inflammatory pain [227]. The results produced in our lab parallel the studies published in pain research showing that inhibition of peripheral, and spinal, NHE1 by administering both a selective and non-selective inhibitor, such as zoniporide, amiloride, and 5-(N,N-dimethyl)-amiloride increased pain behavior in capsaicin, serotonin, and formalin tests [228-231]. There were also electrophysiological studies with evidence that the inhibition of NHE1 can modulate electrical activity of primary nociceptive terminals [227].

This body of research suggests NHE1 plays a crucial role in inflammatory and acute pain in modulating pain transmission in the periphery and spinal cord. Given this information, it is possible NHE1 may have a similar role in the cortex and brainstem in relation to CSD associated headache-like behavior. We discovered a significant decrease in the total protein detection of NHE1 in cortex and PAG at 90 minutes after injection of KCl (peak periorbital allodynia) suggesting brain regions influenced by CSD events and implicated in central sensitization have tightly regulated pH responses to depolarization [232]. Brain function associated with neuronal excitability and neurotransmitter release is extremely sensitive to small changes in pH. There is a high number of pH-sensitive membrane proteins, such as channels, transporters, receptors and ATPase pumps expressed in CNS which can also be investigated in relation to CSD events[233].

To follow up with results from the NHE1 study suggesting transporter facilitated sumatriptan uptake into the rat brain *in vivo*[7, 188], we investigated Oatp1a4. There is evidence suggesting that CSD events can dynamically regulate the functional expression of Oatp1a4 *in vitro* in bEnd.3 cells, and *in vivo* to move sumatriptan from the blood to the brain [7, 145]. OATPs are membrane solute carriers that mitigate bi-directional and sodium-independent transport of amphipathic substrates and are expressed in several tissues throughout the body but OATP1A2 and its rat ortholog OATP1a4 is highly expressed in the brain[154, 161]. It has been shown that inflammation upregulates Oatp1a4 functional expression [156] changing drug pharmacokinetic profiles *in vivo*, such as statins, opioid peptides, and neuro-steroids [154, 156, 161, 164, 234].

CSD can also affect Oatp1a4 expression through means of inflammation and changes in pH as previous studies would suggest [188]. Recent literature published by Albekairi et al., showed that bEND.3 cells express Oatp1a4, but at lower levels than the human endothelial cells

[234]. Our results confirm that bEnd.3 mouse cells express Oatp1a4 providing evidence that this cell-line can be used to assess blood-to-brain uptake of therapeutics *in vitro*. Before performing transport studies, we characterized how Oatp1a4 responds in bEnd.3 mouse cells when exposed to high KCl (60 mM) in relation to a CSD event. Our results concluded that there was no change in either protein detection levels or localization in bEnd.3 cells when exposed to high extracellular KCl compared to controls within 5 minutes.

Moving forward we wanted to assess the activity of Oatp1a4 in uptake of sumatriptan across the BEB using bEnd.3 mouse cells. The triptan class pharmaceuticals are the first-line therapies for episodic migraine and are associated with high therapeutic gains and favorable side-effect profiles [14, 235-238]. Triptans are 5-HT derivatives and constitute about 80% of migraine prescriptions and make up around 50% of the anti-headache total market [237]. In 30-70% of patients, head pain intensity and episode duration is reduced with triptan compounds [93, 237, 239] with many indicating that triptans must be on-board during prodrome for best results [235, 238, 240-242].

To properly test if Oatp1a4 is involved in the transport of sumatriptan in the presence of high extracellular KCl, we performed an uptake experiment within 5 minutes of KCl exposure and 5 minutes post KCl exposure *in vitro* in the presence or absence of an Oatp1a4 inhibitor E3S. Sumatriptan was present on the abluminal side of the bEnd.3 trans-well monolayer during, but not after the abluminal KCl exposure. This result supports the concept that administration of a triptan during the aura phase could improve the efficacy of the drug. Also of note, within the 5 min exposure to high extracellular KCl (60 mM) there was a significant reduction (Figure 10) of sumatriptan in the abluminal well when the monolayer was pretreated with OATP inhibitor E3S, signifying the activity of Oatp1a4 may play an active role in sumatriptan transport *in vitro*. The

fact that there was no change in the 5-minute post KCl exposure collection (Figure 11) in the E3S treated monolayer could suggest the activity of Oatp1a4 is dependent on the extracellular environment and the transporter quickly returns to homeostatic balance. These observations suggest that sensitivity to sumatriptan may be a result of a time-dependent regulation of the transporter in relation to its environment. OATP1A2/Oatp1a4 is implicated in the active transport of triptan compounds in HEK cells *in vitro* [157], coinciding with our results and supporting our hypothesis.

Distinct tissue distribution for Oatp1a4/OATP1A2 is described [161, 243, 244], though CNS regional distribution is relatively unexplored. Distribution of Oatp1a4 varies between BBB, blood-arachnoid-barrier [245], and blood cerebrospinal fluid barrier [246]. The current work showing western blots which indicate Oatp1a4 regulation during CSD events is time dependent within the V1M cortex and brainstem containing PAG and Vc, further suggests that regional differences in active transport for Oatp1a4 substrates exist. This is intriguing given the *in vitro* results, showing the transporter is further affected by the microenvironment of the brain during and after a CSD event.

An *in vivo* study to validate a transport model [158] showed that OATP1A2 did not play a role in sumatriptan transport/uptake under physiological conditions in a humanized mouse model. However, the role of Oatp1a4 has yet to be elucidated during a pathological state such as a CSD event [158]. Our results show that Oatp1a4 does not participate in the brainstem transport of sumatriptan *in vivo* 30- and 90- minutes post CSD induction with pretreatment of Oatp inhibitor E3S as determined by *in situ* brain perfusion (Figure 13). Another observation made from our *in-situ* data is the significant overall increase of sumatriptan crossing into the brain 30-minutes post CSD induction compared to the 90-minute post CSD timepoint across groups

despite treatment and region. Also, the time between 0-60 minutes of sumatriptan application in the presence of an NHE1 inhibitor when assessing periorbital allodynia had shown the most increase in efficacy of the conjunctive treatment. This data taken together suggests pH as well as the timing in which sumatriptan is taken in relevance to when an aura is experienced is critical for antinociceptive efficacy, as well as limiting the time of the headache phase. Our in vivo data suggests Oatp1a4 may not facilitate sumatriptan transport under CSD conditions when administered after induction suggesting an alternative mechanism of transport into the brainstem and cortex despite increases in expression of Oatp1a4 in these regions. Additional investigations are required to elucidate the full complement of transporters influenced by CSD induction. The Organic Cation Transporter (OCT) family specifically OCT1 may be of interest for the transport of sumatriptan during CSD as well as it has been shown to be a substrate [247].

Previous work in this lab showed cortical uptake of sucrose into the brain post CSD induction which parallels sumatriptan, and since they are close in size, this could indicate transient paracellular leaks may have a large role in sumatriptan crossing into the brain [7, 145]. Although NHE1 expression is altered post CSD and may affect sumatriptan efficacy in vivo in regions such as the cortex and brainstem, [145] Oatp1a4 does not facilitate the blood-to-brain transport of the drug. As NHE1 plays a role in pH homeostasis, and sumatriptan is 99% protonated at physiological pH (~ 7.4) [115, 248, 249], the noted dysregulation and increased stress on cellular metabolism leading to the drop in extracellular pH can keep the drug in its protonated state. Organic cation transporters (OCT) at the BBB may play a role in sumatriptan blood-to-brain uptake, as sumatriptan has been described in studies in liver cells to be a substrate for OCT1[250-252]. Future studies are needed to verify the role of these transporters in sumatriptan brain uptake during headache.

In summary, increased sumatriptan transport across the BEB, although, NHE1 inhibition also improves the BEB integrity when exposed to high KCl concentration in vitro [188] indicating an alternative mechanism behind movement of sumatriptan. In addition, the mechanism of increased efficacy of sumatriptan derived from NHE1 inhibition in vivo could mean that pH change from CSD events influences transporter activity. This alone justified investigating transporters, and Oatp1a4 was a good potential target as literature had suggested sumatriptan to be a substrate. However, the incongruity between the in vitro and in vivo data collected in the Oatp1a4 studies we completed highlights the importance of investigating BBB transport mechanisms utilizing multiple models and considering specific events and environments. The BBB is a complex system that is both dynamic and highly selective to tightly control the microenvironment of the brain. This tight regulation further adds to the difficulty in modeling the system. Further studies should use in vivo and ex vivo techniques for functional systems observations, and in vitro techniques for specific intracellular signaling mechanisms to fully elucidate how CSD events dynamically regulate the functional expression of transporters. Oatp1a4 and OCT family of transporters need to be further studied to understand the role they play in the brain uptake of sumatriptan, as well as other migraine therapeutics during headache.

6.2 HSP90 Inhibition Improves BBB Integrity Showing Claudin 5 to be Integral as a Neuroprotective Tight Junction Protein During and After CSD Events

Current results from the study completed in our lab suggests that inhibition of HSP90 with the selective agent 17-AAG reduces CSD associated BBB paracellular leak at the endothelial cell level both in vitro and in vivo via modulation of tight junction expression. This finding correlates with the findings of another group who studied the use of HSP90 inhibitor 17-DMAG in an MCAO model to reduce the associative ischemic tissue damage and neurological

function [245]. The results of that study showed pretreatment with 17-DMAG 1 hour before MCAO decreased infarct size caused by MCAO as well as suppressed the reduction of tight junction (TJ) protein expression of Occludin and ZO-1. Similarly, previous work by our group had shown a transient opening in the BBB post CSD induction by injection of 1 M KCl (0.5 μ L) [7].

There can be several mechanisms as to how HSP90 inhibition is neuroprotective of the BBB. Factors of BBB disruption leading to damage primarily include hypoxic or inflammatory states associated with disease. CSD has been shown to induce neuroinflammation as well as increase reactive oxygen species [60, 123]. Studies have shown that HSP90 inhibition decreases inflammation in models of arthritis and MCAO [124, 245, 253] as well as reduces oxidative stress specifically in the microvasculature of the brain [176]. There has been research showing increased matrix metalloproteinase-9 (MMP-9) expression can further disrupt barrier function allowing for decreased physical integrity [120]. CSD events have been documented to increase MMP-9 expression [60, 167]. HSP90 inhibition decreased MMP-9 expression in a stroke model [245] as well as lowered inflammatory markers. This same group also showed that HSP90 inhibition prevented a reduction in TJ proteins occludin and ZO-1. Our study shows that pretreatment with HSP90 inhibitor 17-AAG increased expression of TJ protein claudin-5 in the cortex and periaqueductal grey (PAG) (**Figure 17**). Increased expression of claudin 5 could add to the positive effects necessary for maintaining BBB integrity during and post CSD. There was some variability noted in the western blot and in situ perfusion, a reason to note could be that we did not account for menstrual cycle in our studies. Hormones are quite influential on blood-brain barrier integrity, specifically tight junction expression.

Although more molecular studies are required to understand the relationship between HSP90 and claudin-5, some studies suggest possible mechanisms of interaction. A recently published study suggests that hypoxia-induced injury of the BBB is reduced through regulation of claudin 5 by autophagy [119]. The groups findings show that in hypoxia induced damage in cells breakdown of the BBB is partially caused by caveolin-1 (CAV1) mediated redistribution of claudin 5 into the cytosol of brain microvascular endothelial cells (BMECs). When they induced autophagy in the cells and noted degradation of CAV1 there was less aggregation of claudin 5 in the cytosol of BMECs [119]. When autophagy was inhibited via genetic or chemical methods this effect was reversed and claudin 5 aggregates formed in the cytosol leading to further BBB breakdown [119]. With this novel mechanism in mind, there has been evidence that HSP90 inhibitor 17-AAG induces the autophagic pathway [254, 255] by stimulating recruitment of LC3-II in vitro and in vivo. This suggests that the increase of claudin 5 seen in the cortex and PAG after 17-AAG treatment could be related to induction of autophagy and degradation of CAV1. Activity of kinases Rho/Rock may also be warranted as physiologically stressful event could lead to hyperphosphorylation of kinases associated with structural proteins. Rho/rock kinases could influence ZO-1 and subsequently claudin 5 proteins. HSP90 protein could be facilitating phosphorylation of rho proteins which could lead to increased activity. HSP90 inhibition could be preventing such activity decreasing structural remodeling in endothelium. The role of HSP90 could be to facilitate stress response activity in the cell which can lead to structural remodeling hindering expression of certain tight junction proteins.

Future studies on BBB dysregulation are required to limit the influence CSD events may have on chance of stroke in patients experiencing migraine with aura. Claudin 5 has been suggested to be a prominent candidate in BBB maintenance and regulation to treat ischemic

stroke [256] and may be a viable target for preventative treatment in people who experience spreading depression. CAV1 in BMECs may be of interest as a target for future studies as well as structural kinases associated with cellular structure. HSP90 inhibition has shown to be a useful method to tease apart new targets for BBB protective properties. For in vivo studies of blood-brain barrier it may be useful to make note of what cycle the female animals are in on the day of testing or tissue harvest as this may be a cause for variation in tight junction or transporter expression.

6.3 HSP90 Inhibition Modulates Endocannabinoid System in the PAG Causing Antinociceptive Effects in a CSD Model of Migraine

HSP90 is a ubiquitously expressed protein and has been documented to be upregulated in several disease states [257]. Initially, we investigated the regions of the female rat brain at 30-, 90-, 180- and 360-minutes post KCl induction of CSD and probed via western blot for the detection levels of HSP90 protein (**Figure 20**). We found that HSP90 protein was upregulated 90 minutes post CSD induction specifically in the PAG. HSP90 upregulation usually indicates increased cellular stress from noxious stimuli [122] indicating the PAG is under stressful stimuli post CSD. Considering the impact of CSD leading to the onset of neurogenic inflammation this result was a bit surprising that HSP90 protein levels were not elevated in the other regions investigated in association with ascending pain transmission suggesting a specific role for HSP90 in the PAG. The activation of the PAG during and after migraine is well documented and can remain active post-cessation of pain by treatment with triptans [21] implicating the PAG to be an important region which modulates nociception from the trigeminovascular system.

HSP90 inhibition has proven useful in pain research, specifically in inflammatory pain. HSP90 inhibition has also shown to enhance the antinociceptive properties of morphine in post-

surgical and neuropathic pain models through opioid receptor signal modulation [121, 122, 257]. We discovered that pretreatment with 0.5 nmol HSP90 inhibitor 17-AAG 24-hours before KCl cortical injection prevented the onset of periorbital allodynia and caused an overall reduction in the number of responders to CSD induction. Considering our results of up regulated HSP90 in the PAG 90 minutes post CSD induction, as well as the ablation of peak pain effect from KCl injection at the 90-minute time point by HSP90 inhibition we wanted to move forward with investigating the PAG region and the potential role of HSP90 inhibition modulating pain after CSD.

Previously in our lab a study was published on sex differences in the endocannabinoid system which may affect the onset of headache pain as migraine affects women 3:1 [188]. The study highlighted significantly lower levels of 2-AG in the PAG region of the brain, correlating with the clinical endocannabinoid deficiency (CED) theory proposing that decreased endocannabinoid activity within the CNS increases frequency of migraine. Another study using DAGL α inhibitor, LEI106, to deplete 2-AG to induce headache had also correlated with the CED theory [188] showing that decreased 2-AG can cause facial allodynia similar to CSD induction. Notably, the HSP90 co-chaperone AHA1 has been shown to directly influence CB1R expression in cells affecting membrane expression and downstream signaling of the CB1R [192]. Therefore, we hypothesized that the beneficial effects of 17-AAG inhibition of HSP90 prior to CSD induction were mediated through increased activity at the CB1R. Blockade of CB1R with rimonabant, a potent antagonist, before CSD induction increased the number of 17-AAG pretreated animals experiencing periorbital allodynia, whereas CB2R receptor antagonism with SR144 showed time-point selective effects and ultimately no change in the pain preventative effects of HSP90 inhibition. This data implicated a role for the CB1R in the 17-AAG mediated

antinociception post CSD induction. 17-AAG has been shown to cross the blood-brain barrier, it is possible that HSP90 inhibition in the PAG had a significant effect specifically through modulation of the CB1R in the PAG. To investigate these findings further we harvested PAG tissue 90 minutes post CSD induction pretreated with 0.5 nmol 17-AAG or vehicle.

Our RT- qPCR and western results showed no change in CB1R or AHA1 detection levels across all groups in the PAG tissue indicating there was no change in receptor tone meaning HSP90 inhibition could be modulating the function of the CB1R to increase activity improving pain outcome in these animals. Using a ^{35}S -GTP γ assay in the presence of a CB1R specific agonist, PrNMI, revealed a right-ward shift in potency in KCl versus aCSF groups and a further right ward shift in the 17-AAG pretreated group 90 minutes post CSD induction in PAG tissue. This shows HSP90 inhibition may play a role in desensitizing the CB1R system in the PAG during CSD suggesting increased activity of this receptor system in response to agonist response.

24-hour pretreatment with 17-AAG may increase the amount of endogenous lipid levels via regulation of enzyme activity responsible for 2-AG or AEA degradation. Results from LC/MS of PAG brain tissue 90 minutes post CSD show a significant decrease of 2-AG and AEA levels compared to naïve post KCl injection but not aCSF. Interestingly, PAG tissues harvested from animals pretreated with HSP90 inhibitor 17-AAG and 90 minutes post KCl injection showed a significant increase of AEA levels compared to vehicle suggesting a selective regulation of the endocannabinoid lipid.

17-AAG is a selective HSP90 inhibitor which when used in animals can increase HSP70 protein levels. HSP70 is a known intracellular chaperone for AEA in the cytosol [196] increased levels of HSP70 could correlate with increased AEA levels. We found no difference in levels of HSP70 between 17-AAG treated and vehicle group in PAG tissues 90 minutes post KCl

induction (**Figure 26**) via western blot. This data pointed to a different interaction between HSP90 and the endocannabinoid system although this does not rule out the role of the HSP70/90 complex entirely. Investigation of the degradative enzyme levels for AEA, FAAH, via western blot revealed that FAAH levels were significantly decreased in the PAG tissue 90 minutes post KCl injection when comparing the 17-AAG group to the vehicle group. Thus, 17AAG inhibition of HSP90 selectively increases AEA in the PAG tissue via decreased FAAH protein levels preventing AEA hydrolysis post CSD. Increased PGE2 noted by use of an Elisa of PAG tissue post aCSF or KCl injection also supports the reduction in AEA levels relevant to KCl cortical injection as it indicates FAAH hydrolytic activity creating more PGE2 as it is a direct metabolite of this pathway. Temporally, there is a rise not at 90 minutes but at 180 minutes suggesting there could be increased hydrolytic activity of AEA which can lead to increased inflammatory markers due to increased PGE2 activity. Results support a role for neuroinflammation within the PAG following CSD induction as a factor in headache-like behavior, as suggested by increased Iba-1 and GFAP detection levels. This data is consistent with other pain models showing that PGE2 in the PAG can facilitate hypersensitivity. Increased PAG functional activity corresponds to pain in migraine and may play a role in central sensitization [78, 116, 258-260]. HSP90 inhibition may be influential in preventing increased inflammation in the PAG through decreased FAAH protein levels. Further investigation of HSP90 inhibition and inflammation in the PAG is warranted.

The PAG is a midbrain structure with direct projections to the medullary and spinal dorsal horn and indirectly through the rostral ventral medulla where it can contribute to descending pain modulation. There has been research which shows electrical stimulation in unconscious rats produces analgesia supporting the PAGs role in endogenous pain modulation [21]. There has also been a study in which rats were given bicuculline, a GABA_A receptor

antagonist, via microinjection into the PAG followed by dural- evoked trigeminovascular stimulation, nociceptive neurons were inhibited as well as basal trigeminal tone in response to the treatment [80, 81]. A group has also studied the effects of AEA in the PAG specifically on GABA neurons using in vivo electrophysiological recordings, they found that AEA specifically produced a reduction in inhibitory GABAergic transmission and this effect was enhanced in the presence of an FAAH inhibitor [155]. An alternate receptor pathway that may be affected by increased AEA levels would be the TRPV1 receptor. Stimulation of the TRPV1 receptor by endocannabinoids in the PAG leads to analgesic effects [261]. HSP90s relationship to AEA and FAAH are currently unknown aside from the fact that increased expression of protein HOP1/STIP1, a co-chaperone to the HSP70/90 complex, is upregulated when AEA levels are increased [262, 263]. These findings overall support the role of endocannabinoids in headache pain associated with CSD correlating with the theory of CED as well as suggests CB1R and TRPV1R as potential therapeutic targets in treatment of migraine.

6.4 2-AG is Essential in Modulating Pain and Maintaining BBB Integrity Post CSD Events

Clinically, reduced endocannabinoid tone is reported during chronic migraine and after medication overuse [199, 208, 264-266]. Previously our group reported results showing PAG levels of 2-AG are reduced after induction of medication overuse headache [116]. We build upon that observation and show that induction of CSD reduces 2-AG levels in the PAG dynamically and that this occurs at times of peak periorbital allodynia. Pharmacological ablation of 2-AG degradation via inhibition of ABHD6 prevented and reversed periorbital allodynia associated with CSD induction. These results support 2-AG degradation as a new target for therapeutic intervention for headache pain occurring during CSD events.

Treatment with the ABHD6 inhibitor prevented and reduced CSD-induced periorbital allodynia, suggesting a new strategy to treat headache pain, supporting prior works [99, 202, 203]. The effects of preventing 2-AG degradation by ABHD6 inhibition before CSD induction were independent of CBR activation, whereas reversal of CSD periorbital allodynia by ABHD6 blockade required CBRs, primarily CB1R (**Figures 30 and 31**). CB1R is expressed by many types of neurons and predominantly localizes on presynaptic terminals to modulate neurotransmitter release [99, 105]. The reversal effect of ABHD6 inhibition likely reflects control of neurotransmitter release via increased 2-AG signaling at CB1Rs. The CBR independent effects of preventative ABHD6 inhibition may represent action of 2-AG at non-CBR sites. Alternatively, ABHD6 also metabolizes other mono-acylglycerols which may be elevated during ABHD6 inhibition that act at other receptor systems (i.e., GPR55, GPR119, PPAR, etc) [267]. Future investigations into these CBR-independent mechanisms of ABHD6 inhibition in preventing CSD-associated allodynia are warranted.

Agonists at CB1R exhibit promising therapeutic efficacy in multiple preclinical rodent pain models [268-270]. We show here that increasing 2-AG signaling at these receptors via inhibition of its hydrolyzing enzymes presents an equally promising route towards analgesia. In the context of the current results and these published reports, it is likely that reversal of CSD-associated allodynia by ABHD6 inhibition reflects control of neurotransmitter release as well as possibly limiting the role of other lipids tied to inflammation. However, enzyme inhibitors and CBR antagonists were applied systemically, and future studies are needed to determine their peripheral versus central sites of action.

Aside from pain modulation 2-AG also seems to play a role in BBB maintenance as a DAGL α inhibitor, LEI106, was applied in vitro to a BEB grown on trans-well plates and was

decrease in TEER in wells treated with LEI106; no compounding effects were seen in wells treated with LEI106 and subject to a 100 mM KCl pulse mimicking a CSD event. We report an increase in paracellular uptake of sucrose in the PAG and a near significant increase in the cortex with no change in the medulla after LEI treatment suggesting 2-AG may be involved in BBB integrity consistent with prior literature [271] Further investigation into tight junction proteins such as occludin and claudin 5 and anchoring proteins such as ZO-1 is warranted. Studies of decreased 2-AG in addition to a CSD event should also be conducted to see if there is an additive effect in vivo.

6.5 Morphine Induced MOH Compromises BBB Integrity In Vivo

Chronic morphine use can lead to medication induced headache in patients. Previously reported from our group was morphine induced MOH reduced 2-AG levels in the PAG region of the female rat brain specifically [188]. Also, we report that female rats given systemic injection of DAGL α inhibitor, LEI106, reduced blood-brain barrier integrity allowing for increased transient paracellular leak specifically in the PAG region of the brain. We wanted to assess how morphine induced headache could affect the BBB. We first report how acute and chronic morphine exposure in vitro affects the brain-endothelial barrier (BEB) utilizing TEER (**Figure 33**). We Found that morphine (35 μ M) applied 15 minutes (acute) and 24 hours (chronic) before TEER measurements showed no reduction in TEER and no additive effect was observed with extracellular KCl. There was a significant difference in reduction in TEER in the acute morphine group compared to the chronic morphine group exposed to KCl suggesting chronic morphine may prevent KCl mediated functional disruption. We confirmed this as sucrose transport was not statistically different from media controls in morphine exposed, KCl pulsed monolayers. Thus, chronic morphine has direct effect on BEB function.

We moved to an in vivo model of an intact BBB utilizing in situ brain perfusions to assess BBB integrity with ¹⁴C-sucrose. We show that continuous morphine uses significantly increased the uptake of sucrose in the PAG but not in the medulla or cortex. Although more control animals are needed at this time, these data correlate with previous data collected in our lab as well as supports the hypothesis that alterations of BBB integrity occur after chronic medication exposure and should be taken into consideration when interpreting data. Future studies are warranted to evaluate tight junction protein expression and other molecular mechanisms by which chronic drug use impact the BBB.

6.7 Concluding Remarks and Significance

In closing, CSD has been linked to changing the pH of the microenvironment of the brain. Our findings suggest that the NHE1 channel may be involved in this dysregulation as we noted inhibition causes periorbital allodynia in female rats with no CSD induction. However, we also noticed NHE1 inhibition had increased the efficacy of sumatriptan in female rat's post CSD induction. Upon further investigation we noticed no change in sumatriptan transport through manipulation Oatp1a4, but our results correlate with previous studies suggesting sumatriptan efficacy is increased when taken closer to the initiation of aura as we observed more uptake of sumatriptan into female rat's brains at earlier timepoints post CSD induction.

Through studies involving the effects of HSP90 inhibition in our in vitro and in vivo models of CSD we concluded that tight junction protein claudin 5 may have a large role in maintaining BBB integrity post CSD and may be beneficial in limiting ischemic stress from CSD events and over time preventing likelihood of ischemic stroke in patients suffering from migraine with aura. Furthermore, the use of HSP90 inhibition in our in vivo model of CSD gave insight into the role of the endocannabinoid system in modulating pain associated with migraine with

aura. We found that endocannabinoid levels were low post CSD in the PAG, increased activity through AEA at the CB1R influenced by HSP90 inhibition hypothetically led to increased pain modulation via the descending pain pathway. Therapeutics enacting on this pathway have potential for treating migraine pain.

ABHD6 inhibitors which decrease the breakdown of 2-AG in the postsynaptic neurons show prevention and reversal of headache pain associated with CSD. Reversal effects of ABHD6 inhibition is tied to CB1R activity which further suggests the role of descending pain modulation in CSD events leading to headache pain as well as its correlation with endocannabinoid deficiency. 2-AG seems to have a role in BBB regulation and maintenance as well, we showed 2-AG deficiency affected BBB integrity in the PAG. Similarly, morphine induced MOH caused a transient leak in the BBB specifically in the PAG, previous studies had shown 2-AG to be significantly reduced in the PAG in a morphine induced MOH model in vivo. these results suggest future studies into how drug delivery can be affected in the endocannabinoid deficient models of headache.

The data reported in this dissertation shows the significance of BBB integrity during CSD and its effects on drug efficacy and delivery. Additionally, it provides molecular insights of how endocannabinoid deficiency can lead to headache pain as well as blood brain barrier disruption. Targeting proteins such as ABHD6 and claudin for therapeutic treatment could be beneficial to patients suffering from migraine with aura.

Appendix:

Publications used in this dissertation

“Liktov-Busa, E., et al., *Functional NHE1 expression is critical to blood brain barrier integrity and sumatriptan blood to brain uptake*. PloS one, 2020. **15**(5): p. e0227463.”

“Verkhovsky V., Palomino S., Blawn K. et. al. *Oatp1a4 promotes blood to brain uptake of sumatriptan dosed prophylactically, but not after, cortical spreading depression induction*. In submission.”

“Palomino S., et. al., *Inhibition of HSP90 preserves blood-brain barrier integrity after cortical spreading depression via claudin 5 upregulation*. In submission.”

“Palomino S., et. al., *HSP90 inhibition mitigates facial allodynia in a CSD model through modulation of the endocannabinoid enzyme FAAH in the PAG*. In preparation.”

“Levine A., Liktov-Busa E. et. al., *ABHD6 and MAGL control 2-AG levels in the PAG and CSD-induced periorbital allodynia*. In preparation”

References

1. Saylor, D. and T.J. Steiner, *The Global Burden of Headache*. Semin Neurol, 2018. **38**(2): p. 182-190.
2. *Global, regional, and national burden of migraine and tension-type headache, 1990-2016: a systematic analysis for the Global Burden of Disease Study 2016*. Lancet Neurol, 2018. **17**(11): p. 954-976.
3. Benoliel, R. and E. Eliav, *Primary headache disorders*. Dent Clin North Am, 2013. **57**(3): p. 513-39.
4. Burch, R.C., D.C. Buse, and R.B. Lipton, *Migraine: Epidemiology, Burden, and Comorbidity*. Neurol Clin, 2019. **37**(4): p. 631-649.
5. Bahra, A., *Other primary headaches-thunderclap-, cough-, exertional-, and sexual headache*. J Neurol, 2020. **267**(5): p. 1554-1566.
6. Chou, D.E., *Secondary Headache Syndromes*. Continuum (Minneap Minn), 2018. **24**(4, Headache): p. 1179-1191.
7. Cottier, K.E., et al., *Loss of blood-brain barrier integrity in a KCl-induced model of episodic headache enhances CNS drug delivery*. Eneuro, 2018. **5**(4).
8. Eikermann-Haerter, K., et al., *Genetic and hormonal factors modulate spreading depression and transient hemiparesis in mouse models of familial hemiplegic migraine type 1*. The Journal of clinical investigation, 2009. **119**(1): p. 99-109.
9. Ayata, C. and M. Lauritzen, *Spreading depression, spreading depolarizations, and the cerebral vasculature*. Physiological reviews, 2015. **95**(3): p. 953-993.
10. Sutherland, H.G., C.L. Albury, and L.R. Griffiths, *Advances in genetics of migraine*. J Headache Pain, 2019. **20**(1): p. 72.

11. Sutherland, H.G. and L.R. Griffiths, *Genetics of Migraine: Insights into the Molecular Basis of Migraine Disorders*. Headache, 2017. **57**(4): p. 537-569.
12. Bron, C., H.G. Sutherland, and L.R. Griffiths, *Exploring the Hereditary Nature of Migraine*. Neuropsychiatr Dis Treat, 2021. **17**: p. 1183-1194.
13. de Boer, I., G.M. Terwindt, and A. van den Maagdenberg, *Genetics of migraine aura: an update*. J Headache Pain, 2020. **21**(1): p. 64.
14. Ferrari, M.D., et al., *Migraine pathophysiology: lessons from mouse models and human genetics*. Lancet Neurol, 2015. **14**(1): p. 65-80.
15. Aurora, S.K. and M.F. Brin, *Chronic Migraine: An Update on Physiology, Imaging, and the Mechanism of Action of Two Available Pharmacologic Therapies*. Headache, 2017. **57**(1): p. 109-125.
16. Burch, R.C., et al., *The prevalence and burden of migraine and severe headache in the United States: updated statistics from government health surveillance studies*. Headache: The Journal of Head and Face Pain, 2015. **55**(1): p. 21-34.
17. Ayata, C., *Cortical spreading depression triggers migraine attack: pro*. Headache: The Journal of Head and Face Pain, 2010. **50**(4): p. 725-730.
18. Lucas, C., *Migraine with aura*. Rev Neurol (Paris), 2021. **177**(7): p. 779-784.
19. Chen, S.-P. and C. Ayata, *Spreading Depression in Primary and Secondary Headache Disorders*. Current Pain and Headache Reports, 2016. **20**(7).
20. Charles, A. and K. Brennan, *The neurobiology of migraine*, in *Handbook of clinical neurology*. 2010, Elsevier. p. 99-108.
21. Goadsby, P.J., et al., *Pathophysiology of migraine: a disorder of sensory processing*. Physiological reviews, 2017.

22. Lipton, R.B. and S.D. Silberstein, *Episodic and chronic migraine headache: breaking down barriers to optimal treatment and prevention*. Headache, 2015. **55 Suppl 2**: p. 103-22; quiz 123-6.
23. *Headache Classification Committee of the International Headache Society (IHS) The International Classification of Headache Disorders, 3rd edition*. Cephalalgia, 2018. **38**(1): p. 1-211.
24. Jay, G.W. and R.L. Barkin, *Primary Headache Disorders Part I- Migraine and the Trigeminal Autonomic Cephalalgias*. Dis Mon, 2017. **63**(11): p. 308-338.
25. Russell, M.B. and A. Ducros, *Sporadic and familial hemiplegic migraine: pathophysiological mechanisms, clinical characteristics, diagnosis, and management*. The Lancet Neurology, 2011. **10**(5): p. 457-470.
26. Kaunisto, M.A., et al., *A novel missense ATP1A2 mutation in a Finnish family with familial hemiplegic migraine type 2*. Neurogenetics, 2004. **5**(2): p. 141-146.
27. Todt, U., et al., *Rare missense variants in ATP1A2 in families with clustering of common forms of migraine*. Human mutation, 2005. **26**(4): p. 315-321.
28. Dreier, J., et al., *Opening of the blood-brain barrier preceding cortical edema in a severe attack of FHM type II*. Neurology, 2005. **64**(12): p. 2145-2147.
29. Hansen, A.J. and T. Zeuthen, *Extracellular ion concentrations during spreading depression and ischemia in the rat brain cortex*. Acta Physiologica Scandinavica, 1981. **113**(4): p. 437-445.
30. Heinemann, U. and H.D. Lux, *Ceiling of stimulus induced rises in extracellular potassium concentration in the cerebral cortex of cat*. Brain research, 1977. **120**(2): p. 231-249.

31. Lothman, E., et al., *Responses of electrical potential, potassium levels, and oxidative metabolic activity of the cerebral neocortex of cats*. Brain research, 1975. **88**(1): p. 15-36.
32. Maslarova, A., et al., *Chronically epileptic human and rat neocortex display a similar resistance against spreading depolarization in vitro*. Stroke, 2011. **42**(10): p. 2917-2922.
33. Buresova, B.J., 0, Krivanek J. *The mechanism and applications of Leaos spreading depression of electroencephalographic activity*. Publ House Czech Acad Sci, Prague, 1974: p. 410.
34. Katzman, R. *Maintenance of a constant brain extracellular potassium*. in *Federation proceedings*. 1976.
35. Prince, D., H. Lux, and E. Neher, *Measurement of extracellular potassium activity in cat cortex*. Brain research, 1973. **50**(2): p. 489-495.
36. Vyskočil, F.e., N. Kríž, and J. Bures, *Potassium-selective microelectrodes used for measuring the extracellular brain potassium during spreading depression and anoxic depolarization in rats*. Brain research, 1972. **39**(1): p. 255-259.
37. Freygang Jr, W. and W.M. Landau, *Some relations between resistivity and electrical activity in the cerebral cortex of the cat*. Journal of Cellular and Comparative Physiology, 1955. **45**(3): p. 377-392.
38. Nicholson, C., et al., *Calcium and potassium changes in extracellular microenvironment of cat cerebellar cortex*. Journal of neurophysiology, 1978. **41**(4): p. 1026-1039.
39. Fabricius, M., L.H. Jensen, and M. Lauritzen, *Microdialysis of interstitial amino acids during spreading depression and anoxic depolarization in rat neocortex*. Brain research, 1993. **612**(1-2): p. 61-69.

40. Molchanova, S., et al., *Interstitial concentrations of amino acids in the rat striatum during global forebrain ischemia and potassium-evoked spreading depression*. *Neurochemical research*, 2004. **29**(8): p. 1519-1527.
41. Lindquist, B.E. and C.W. Shuttleworth, *Adenosine receptor activation is responsible for prolonged depression of synaptic transmission after spreading depolarization in brain slices*. *Neuroscience*, 2012. **223**: p. 365-376.
42. Dreier, J.P., et al., *Recording, analysis, and interpretation of spreading depolarizations in neurointensive care: review and recommendations of the COSBID research group*. *Journal of Cerebral Blood Flow & Metabolism*, 2017. **37**(5): p. 1595-1625.
43. Santos, I., et al., *Job stress is associated with migraine in current workers: The Brazilian Longitudinal Study of Adult Health (ELSA-Brazil)*. *European Journal of Pain*, 2014. **18**(9): p. 1290-1297.
44. Fujita, S., et al., *Cytoarchitecture-dependent decrease in propagation velocity of cortical spreading depression in the rat insular cortex revealed by optical imaging*. *Cerebral Cortex*, 2016. **26**(4): p. 1580-1589.
45. Chuquet, J., L. Hollender, and E.A. Nimchinsky, *High-resolution in vivo imaging of the neurovascular unit during spreading depression*. *Journal of Neuroscience*, 2007. **27**(15): p. 4036-4044.
46. Gault, L.M., et al., *Changes in energy metabolites, cGMP and intracellular pH during cortical spreading depression*. *Brain research*, 1994. **641**(1): p. 176-180.
47. Mies, G. and W. Paschen, *Regional changes of blood flow, glucose, and ATP content determined on brain sections during a single passage of spreading depression in rat brain cortex*. *Experimental neurology*, 1984. **84**(2): p. 249-258.

48. Lauritzen, M., et al., *Cortical spreading depression is associated with arachidonic acid accumulation and preservation of energy charge*. Journal of Cerebral Blood Flow & Metabolism, 1990. **10**(1): p. 115-122.
49. Moghaddam, B., et al., *Temporal relationship between neurotransmitter release and ion flux during spreading depression and anoxia*. Canadian journal of physiology and pharmacology, 1987. **65**(5): p. 1105-1110.
50. Gjedde, A., A.J. Hansen, and B. Quistorff, *Blood-brain glucose transfer in spreading depression*. Journal of neurochemistry, 1981. **37**(4): p. 807-812.
51. Kocher, M., *Metabolic and hemodynamic activation of postischemic rat brain by cortical spreading depression*. Journal of Cerebral Blood Flow & Metabolism, 1990. **10**(4): p. 564-571.
52. Csiba, L., W. Paschen, and G. Mies, *Regional changes in tissue pH and glucose content during cortical spreading depression in rat brain*. Brain research, 1985. **336**(1): p. 167-170.
53. Mutch, W. and A. Hansen, *Extracellular pH changes during spreading depression and cerebral ischemia: mechanisms of brain pH regulation*. Journal of Cerebral Blood Flow & Metabolism, 1984. **4**(1): p. 17-27.
54. Rapoport, S.I. and W.H. Marshall, *Measurement of cortical pH in spreading cortical depression*. American Journal of Physiology-Legacy Content, 1964. **206**(5): p. 1177-1180.
55. Scheller, D., J. Kolb, and F. Tegtmeier, *Lactate and pH change in close correlation in the extracellular space of the rat brain during cortical spreading depression*. Neuroscience letters, 1992. **135**(1): p. 83-86.

56. Chesler, M. and R. Kraig, *Intracellular pH of astrocytes increases rapidly with cortical stimulation*. American Journal of Physiology-Regulatory, Integrative and Comparative Physiology, 1987. **253**(4): p. R666-R670.
57. Hashemi, P., et al., *Persisting depletion of brain glucose following cortical spreading depression, despite apparent hyperaemia: evidence for risk of an adverse effect of Leao's spreading depression*. Journal of Cerebral Blood Flow & Metabolism, 2009. **29**(1): p. 166-175.
58. Gorji, A., *Spreading depression: a review of the clinical relevance*. Brain Research Reviews, 2001. **38**(1-2): p. 33-60.
59. Somjen, G.G., *Mechanisms of spreading depression and hypoxic spreading depression-like depolarization*. Physiological reviews, 2001. **81**(3): p. 1065-1096.
60. Gao, H.M., et al., *Impact of migraine attacks on the blood-brain barrier*. Chin Med J (Engl), 2010. **123**(18): p. 2559-61.
61. Zhao, H., et al., *Emerging roles of Na⁺/H⁺ exchangers in epilepsy and developmental brain disorders*. Progress in neurobiology, 2016. **138**: p. 19-35.
62. Iyengar, S., et al., *CGRP and the trigeminal system in migraine*. Headache: The Journal of Head and Face Pain, 2019. **59**(5): p. 659-681.
63. Nosedá, R. and R. Burstein, *Migraine pathophysiology: anatomy of the trigeminovascular pathway and associated neurological symptoms, cortical spreading depression, sensitization, and modulation of pain*. Pain, 2013. **154 Suppl 1**: p. S44-53.
64. Cottier, K.E., T.W. Vanderah, and T.M. Largent-Milnes, *The CNS as a primary target for migraine therapeutics*. Current Topics in Pharmacology, 2017. **21**: p. 1-16.

65. Go, J.L., P.E. Kim, and C.-S. Zee. *The trigeminal nerve*. in *Seminars in ultrasound, CT and MRI*. 2001. Elsevier.
66. Millan, M.J., *Descending control of pain*. *Progress in neurobiology*, 2002. **66**(6): p. 355-474.
67. Burstein, R., et al., *Chemical stimulation of the intracranial dura induces enhanced responses to facial stimulation in brain stem trigeminal neurons*. *Journal of neurophysiology*, 1998. **79**(2): p. 964-982.
68. Liu, Y., J. Broman, and L. Edvinsson, *Central projections of sensory innervation of the rat superior sagittal sinus*. *Neuroscience*, 2004. **129**(2): p. 431-437.
69. Cechetto, D.F., D.G. Standaert, and C.B. Saper, *Spinal and trigeminal dorsal horn projections to the parabrachial nucleus in the rat*. *Journal of Comparative Neurology*, 1985. **240**(2): p. 153-160.
70. Dallel, R., O. Ricard, and P. Raboisson, *Organization of parabrachial projections from the spinal trigeminal nucleus oralis: an anterograde tracing study in the rat*. *Journal of Comparative Neurology*, 2004. **470**(2): p. 181-191.
71. Rodriguez, E., et al., *A craniofacial-specific monosynaptic circuit enables heightened affective pain*. *Nature neuroscience*, 2017. **20**(12): p. 1734-1743.
72. Goadsby, P.J. and P.R. Holland, *An Update: Pathophysiology of Migraine*. *Neurol Clin*, 2019. **37**(4): p. 651-671.
73. Romero-Reyes, M. and S. Akerman, *Update on animal models of migraine*. *Current pain and headache reports*, 2014. **18**(11): p. 1-12.
74. Munro, G., I. Jansen-Olesen, and J. Olesen, *Animal models of pain and migraine in drug discovery*. *Drug discovery today*, 2017. **22**(7): p. 1103-1111.

75. Zagami, A. and G. Lambert, *Stimulation of cranial vessels excites nociceptive neurones in several thalamic nuclei of the cat*. Experimental brain research, 1990. **81**(3): p. 552-566.
76. Weiller, C., et al., *Brain stem activation in spontaneous human migraine attacks*. Nature medicine, 1995. **1**(7): p. 658-660.
77. Domínguez, C., et al., *Iron deposition in periaqueductal gray matter as a potential biomarker for chronic migraine*. Neurology, 2019. **92**(10): p. e1076-e1085.
78. Solstrand Dahlberg, L., et al., *Responsivity of periaqueductal gray connectivity is related to headache frequency in episodic migraine*. Frontiers in neurology, 2018. **9**: p. 61.
79. Knight, Y. and P. Goadsby, *The periaqueductal grey matter modulates trigeminovascular input: a role in migraine?* Neuroscience, 2001. **106**(4): p. 793-800.
80. Knight, Y.E., T. Bartsch, and P.J. Goadsby, *Trigeminal antinociception induced by bicuculline in the periaqueductal gray (PAG) is not affected by PAG P/Q-type calcium channel blockade in rat*. Neuroscience letters, 2003. **336**(2): p. 113-116.
81. Knight, Y.E., et al., *P/Q-type calcium-channel blockade in the periaqueductal gray facilitates trigeminal nociception: a functional genetic link for migraine?* Journal of Neuroscience, 2002. **22**(5): p. RC213-RC213.
82. Chong, C.D., et al., *Migraine classification using magnetic resonance imaging resting-state functional connectivity data*. Cephalalgia, 2017. **37**(9): p. 828-844.
83. Pozo-Rosich, P., et al., *Periaqueductal gray calcitonin gene-related peptide modulates trigeminovascular neurons*. Cephalalgia, 2015. **35**(14): p. 1298-1307.
84. Bartsch, T., Y.E. Knight, and P.J. Goadsby, *Activation of 5-HT_{1B/1D} receptor in the periaqueductal gray inhibits nociception*. Annals of neurology, 2004. **56**(3): p. 371-381.

85. Charles, A., *The migraine aura*. Continuum: Lifelong learning in Neurology, 2018. **24**(4): p. 1009-1022.
86. Li, L., et al., *Involvement of adenosine monophosphate-activated protein kinase in morphine-induced cardioprotection*. Journal of Surgical Research, 2011. **169**(2): p. 179-187.
87. Eftekhari, S., et al., *Differentiation of nerve fibers storing CGRP and CGRP receptors in the peripheral trigeminovascular system*. The Journal of Pain, 2013. **14**(11): p. 1289-1303.
88. Ottosson, A. and L. Edvinsson, *Release of histamine from dural mast cells by substance P and calcitonin gene-related peptide*. Cephalalgia, 1997. **17**(3): p. 166-174.
89. Hamel, E., *Serotonin and migraine: biology and clinical implications*. Cephalalgia, 2007. **27**(11): p. 1293-300.
90. Jacobs, B.L. and E.C. Azmitia, *Structure and function of the brain serotonin system*. Physiological reviews, 1992. **72**(1): p. 165-229.
91. Hornung, J.-P., *The human raphe nuclei and the serotonergic system*. Journal of chemical neuroanatomy, 2003. **26**(4): p. 331-343.
92. Hannon, J. and D. Hoyer, *Molecular biology of 5-HT receptors*. Behavioural brain research, 2008. **195**(1): p. 198-213.
93. Cameron, C., et al., *Triptans in the Acute Treatment of Migraine: A Systematic Review and Network Meta-Analysis*. Headache, 2015. **55 Suppl 4**: p. 221-35.
94. de Vries, T., C.M. Villalón, and A. MaassenVanDenBrink, *Pharmacological treatment of migraine: CGRP and 5-HT beyond the triptans*. Pharmacol Ther, 2020. **211**: p. 107528.

95. Schuh-Hofer, S., et al., *Increased serotonin transporter availability in the brainstem of migraineurs*. Journal of neurology, 2007. **254**(6): p. 789-796.
96. Evers, S., et al., *Efficacy of frovatriptan as compared to other triptans in migraine with aura*. J Headache Pain, 2015. **16**: p. 514.
97. Hansen, J.M., P.J. Goadsby, and A. Charles, *Reduced efficacy of sumatriptan in migraine with aura vs without aura*. Neurology, 2015. **84**(18): p. 1880-5.
98. Tietjen, G.E., et al., *Allodynia in migraine: association with comorbid pain conditions*. Headache: The Journal of Head and Face Pain, 2009. **49**(9): p. 1333-1344.
99. Greco, R., et al., *Endocannabinoid System and Migraine Pain: An Update*. Front Neurosci, 2018. **12**: p. 172.
100. Blawn, K.T., et al., *Sex hormones regulate NHE1 functional expression and brain endothelial proteome to control paracellular integrity of the blood endothelial barrier*. Brain Research, 2021. **1763**: p. 147448.
101. Bodor, Á.L., et al., *Endocannabinoid signaling in rat somatosensory cortex: laminar differences and involvement of specific interneuron types*. Journal of Neuroscience, 2005. **25**(29): p. 6845-6856.
102. Hu, S.S.-J. and K. Mackie, *Distribution of the endocannabinoid system in the central nervous system*. Endocannabinoids, 2015: p. 59-93.
103. Navarrete, M. and A. Araque, *Endocannabinoids mediate neuron-astrocyte communication*. Neuron, 2008. **57**(6): p. 883-893.
104. Lauckner, J.E., B. Hille, and K. Mackie, *The cannabinoid agonist WIN55, 212-2 increases intracellular calcium via CB1 receptor coupling to Gq/11 G proteins*. Proceedings of the National Academy of Sciences, 2005. **102**(52): p. 19144-19149.

105. Lu, H.-C. and K. Mackie, *Review of the endocannabinoid system*. *Biological Psychiatry: Cognitive Neuroscience and Neuroimaging*, 2021. **6**(6): p. 607-615.
106. Nyiri, G., et al., *CB1 cannabinoid receptors are enriched in the perisynaptic annulus and on preterminal segments of hippocampal GABAergic axons*. *Neuroscience*, 2005. **136**(3): p. 811-822.
107. Di Marzo, V., *New approaches and challenges to targeting the endocannabinoid system*. *Nature Reviews Drug Discovery*, 2018. **17**(9): p. 623-639.
108. Morales, P. and P.H. Reggio, *An update on non-CB1, non-CB2 cannabinoid related G-protein-coupled receptors*. *Cannabis and cannabinoid research*, 2017. **2**(1): p. 265-273.
109. Nomura, D.K., et al., *Endocannabinoid hydrolysis generates brain prostaglandins that promote neuroinflammation*. *Science*, 2011. **334**(6057): p. 809-813.
110. Tassorelli, C., R. Greco, and S.D. Silberstein, *The endocannabinoid system in migraine: from bench to pharmacy and back*. *Curr Opin Neurol*, 2019. **32**(3): p. 405-412.
111. Kandasamy, R., et al., *Anti-migraine effect of Δ^9 -tetrahydrocannabinol in the female rat*. *European journal of pharmacology*, 2018. **818**: p. 271-277.
112. Akerman, S., P.R. Holland, and P.J. Goadsby, *Cannabinoid (CB1) receptor activation inhibits trigeminovascular neurons*. *Journal of Pharmacology and Experimental Therapeutics*, 2007. **320**(1): p. 64-71.
113. Akerman, S., et al., *Endocannabinoids in the brainstem modulate dural trigeminovascular nociceptive traffic via CB1 and "triptan" receptors: implications in migraine*. *Journal of Neuroscience*, 2013. **33**(37): p. 14869-14877.
114. Maione, S., et al., *Elevation of endocannabinoid levels in the ventrolateral periaqueductal grey through inhibition of fatty acid amide hydrolase affects descending*

- nociceptive pathways via both cannabinoid receptor type 1 and transient receptor potential vanilloid type-1 receptors. Journal of Pharmacology and Experimental Therapeutics, 2006. 316(3): p. 969-982.*
115. Burston, J.J. and S.G. Woodhams, *Endocannabinoid system and pain: an introduction. Proceedings of the nutrition society, 2014. 73(1): p. 106-117.*
116. Levine, A., et al., *Sex differences in the expression of the endocannabinoid system within VIM cortex and PAG of Sprague Dawley rats. Biol Sex Differ, 2021. 12(1): p. 60.*
117. Hawkins, B.T. and T.P. Davis, *The blood-brain barrier/neurovascular unit in health and disease. Pharmacol Rev, 2005. 57(2): p. 173-85.*
118. Urquhart, B.L. and R.B. Kim, *Blood– brain barrier transporters and response to CNS-active drugs. European journal of clinical pharmacology, 2009. 65(11): p. 1063-1070.*
119. Zou, D., et al., *Rapid orderly migration of neutrophils after traumatic brain injury depends on MMP9/13. Biochemical and Biophysical Research Communications, 2021. 579: p. 161-167.*
120. Islam, Y., et al., *Development of brain targeting peptide based MMP-9 inhibiting nanoparticles for the treatment of brain diseases with elevated MMP-9 activity. Journal of pharmaceutical sciences, 2020. 109(10): p. 3134-3144.*
121. Schopf, F.H., M.M. Biebl, and J. Buchner, *The HSP90 chaperone machinery. Nat Rev Mol Cell Biol, 2017. 18(6): p. 345-360.*
122. Streicher, J.M., *The role of heat shock proteins in regulating receptor signal transduction. Molecular Pharmacology, 2019. 95(5): p. 468-474.*

123. Duron, D.I., et al., *Inhibition of Hsp90 in the spinal cord enhances the antinociceptive effects of morphine by activating an ERK-RSK pathway*. *Science signaling*, 2020. **13**(630): p. eaaz1854.
124. Khan, A.U., et al., *Inhibition of NF- κ B signaling and HSP70/HSP90 proteins by newly synthesized hydrazide derivatives in arthritis model*. *Naunyn Schmiedebergs Arch Pharmacol*, 2021. **394**(7): p. 1497-1519.
125. Casey, J.R., S. Grinstein, and J. Orlowski, *Sensors and regulators of intracellular pH*. *Nature reviews Molecular cell biology*, 2010. **11**(1): p. 50-61.
126. Yao, H., et al., *Intracellular pH regulation of CA1 neurons in Na⁺/H⁺ isoform 1 mutant mice*. *The Journal of clinical investigation*, 1999. **104**(5): p. 637-645.
127. Cui, Y., et al., *11C-PK11195 PET for the in vivo evaluation of neuroinflammation in the rat brain after cortical spreading depression*. *Journal of Nuclear Medicine*, 2009. **50**(11): p. 1904-1911.
128. Putney, L., *Denker SP, and Barber DL*. The changing face of the Na⁺/H⁺ exchanger, NHE1: structure, regulation, and cellular actions. *Annu Rev Pharmacol Toxicol*, 2002. **42**: p. 527-552.
129. Bkaily, G., et al., *Immunofluorescence revealed the presence of NHE-1 in the nuclear membranes of rat cardiomyocytes and isolated nuclei of human, rabbit, and rat aortic and liver tissues*. *Canadian journal of physiology and pharmacology*, 2004. **82**(8-9): p. 805-811.
130. Park, S.L., et al., *The effect of Na⁺/H⁺ exchanger-1 inhibition by sabiporide on blood-brain barrier dysfunction after ischemia/hypoxia in vivo and in vitro*. *Brain research*, 2010. **1366**: p. 189-196.

131. Ferrari, M.D., et al., *Migraine*. Nat Rev Dis Primers, 2022. **8**(1): p. 2.
132. Begum, G., et al., *Selective knockout of astrocytic Na⁺/H⁺ exchanger isoform 1 reduces astrogliosis, BBB damage, infarction, and improves neurological function after ischemic stroke*. Glia, 2018. **66**(1): p. 126-144.
133. Abbott, N.J., et al., *Structure and function of the blood–brain barrier*. Neurobiology of disease, 2010. **37**(1): p. 13-25.
134. Nagy, Z., M. Szabo, and I. Hüttner, *Blood-brain barrier impairment by low pH buffer perfusion via the internal carotid artery in rat*. Acta neuropathologica, 1985. **68**(2): p. 160-163.
135. Rapoport, S., *Cortical pH and the blood-brain barrier*. The Journal of Physiology, 1964. **170**(2): p. 238.
136. Wong, A., et al., *The blood-brain barrier: an engineering perspective* Front. 2013, Neuroengineering.
137. Oldendorf, W., L. Braun, and E. Cornford, *pH dependence of blood-brain barrier permeability to lactate and nicotine*. Stroke, 1979. **10**(5): p. 577-581.
138. Shi, Y., et al., *Role of sodium/hydrogen exchanger isoform 1 in microglial activation and proinflammatory responses in ischemic brains*. Journal of neurochemistry, 2011. **119**(1): p. 124-135.
139. Fioravanti, B., et al., *Evaluation of cutaneous allodynia following induction of cortical spreading depression in freely moving rats*. Cephalalgia, 2011. **31**(10): p. 1090-1100.
140. Edelmayer, R.M., et al., *Medullary pain facilitating neurons mediate allodynia in headache-related pain*. Annals of Neurology: Official Journal of the American Neurological Association and the Child Neurology Society, 2009. **65**(2): p. 184-193.

141. Edelmayer, R.M., M.H. Ossipov, and F. Porreca, *An experimental model of headache-related pain*, in *Pain Research*. 2012, Springer. p. 109-120.
142. Andrew, R.D., Y.-T. Hsieh, and C.D. Brisson, *Spreading depolarization triggered by elevated potassium is weak or absent in the rodent lower brain*. *Journal of Cerebral Blood Flow & Metabolism*, 2017. **37**(5): p. 1735-1747.
143. McCaffrey, G., et al., *Tight junctions contain oligomeric protein assembly critical for maintaining blood–brain barrier integrity in vivo*. *Journal of neurochemistry*, 2007. **103**(6): p. 2540-2555.
144. Tome, M.E., et al., *Acute pain alters P-glycoprotein-containing protein complexes in rat cerebral microvessels: Implications for P-glycoprotein trafficking*. *Journal of Cerebral Blood Flow & Metabolism*, 2018. **38**(12): p. 2209-2222.
145. Liktor-Busa, E., et al., *Functional NHE1 expression is critical to blood brain barrier integrity and sumatriptan blood to brain uptake*. *PloS one*, 2020. **15**(5): p. e0227463.
146. Menyhárt, Á., et al., *Age or ischemia uncouples the blood flow response, tissue acidosis, and direct current potential signature of spreading depolarization in the rat brain*. *American Journal of Physiology-Heart and Circulatory Physiology*, 2017. **313**(2): p. H328-H337.
147. Lourenço, C.F., et al., *Neurometabolic and electrophysiological changes during cortical spreading depolarization: Multimodal approach based on a lactate-glucose dual microbiosensor arrays*. *Scientific reports*, 2017. **7**(1): p. 1-12.
148. Mainero, C., J. Boshyan, and N. Hadjikhani, *Altered functional magnetic resonance imaging resting-state connectivity in periaqueductal gray networks in migraine*. *Annals of neurology*, 2011. **70**(5): p. 838-845.

149. Crimi, E., et al., *Effects of intracellular acidosis on endothelial function: an overview*. Journal of critical care, 2012. **27**(2): p. 108-118.
150. Mason, B.N. and A.F. Russo, *Vascular contributions to migraine: time to revisit?* Frontiers in cellular neuroscience, 2018: p. 233.
151. Zhao, J. and D. Levy, *Cortical spreading depression promotes persistent mechanical sensitization of intracranial meningeal afferents: implications for the intracranial mechanosensitivity of migraine*. Eneuro, 2016. **3**(6).
152. Charles, A. and K. Brennan, *Cortical spreading depression—new insights and persistent questions*. Cephalalgia, 2009. **29**(10): p. 1115-1124.
153. Hladky, S.B. and M.A. Barrand, *Fluid and ion transfer across the blood–brain and blood–cerebrospinal fluid barriers; a comparative account of mechanisms and roles*. Fluids and Barriers of the CNS, 2016. **13**(1): p. 1-69.
154. Roth, M., A. Obaidat, and B. Hagenbuch, *OATPs, OATs and OCTs: the organic anion and cation transporters of the SLCO and SLC22A gene superfamilies*. British journal of pharmacology, 2012. **165**(5): p. 1260-1287.
155. Thompson, B.J., et al., *Hypoxia/reoxygenation stress signals an increase in organic anion transporting polypeptide 1a4 (Oatp1a4) at the blood–brain barrier: relevance to CNS drug delivery*. Journal of Cerebral Blood Flow & Metabolism, 2014. **34**(4): p. 699-707.
156. Ronaldson, P.T., et al., *Inflammatory pain signals an increase in functional expression of organic anion transporting polypeptide 1a4 at the blood-brain barrier*. Journal of Pharmacology and Experimental Therapeutics, 2011. **336**(3): p. 827-839.

157. Cheng, Z., et al., *Hydrophilic anti-migraine triptans are substrates for OATP1A2, a transporter expressed at human blood-brain barrier*. *Xenobiotica*, 2012. **42**(9): p. 880-890.
158. Sano, Y., et al., *Evaluation of organic anion transporter 1A2-knock-in mice as a model of human blood-brain barrier*. *Drug Metabolism and Disposition*, 2018. **46**(11): p. 1767-1775.
159. Seelbach, M.J., et al., *Peripheral inflammatory hyperalgesia modulates morphine delivery to the brain: a role for P-glycoprotein*. *Journal of neurochemistry*, 2007. **102**(5): p. 1677-1690.
160. Ronaldson, P.T., et al., *Transforming growth factor- β signaling alters substrate permeability and tight junction protein expression at the blood-brain barrier during inflammatory pain*. *Journal of Cerebral Blood Flow & Metabolism*, 2009. **29**(6): p. 1084-1098.
161. Kalliokoski, A. and M. Niemi, *Impact of OATP transporters on pharmacokinetics*. *British journal of pharmacology*, 2009. **158**(3): p. 693-705.
162. Franke, R.M., L.A. Scherkenbach, and A. Sparreboom, *Pharmacogenetics of the organic anion transporting polypeptide 1A2*. 2009.
163. Imai, S., et al., *DNA methylation and histone modification profiles of mouse organic anion transporting polypeptides*. *Drug Metabolism and Disposition*, 2013. **41**(1): p. 72-78.
164. Abdullahi, W., et al., *Functional expression of organic anion transporting polypeptide 1a4 is regulated by transforming growth factor- β /Activin receptor-like kinase 1 signaling at the blood-brain barrier*. *Molecular pharmacology*, 2018. **94**(6): p. 1321-1333.

165. Lauritzen, M., et al., *Clinical Relevance of Cortical Spreading Depression in Neurological Disorders: Migraine, Malignant Stroke, Subarachnoid and Intracranial Hemorrhage, and Traumatic Brain Injury*. *Journal of Cerebral Blood Flow & Metabolism*, 2011. **31**(1): p. 17-35.
166. Enger, R., et al., *Dynamics of Ionic Shifts in Cortical Spreading Depression*. *Cereb Cortex*, 2015. **25**(11): p. 4469-76.
167. Gursoy-Ozdemir, Y., et al., *Cortical spreading depression activates and upregulates MMP-9*. 2004. **113**(10): p. 1447-1455.
168. Thuringer, D. and C. Garrido, *Molecular chaperones in the brain endothelial barrier: neurotoxicity or neuroprotection?* *The FASEB Journal*, 2019. **33**(11): p. 11629-11639.
169. Aridon, P., et al., *Protective role of heat shock proteins in Parkinson's disease*. *Neurodegenerative diseases*, 2011. **8**(4): p. 155-168.
170. Lei, W., et al., *Heat-shock protein 90 (Hsp90) promotes opioid-induced anti-nociception by an ERK mitogen-activated protein kinase (MAPK) mechanism in mouse brain*. *Journal of Biological Chemistry*, 2017. **292**(25): p. 10414-10428.
171. Kruse, R., et al., *Characterization of the CLASP2 protein interaction network identifies SOGA1 as a microtubule-associated protein*. *Molecular & Cellular Proteomics*, 2017. **16**(10): p. 1718-1735.
172. Srinivasan, B., et al., *TEER measurement techniques for in vitro barrier model systems*. *Journal of laboratory automation*, 2015. **20**(2): p. 107-126.
173. Kadry, H., B. Noorani, and L. Cucullo, *A blood-brain barrier overview on structure, function, impairment, and biomarkers of integrity*. *Fluids and Barriers of the CNS*, 2020. **17**(1): p. 1-24.

174. Qi, J., et al., *Heat shock protein 90 inhibition by 17-Dimethylaminoethylamino-17-demethoxygeldanamycin protects blood-brain barrier integrity in cerebral ischemic stroke*. American Journal of Translational Research, 2015. **7**(10): p. 1826.
175. Schubert-Unkmeir, A., et al., *Gene expression pattern in human brain endothelial cells in response to Neisseria meningitidis*. Infection and immunity, 2007. **75**(2): p. 899-914.
176. Uddin, M.A., et al., *Hsp90 inhibition protects the brain microvascular endothelium against oxidative stress*. Brain Disorders, 2021. **1**: p. 100001.
177. Lu, T.-S., et al., *Heat shock treatment protects osmotic stress–induced dysfunction of the blood-brain barrier through preservation of tight junction proteins*. Cell stress & chaperones, 2004. **9**(4): p. 369.
178. Miles, V.N., et al., *The Effect of Heat Shock Protein 90 Inhibitor on Pain in Cancer Patients: A Systematic Review and Meta-Analysis*. Medicina, 2020. **57**(1): p. 5.
179. Filipeanu, C.M., et al., *Δ9-THC increases endogenous AHA1 expression in rat cerebellum and may modulate CB1 receptor function during chronic use*. Journal of neurochemistry, 2011. **118**(6): p. 1101-1112.
180. Russo, E.B., *Clinical endocannabinoid deficiency (CECD): can this concept explain therapeutic benefits of cannabis in migraine, fibromyalgia, irritable bowel syndrome and other treatment-resistant conditions?* Neuro endocrinology letters, 2008. **29**(2): p. 192-200.
181. Greco, R., et al., *Dual Inhibition of FAAH and MAGL Counteracts Migraine-like Pain and Behavior in an Animal Model of Migraine*. Cells, 2021. **10**(10).
182. Leimuranta, P., L. Khiroug, and R. Giniatullin, *Emerging Role of (Endo)Cannabinoids in Migraine*. Front Pharmacol, 2018. **9**: p. 420.

183. Zou, S. and U. Kumar, *Cannabinoid Receptors and the Endocannabinoid System: Signaling and Function in the Central Nervous System*. Int J Mol Sci, 2018. **19**(3).
184. Clayton, J.A. and F.S. Collins, *Policy: NIH to balance sex in cell and animal studies*. Nature, 2014. **509**(7500): p. 282-283.
185. Bolay, H., N.E. Berman, and D. Akcali, *Sex-related differences in animal models of migraine headache*. Headache: The Journal of Head and Face Pain, 2011. **51**(6): p. 891-904.
186. Chai, N.C., B.L. Peterlin, and A.H. Calhoun, *Migraine and estrogen*. Current opinion in neurology, 2014. **27**(3): p. 315.
187. Wilkerson, E.M., et al., *The peripheral blood eosinophil proteome*. Journal of proteome research, 2016. **15**(5): p. 1524-1533.
188. Levine, A., et al., *DAGL α Inhibition as a Non-invasive and Translational Model of Episodic Headache*. Front Pharmacol, 2020. **11**: p. 615028.
189. Alcazar, A. and C. Cid, *High cytotoxic sensitivity of the oligodendrocyte precursor cells to HSP90 inhibitors in cell cultures*. Experimental neurology, 2009. **216**(2): p. 511-514.
190. Pastvova, N., P. Dolezel, and P. Mlejnek, *Heat Shock Protein Inhibitor 17-Allyl-17-Demethoxygeldanamycin, a Potent Inductor of Apoptosis in Human Glioma Tumor Cell Lines, Is a Weak Substrate for ABCB1 and ABCG2 Transporters*. Pharmaceuticals, 2021. **14**(2): p. 107.
191. Singh, J.K., et al., *Management of Hsp90-Dependent protein folding by small molecules targeting the Aha1 Co-Chaperone*. Cell chemical biology, 2020. **27**(3): p. 292-305. e6.

192. Filipeanu, C.M., et al., *Modulation of $\alpha 2C$ adrenergic receptor temperature-sensitive trafficking by HSP90*. *Biochimica et Biophysica Acta (BBA)-Molecular Cell Research*, 2011. **1813**(2): p. 346-357.
193. Oroz, J., L.J. Blair, and M. Zweckstetter, *Dynamic Aha1 co-chaperone binding to human Hsp90*. *Protein Science*, 2019. **28**(9): p. 1545-1551.
194. Yamamoto, T., et al., *Selective targeting of peripheral cannabinoid receptors prevents behavioral symptoms and sensitization of trigeminal neurons in mouse models of migraine and medication overuse headache*. *Pain*, 2021. **160**(8): p. 2246-2262.
195. Seltzman, H.H., et al., *Peripherally selective cannabinoid 1 receptor (CB1R) agonists for the treatment of neuropathic pain*. *Journal of medicinal chemistry*, 2016. **59**(16): p. 7525-7543.
196. Batulan, Z., et al., *Induction of multiple heat shock proteins and neuroprotection in a primary culture model of familial amyotrophic lateral sclerosis*. *Neurobiology of disease*, 2006. **24**(2): p. 213-225.
197. Woodhams, S.G., et al., *The cannabinoid system and pain*. *Neuropharmacology*, 2017. **124**: p. 105-120.
198. Greco, R., et al., *The endocannabinoid system and migraine*. *Experimental neurology*, 2010. **224**(1): p. 85-91.
199. Cupini, L., et al., *Biochemical changes in endocannabinoid system are expressed in platelets of female but not male migraineurs*. *Cephalalgia*, 2006. **26**(3): p. 277-281.
200. Sarchielli, P., et al., *Endocannabinoids in chronic migraine: CSF findings suggest a system failure*. *Neuropsychopharmacology*, 2007. **32**(6): p. 1384-1390.

201. Rossi, C., et al., *Endocannabinoids in platelets of chronic migraine patients and medication-overuse headache patients: relation with serotonin levels*. *European journal of clinical pharmacology*, 2008. **64**(1): p. 1-8.
202. Greco, R., et al., *Effects of peripheral FAAH blockade on NTG-induced hyperalgesia—evaluation of URB937 in an animal model of migraine*. *Cephalalgia*, 2015. **35**(12): p. 1065-1076.
203. Nozaki, C., A. Markert, and A. Zimmer, *Inhibition of FAAH reduces nitroglycerin-induced migraine-like pain and trigeminal neuronal hyperactivity in mice*. *European Neuropsychopharmacology*, 2015. **25**(8): p. 1388-1396.
204. Kaur, R., P. Sidhu, and S. Singh, *What failed BIA 10–2474 Phase I clinical trial? Global speculations and recommendations for future Phase I trials*. *Journal of pharmacology & pharmacotherapeutics*, 2016. **7**(3): p. 120.
205. Ghaemi, A., et al., *Astrocyte-mediated inflammation in cortical spreading depression*. *Cephalalgia*, 2018. **38**(4): p. 626-638.
206. Hsu, K.-L., et al., *Discovery and optimization of piperidyl-1, 2, 3-triazole ureas as potent, selective, and in vivo-active inhibitors of α/β -hydrolase domain containing 6 (ABHD6)*. *Journal of medicinal chemistry*, 2013. **56**(21): p. 8270-8279.
207. Yousif, S., et al., *Effect of chronic exposure to morphine on the rat blood–brain barrier: focus on the P-glycoprotein*. *Journal of neurochemistry*, 2008. **107**(3): p. 647-657.
208. Collaborators, G.B.o.D., *Global, regional, and national burden of neurological disorders, 1990–2016: a systematic analysis for the Global Burden of Disease Study 2016*. 2019.

209. Sueiras, M., et al., *Cortical spreading depression phenomena are frequent in ischemic and traumatic penumbra: a prospective study in patients with traumatic brain injury and large hemispheric ischemic stroke*. Journal of Clinical Neurophysiology, 2021. **38**(1): p. 47-55.
210. Øie, L.R., et al., *Migraine and risk of stroke*. Journal of Neurology, Neurosurgery & Psychiatry, 2020. **91**(6): p. 593-604.
211. Chiang, M.-C., et al., *Migraine with Visual aura and the Risk of Stroke-a Narrative Review*. Journal of Stroke and Cerebrovascular Diseases, 2021. **30**(11): p. 106067.
212. Pearn, M.L., et al., *Pathophysiology associated with traumatic brain injury: current treatments and potential novel therapeutics*. Cellular and molecular neurobiology, 2017. **37**(4): p. 571-585.
213. Bernardo-Castro, S., et al., *Pathophysiology of blood–brain barrier permeability throughout the different stages of ischemic stroke and its implication on hemorrhagic transformation and recovery*. Frontiers in Neurology, 2020: p. 1605.
214. Feigin, V.L., et al., *Burden of neurological disorders across the US from 1990-2017: a global burden of disease study*. JAMA neurology, 2021. **78**(2): p. 165-176.
215. Burton, W.N., et al., *The economic burden of lost productivity due to migraine headache: a specific worksite analysis*. Journal of occupational and environmental medicine, 2002: p. 523-529.
216. Schwedt, T.J., *Chronic migraine*. Bmj, 2014. **348**: p. g1416.
217. Andreou, A.P. and L. Edvinsson, *Mechanisms of migraine as a chronic evolutive condition*. J Headache Pain, 2019. **20**(1): p. 117.

218. Marmura, M.J., S.D. Silberstein, and T.J. Schwedt, *The acute treatment of migraine in adults: the american headache society evidence assessment of migraine pharmacotherapies*. Headache, 2015. **55**(1): p. 3-20.
219. Burstein, R., B. Collins, and M. Jakubowski, *Defeating migraine pain with triptans: a race against the development of cutaneous allodynia*. Annals of Neurology: Official Journal of the American Neurological Association and the Child Neurology Society, 2004. **55**(1): p. 19-26.
220. Beydoun, R., et al., *Na⁺/H⁺ exchanger 9 regulates iron mobilization at the blood-brain barrier in response to iron starvation*. Journal of Biological Chemistry, 2017. **292**(10): p. 4293-4301.
221. Yuen, N.Y., et al., *Exacerbated brain edema in a rat streptozotocin model of hyperglycemic ischemic stroke: Evidence for involvement of blood–brain barrier Na–K–Cl cotransport and Na/H exchange*. Journal of Cerebral Blood Flow & Metabolism, 2019. **39**(9): p. 1678-1692.
222. Luo, J., Chen H, Kintner DB, Shull GE, Sun D. Decreased neuronal death in Na⁺/H⁺ exchanger isoform: p. 11256-11268.
223. Viana, M., et al., *Triptan nonresponders: do they exist and who are they?* Cephalalgia, 2013. **33**(11): p. 891-896.
224. Bressler, J., K. Clark, and C. O’Driscoll, *Assessing Blood–Brain Barrier Function Using In Vitro Assays*, in *Cell-Cell Interactions*. 2013, Springer. p. 67-79.
225. Witt, K.A., et al., *Peptide drug modifications to enhance bioavailability and blood-brain barrier permeability*. Peptides, 2001. **22**(12): p. 2329-2343.

226. Gentile, S., et al., *Reversible MRI abnormalities in a patient with recurrent status migrainosus*. Cephalalgia, 2009. **29**(6): p. 687-690.
227. Torres-López, J.E., et al., *Role of NHE1 in Nociception*. Pain Research and Treatment, 2013. **2013**.
228. Castañeda-Corral, G., et al., *Role of the spinal Na⁺/H⁺ exchanger in formalin-induced nociception*. Neuroscience letters, 2011. **501**(1): p. 4-9.
229. Castañeda-Corral, G., et al., *Blockade of peripheral and spinal Na⁺/H⁺ exchanger increases formalin-induced long-lasting mechanical allodynia and hyperalgesia in rats*. Brain research, 2012. **1475**: p. 19-30.
230. Rocha-Gonzalez, H.I., et al., *Identification of the Na⁺/H⁺ exchanger 1 in dorsal root ganglion and spinal cord: its possible role in inflammatory nociception*. Neuroscience, 2009. **160**(1): p. 156-164.
231. Steen, K.H., H. Wegner, and P.W. Reeh, *The pH response of rat cutaneous nociceptors correlates with extracellular [Na⁺] and is increased under amiloride*. European Journal of Neuroscience, 1999. **11**(8): p. 2783-2792.
232. Xiong, Z.-Q. and J.L. Stringer, *Extracellular pH responses in CA1 and the dentate gyrus during electrical stimulation, seizure discharges, and spreading depression*. Journal of neurophysiology, 2000. **83**(6): p. 3519-3524.
233. Sinning, A. and C.A. Hübner, *Minireview: pH and synaptic transmission*. FEBS letters, 2013. **587**(13): p. 1923-1928.
234. Albekairi, T.H., et al., *Brain delivery of a potent opioid receptor agonist, biphalin during ischemic stroke: role of organic anion transporting polypeptide (OATP)*. Pharmaceutics, 2019. **11**(9): p. 467.

235. Gilmore, B. and M. Michael, *Treatment of acute migraine headache*. American family physician, 2011. **83**(3): p. 271-280.
236. Humphrey, P.P., et al., *Serotonin and migraine*. Annals of the new York Academy of Sciences, 1990.
237. Smitherman, T.A., et al., *The Prevalence, Impact, and Treatment of Migraine and Severe Headaches in the United States: A Review of Statistics From National Surveillance Studies*. Headache: The Journal of Head and Face Pain, 2013. **53**(3): p. 427-436.
238. Thorlund, K., et al., *Comparative efficacy of triptans for the abortive treatment of migraine: a multiple treatment comparison meta-analysis*. Cephalalgia, 2014. **34**(4): p. 258-267.
239. Burgos-Vega, C., J. Moy, and G. Dussor, *Meningeal afferent signaling and the pathophysiology of migraine*. Progress in molecular biology and translational science, 2015. **131**: p. 537-564.
240. Bigal, M.E. and R.B. Lipton, *Excessive acute migraine medication use and migraine progression*. Neurology, 2008. **71**(22): p. 1821-1828.
241. Bigal, M.E., A.V. Krymchantowski, and T. Ho, *Migraine in the triptan era: progresses achieved, lessons learned and future developments*. Arquivos de neuro-psiquiatria, 2009. **67**(2B): p. 559-569.
242. Martelletti, P., *The therapeutic armamentarium in migraine is quite elderly*. 2015, Taylor & Francis. p. 175-177.
243. Gao, B., et al., *Differential cellular expression of organic anion transporting peptides OATP1A2 and OATP2B1 in the human retina and brain: implications for carrier-*

- mediated transport of neuropeptides and neurosteroids in the CNS.* Pflügers Archiv-European Journal of Physiology, 2015. **467**(7): p. 1481-1493.
244. Kramer, D.R., et al., *Cortical spreading depolarization: Pathophysiology, implications, and future directions.* J Clin Neurosci, 2016. **24**: p. 22-7.
245. Yaguchi, Y., et al., *Organic anion-transporting polypeptide 1a4 (Oatp1a4/Slco1a4) at the blood–arachnoid barrier is the major pathway of sulforhodamine-101 clearance from cerebrospinal fluid of rats.* Molecular pharmaceutics, 2019. **16**(5): p. 2021-2027.
246. Burch, R., P. Rizzoli, and E. Loder, *The prevalence and impact of migraine and severe headache in the United States: Updated age, sex, and socioeconomic-specific estimates from government health surveys.* Headache, 2021. **61**(1): p. 60-68.
247. Bokelmann, K., J. Brockmüller, and M.V. Tzvetkov, *Impact of promoter polymorphisms on the transcriptional regulation of the organic cation transporter OCT1 (SLC22A1).* Journal of personalized medicine, 2018. **8**(4): p. 42.
248. Wood, I. and M. Pickholz, *Triptan partition in model membranes.* Journal of molecular modeling, 2014. **20**(10): p. 1-8.
249. Wood, I. and M. Pickholz, *Concentration effects of sumatriptan on the properties of model membranes by molecular dynamics simulations.* European Biophysics Journal, 2013. **42**(11): p. 833-841.
250. Meyer, M.J., et al., *Effects of genetic polymorphisms on the OCT1 and OCT2-mediated uptake of ranitidine.* PloS one, 2017. **12**(12): p. e0189521.
251. Römer, S., et al., *Effects of a Common Eight Base Pairs Duplication at the Exon 7-Intron 7 Junction on Splicing, Expression, and Function of OCT1.* Frontiers in pharmacology, 2021. **12**.

252. Matthaiei, J., et al., *OCT1 mediates hepatic uptake of sumatriptan and loss-of-function OCT1 polymorphisms affect sumatriptan pharmacokinetics*. *Clinical Pharmacology & Therapeutics*, 2016. **99**(6): p. 633-641.
253. Nascimento, D.S.M., et al., *Drug-induced HSP90 inhibition alleviates pain in monoarthritic rats and alters the expression of new putative pain players at the DRG*. *Molecular Neurobiology*, 2018. **55**(5): p. 3959-3975.
254. Riedel, M., et al., *17-AAG induces cytoplasmic α -synuclein aggregate clearance by induction of autophagy*. *PloS one*, 2010. **5**(1): p. e8753.
255. Petersen, A.L.d.O., et al., *17-AAG-induced activation of the autophagic pathway in Leishmania is associated with parasite death*. *Microorganisms*, 2021. **9**(5): p. 1089.
256. Dodick, D.W., *Migraine*. *Lancet*, 2018. **391**(10127): p. 1315-1330.
257. Hoter, A., M.E. El-Sabban, and H.Y. Naim, *The HSP90 Family: Structure, Regulation, Function, and Implications in Health and Disease*. *Int J Mol Sci*, 2018. **19**(9).
258. Palazzo, E., et al., *EPI Receptor within the Ventrolateral Periaqueductal Grey Controls Thermonociception and Rostral Ventromedial Medulla Cell Activity in Healthy and Neuropathic Rat*. *Molecular pain*, 2011. **7**: p. 1744-8069-7-82.
259. Carrive, P. and M.M. Morgan, *Periaqueductal gray*. *The human nervous system*, 2012. **3**: p. 368-401.
260. Wilson-Poe, A.R., et al., *Effects of inflammatory pain on CBI receptor in the midbrain periaqueductal gray*. *Pain reports*, 2021. **6**(1).
261. Palazzo, E., F. Rossi, and S. Maione, *Role of TRPV1 receptors in descending modulation of pain*. *Molecular and cellular endocrinology*, 2008. **286**(1-2): p. S79-S83.

262. Pasquariello, N., et al., *Characterization of the endocannabinoid system in human neuronal cells and proteomic analysis of anandamide-induced apoptosis*. Journal of Biological Chemistry, 2009. **284**(43): p. 29413-29426.
263. Bhattacharya, K. and D. Picard, *The Hsp70–Hsp90 go-between Hop/Stip1/Sti1 is a proteostatic switch and may be a drug target in cancer and neurodegeneration*. Cellular and Molecular Life Sciences, 2021. **78**(23): p. 7257-7273.
264. Karlı, N., et al., *Impact of sex hormonal changes on tension-type headache and migraine: a cross-sectional population-based survey in 2,600 women*. The journal of headache and pain, 2012. **13**(7): p. 557-565.
265. Buse, D.C., et al., *Sex Differences in the Prevalence, Symptoms, and Associated Features of Migraine, Probable Migraine and Other Severe Headache: Results of the American Migraine Prevalence and Prevention (AMPP) Study*. Headache: The Journal of Head and Face Pain, 2013. **53**(8): p. 1278-1299.
266. Borsook, D., et al., *Sex and the migraine brain*. Neurobiology of disease, 2014. **68**: p. 200-214.
267. Poursharifi, P., S.R.M. Madiraju, and M. Prentki, *Monoacylglycerol signalling and ABHD6 in health and disease*. Diabetes, Obesity and Metabolism, 2017. **19**: p. 76-89.
268. Davis, M.P., *Cannabinoids in pain management: CB1, CB2 and non-classic receptor ligands*. Expert opinion on investigational drugs, 2014. **23**(8): p. 1123-1140.
269. Datta, U., et al., *Positive allosteric modulation of the cannabinoid type-1 receptor (CB1R) in periaqueductal gray (PAG) antagonizes anti-nociceptive and cellular effects of a mu-opioid receptor agonist in morphine-withdrawn rats*. Psychopharmacology, 2020. **237**(12): p. 3729-3739.

270. Hashiesh, H.M., et al., *Pharmacological Properties, Therapeutic Potential and Molecular Mechanisms of JWH133, a CB2 Receptor-Selective Agonist*. *Frontiers in Pharmacology*, 2021. **12**.
271. Panikashvili, D., et al., *The endocannabinoid 2-AG protects the blood–brain barrier after closed head injury and inhibits mRNA expression of proinflammatory cytokines*. *Neurobiology of disease*, 2006. **22**(2): p. 257-264.